Study on Photoreaction Mechanisms of Aromatic Carboxylic Acids

Masaya Miyagawa

Department of Chemical and Material Systems

Graduate School of Bio-Applications and Systems Engineering

Tokyo University of Agriculture and Technology

Study on Photoreaction Mechanisms

of Aromatic Carboxylic Acids

Contents

Chapter 1: General Introduction

1.1. Monomeric structure of carboxylic acid

Carboxylic acid (CA, hereafter), generally written as R−COOH, is widely distributed throughout nature such as soil and atmosphere, and also applied industrially as fungicides, photostabilizers and drugs. Since CAs have both a hydrogen donor of the O−H part and two hydrogen acceptors of the C=O and C−O parts, they can easily form a hydrogen bond, and exist as a monomer, a dimer or an anion. Reactions of CAs are also strongly affected by hydrogen bonds. Thus, conformations of CAs have been investigated energetically.

Many spectroscopic studies on structures of CAs have been done in solution. Unlike many organic compounds, CAs are relatively soluble in water, because CAs have the O−H part to release the proton and exist as an anion, $R-COO^-$. In contrast, studies on the neutral form have been done in dilute non-polar solutions such as carbon tetrachloride and cyclohexane, where a structure of a complex with an additive such as ethanol is also investigated [1−13]. However, the intermolecular interaction can stabilize or destabilize a conformer or a reaction product. Thus measurements in the gas phase are adequate to study monomeric CAs and their photoreactions [12,14−32].

Monomeric CAs have two rotational axes, R−C and C−O. While the internal rotation around the R−C bond does not always have to be considered due to symmetry, the one around the C−O bond must always be considered. Thus, there are at least two conformations, *cis* and *trans* around the OC−OH bond shown in Fig. 1.1. In general CAs with no intramolecular hydrogen bond (IMHB, hereafter), the *trans* conformer is less stable than the *cis* due to electronic repulsion of lone pairs of the two O atoms by more than 20 kJ mol^{-1} calculated by quantum chemical calculations [33]. Furthermore, the *trans* conformer isomerizes to the *cis* in darkness by

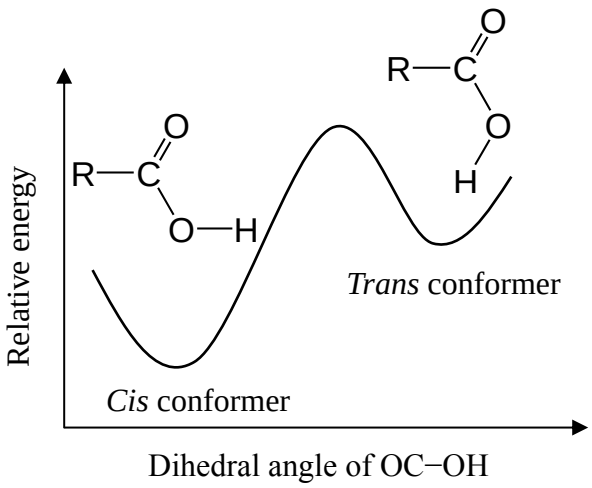

Fig. 1.1. *Cis* and *trans* conformers of carboxylic acids.

hydrogen-atom tunneling in the electronic ground state even at several kelvins. Thus it was once thought that the *trans* conformer can not be observed even if it is produced from the *cis*. However, photoproduction and temporal existence of the *trans* conformer of formic acid was reported in an argon matrix upon near infrared (IR) radiation [33−39]. Similarly, the *trans* conformer of benzoic acid and its *para*-substituted derivatives was also reported in an argon matrix and the effect of the substitution was investigated [33]. Since the low-temperature matrix-isolation technique enables unstable photoproducts to exist, photoreaction mechanisms have been investigated with this technique. However, such studies have not been done deeply in CAs as described in section 1.3.

Since the carboxy group has the hydrogen donor, stabilization of the *trans* conformer by an IMHB of X···HOOC has been attempted, where X represents the hydrogen acceptor [27,40−46]. For example, in 2-chloroacetic acid, the energy difference is lowered to 7.8 kJ mol^{-1} by the IMHB of Cl···HOOC calculated at DFT/B3LYP/6-31++G** level. As a result, a small amount of the *trans* conformer is observed in an argon matrix, and does not change to the *cis* conformer by hydrogen-atom tunneling [47]. This fact indicates that the IMHB may cause a significant change on the asymmetric potential surfaces in relation to both *cis* and *trans* conformers. The inversion of relative energy is reported in pyruvic acid (CH_3−CO−COOH), where the strong IMHB of C=O···HOOC is formed [46]. As a result, the *trans* is more stable than the *cis* by 9.5 kJ mol^{-1} in contrast to the result of 2-chloroacetic acid. The difference between these two molecules is not only due to the difference of the hydrogen acceptor, the Cl or O atom, but also due to that of the hybrid orbital of the lone pair. In other words, compared to the IMHB originating from the out-of-plane sp^3 hybrid orbital, the one originating from the in-plane sp^2 hybrid orbital is strong, resulting in the inversion of the relative energies of the *cis* and the *trans* conformers. On the other hand, stabilization of the *trans* conformer due to an IMHB was also attempted in aromatic CAs, where the *cis* conformer is more stable and the *trans* can not exist stably in halogenated benzoic acid or 2-furancarboxylic acid in spite of destabilization due to the repulsion of lone pairs of the O atom and the halogen atom or another O atom in the furan ring [42,48,49].

As well as the conformers around the OC−OH bond, the conformers around the

R−COOH bond have also been found in aliphatic CAs because their chain-like molecular frames do not give large energy differences [43,47,50,51]. In contrast, in *ortho*-substituted aromatic CAs, the energy difference between the two conformers around the R−C bond is strongly affected by the presence and the strength of the IMHB [21,24,48]. For example, while the energy difference in 2-fluorobenzoic acid with no IMHB is calculated to be 2.8 kJ mol^{-1} at DFT/B3LYP/6-311++G** level, that in salicylic acid is 16.4 kJ mol^{-1} at DFT/B3LYP/6-31G** due to the different IMHBs of C=O···HO−Ph and C−O···HO−Ph shown in Fig. 1.2 and 1.3, respectively. The presence of IMHB is confirmed experimentally by the lower-wavenumber shifts of the C=O and O−H stretching modes. Such conformational difference is important because photoreactions often depend on conformations and IMHBs, which will be described in section 1.3.

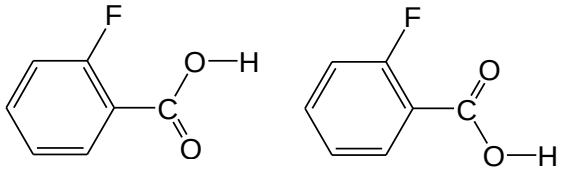

ΔE / kJ mol^{-1} 0.0 2.8

Fig. 1.2. Conformers of 2-fluorobenzoic acid.

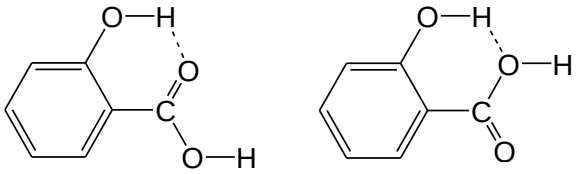

ΔE / kJ mol^{-1} 0.0 16.4

Fig. 1.3. Conformers of salicylic acid.

1.2. Dimeric structure of carboxylic acid

Since the carboxy group has both the hydrogen donor and the acceptor of the O−H and C=O parts respectively, CAs easily dimerize in high concentration in the gas or liquid phase through the two intermolecular hydrogen bonds of C=O···H−O. A dimer consisting of the same kind or different kinds of CA is called homodimer or heterodimer, respectively. Structural studies of dimers have been done in supersonic-jet expansion and in a noble-gas matrix [21,24,48,52]. Unlike a homodimer, a heterodimer has an asymmetric structure, and the double hydrogen-atom transfer between the two carboxy groups is often investigated, using a simple CA as the counterpart such as formic acid or benzoic acid [53−58].

In *ortho*-substituted benzoic acid derivatives, the electronic repulsion between the substituent groups plays an important role in the relative energy of a homodimer as well as the IMHB [21,48]. For example, in 2-fluorobenzoic acid, the homodimer composed of the less stable conformers is more stable than the one composed of the more stable conformers by 3.1 kJ mol^{-1} calculated at DFT/B3LYP/6-311++G** level shown in Fig. 1.4.

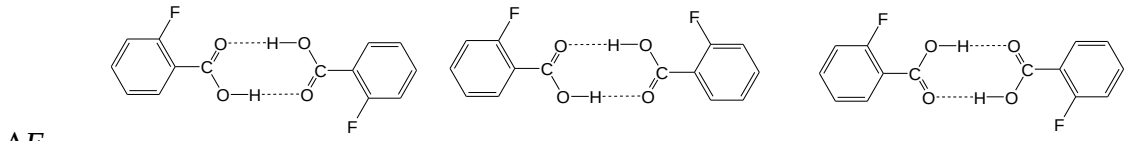

ΔE / kJ mol^{-1} 0.0 0.92 3.1

Fig. 1.4. Homodimers of 2-fluorobenzoic acid.

As a result, three kinds of homodimers are observed in supersonic-jet expansion [48]. The inversion of the relative energy is explained by weakened repulsive interaction between the F atom and the C=O part due to the formation of the intermolecular hydrogen bonds. In contrast, in salicylic acid, the energy difference between the two homodimers is calculated to be 16.4 kJ mol^{-1} at DFT/B3LYP/6-31G** level. As a result, only the most stable homodimer is observed shown in Fig. 1.5.

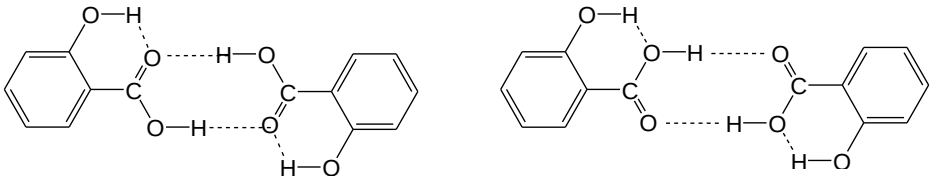

ΔE / kJ mol^{-1} 0.0 16.4

Fig. 1.5. Homodimers of salicylic acid.

Dimerization is often confirmed by the IR-band shifts of the C=O and O−H

stretching modes. For example, the former is reported in benzoic acid in an argon matrix [19]. The band assigned to the monomer appears at 1752 cm^{-1}, while new bands appear at 1737 and 1699 cm^{-1} by annealing the matrix sample. The former or latter band is assigned to a dimer with one or two intermolecular hydrogen bonds respectively, shown in Fig. 1.6. In contrast, the O−H stretching mode of the dimeric CAs is often too broad and too weak to be observed. Thus, the lower-wavenumber shift of the C=O stretching mode is used as the signature of the dimerization.

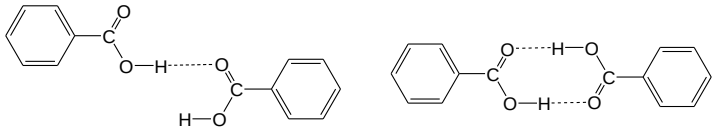

Fig. 1.6. Dimeric structures of benzoic acid.

1.3. Photoreactions of single molecules

Including CAs, numerous studies have ever been done on structures and photoreactions of single molecules mainly in a low-temperature noble-gas matrix or in supersonic-jet expansion. In this section, the author describes the fundamental reactions and their examples.

One of the simplest photoreactions is probably stereoisomerization from pyridines to Dewar pyridines by UV irradiation shown in Scheme 1.1 [59−61]. Such a slight difference is distinguished successfully by comparison with calculated spectral patterns obtained by the quantum chemical calculations. In compounds with a rotational axis, light-induced conformational changes are often observed, and the vibrational assignments are done as well [62−69]. Among many molecules, phenol derivatives have attracted much attention because they have simple structures with the rotational axis of the Ph−OH bond and they can form an IMHB with O, N or a halogen atom at the *ortho* position. As a result, not only the conformational change but also

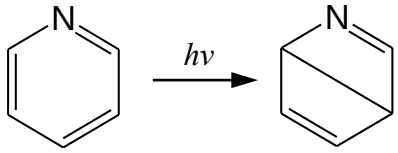

Scheme 1.1. Photoproduction of Dewar pyridine by UV irradiation.

hydrogen-atom tunneling and dissociation with other atoms are reported, which will be described later. In contrast, conformational changes have scarcely been investigated in aromatic CAs [43,47,50,51]. Studies on those of 2-chlorobenzoic acid and 2-furancarboxylic acid suggest the strength of the IMHB affects the stability of the *trans* conformer around the OC−OH bond [42,49]. In addition, Orton et al. pointed out the difference of the IMHB of C=O···HO−Ph and C−O···HO−Ph affects the relative energies greatly in the study on the conformational change of methyl salicylate [70]. In *ortho*-substituted aromatic CAs, the effect of the IMHB on its fluorescence has been investigated more deeply than the conformational changes. For example, Weller reported a dual emission in salicylic acid (2-hydroxybenzoic acid) when it is excited upon UV irradiation. At first, this emission was assumed to originate from two tautomers produced by the hydrogen-atom dissociation and the following transfer from the O−H to the C=O part in the hydroxy and carboxy groups respectively, but later works concluded that such a tautomerization does not occur and the dual emission originates from the S_1−S_0 transition of two conformers having different IMHBs. The photoreaction mechanisms will be described in detail in section 3.1 [21,24,29].

Light-induced hydrogen-atom dissociation has been found in aromatic compounds [68,69,71−82]. In this reaction, there are three possibilities of the further reaction: the first one is the back reaction induced thermally. The second one is tautomerization, where the dissociated H atom migrates to the aromatic ring or a hydrogen acceptor such as carbonyl and imino groups, and the third one is that another atom such as a halogen or an H atom dissociates to produce a hydrogen halide or an hydrogen molecule, respectively.

Various tautomerization is reported in aromatic compounds having a hydroxy or an amino group [63,71,83−89]. Typical examples are keto-enol and amino-imino tautomerization caused by hydrogen-atom transfer, which is reviewed in Refs. [90−92]. Since the equilibrium between the two tautomers is affected by the dipole moment of solvent molecules, many studies have been done in low-temperature noble-gas matrices. The absorption wavelength, the equilibrium, and the photoreaction mechanisms have been investigated especially in DNA bases such as adenine because the tautomerization induces the loss of the genetic information on replications [89,71,93,94]. As their parent molecules, pyridine and pyrimidine derivatives have also been investigated even though

they also show a ring-opening reaction. In aromatic CAs, conformations of orotic acid (6-carboxyuracil) have recently been determined as a fundamental molecule for biosynthesis of nucleic acids [95]. However, no tautomerization to produce $R=C(OH)_2$ from $R-COOH$ has been reported, indicating $R=C-(OH)_2$ has no potential minimum at the ground state or is unstable and the back reaction easily occurs.

Dissociation of a small molecule is sometimes related to the presence of IMHB. For example, an HCl molecule dissociates from the *trans* conformer of 2-chloropropionic acid having the IMHB of Cl···HOOC, resulting in methyloxiranone, a 3-membered lactone, even though the observation of the carboxy radical has not been reported in any CAs. On the other hand, there is another photodissociation in aromatic compounds, where one H radical dissociates upon light irradiation and it dissociates another H radical to produce an H_2 molecule. In this case, production of a bicyclo compound is reported in *ortho*-substituted aromatic compounds such as *o*-diaminobenzene shown in Scheme 1.2.

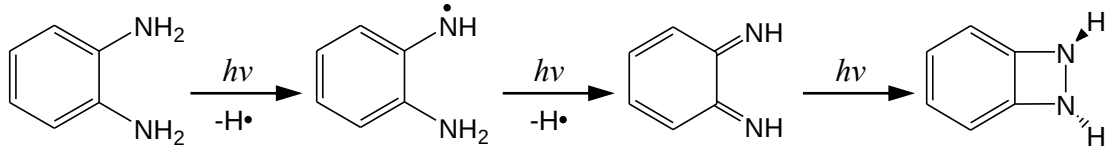

Scheme 1.2. Hydrogen-atom dissociation from 1,2-diaminobenzene and the following production of 7,8-diazabicyclo[4.2.0]octa-1,3,5-triene upon UV irradiation.

No bicyclo compound has been reported from benzoic acid derivatives, even though Chapman et al. reported a similar back reaction from a bicyclo compound, where methyl salicylate is produced from methanol and 7-oxabicyclo[4,2,0]octa-1,3,5-trien-8-one in an argon matrix by a ring-opening reaction shown in Scheme 1.3 [96].

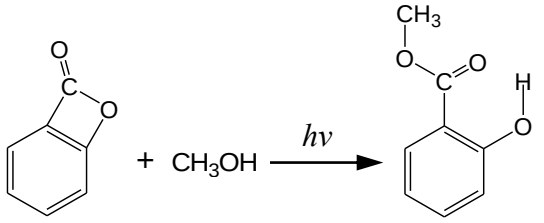

Scheme 1.3. Photoproduction of methyl salicylate from 7-oxabicyclo[4,2,0]octa-1,3,5-trien-8-one and methanol upon UV irradiation.

Ring-opening reactions by UV irradiation have been reported in π-conjugated cyclic compounds [86,74,97−103]. A typical example is *α*-pyrone, where the C−O bond in the pyran ring cleavages and a chain-like conjugated ketene compound is produced. The back reaction occurs thermally, as shown in Scheme 1.4. Since ketenes have been invoked as intermediates in many photochemical reactions of unsaturated ketones, this reaction attracted much attention, and similar reactions were also reported later in pyridine and pyrimidine derivatives. However, there is no report in aromatic CAs. The author assumes that the required energy to open the aromatic ring is so high that a decomposition reaction occurs preferentially.

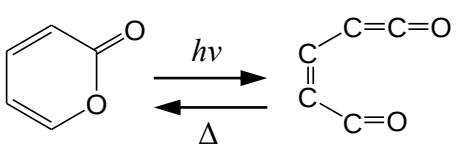

Scheme 1.4. Open-ring reaction and its back reaction of α-pyrone.

Since CAs are present in nature and also applied industrially, their decomposition reactions have also been investigated [41,104−110]. Faust et al. studied photolysis of *α*,*β*-unsaturated CAs ($R-C_{\beta}=C_{\alpha}-COOH$) and suggested two reaction pathways: one is the cleavage of the $C_{\alpha}-COOH$ bond and the other is that of the C−O bond. The reaction mechanisms are shown in Scheme 1.5(a) and (b), respectively. On the other hand, since aromatic CAs are relatively stable by light irradiation compared to aliphatic CAs, photolysis of aromatic CAs has often been investigated in solution by use of photocatalysts such as TiO_2 or in the presence of oxidants such as H_2O_2 [111−114].

Studies on CAs performed by various methods are summarized in Table 1.1. In aromatic CAs, most of the studies focused on the conformational change around the OC−OH bond or the dual emission. In the former case, stable existence of the *trans* conformer has not been reported in aromatic CAs, indicating the IMHB is relatively weak, while the IMHB plays an important role in the latter case.

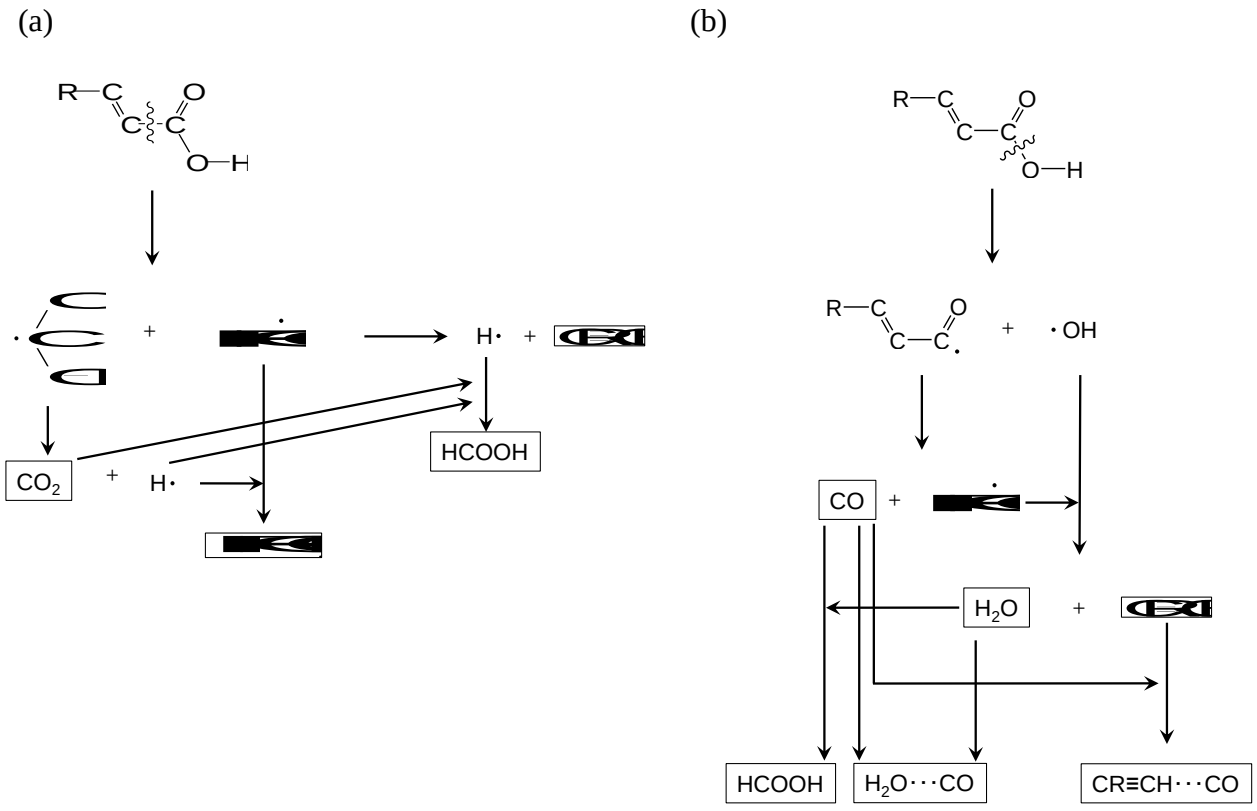

Scheme 1.5. Photolysis of *α,β*-unsaturated carboxylic acids.

Table 1.1. History of studies on carboxylic acids.

Year	Author	Sample molecule	Condition of sample	Measure-ment	Characteristics	Ref.
1955	Weller	Salicylic acid (SA), Methylsalicylate	Solution (Sol)	emission	Dual emissions, Excited-state intramolecualr proton transfer (ESIPT), double minimum potential	13
1990	Joshi	SA-Diethylether complex	Sol	emission	ESIPT in complex	1
1992	Kulbida	Chloroacetic acid	Matrix isolation (MI)	IR	Temporary existence of the trans form, Hydorogen-atom tunneling	27
1994	Pant	SA	Sol	UV-vis, emission	ESIPT in dimer	2
1995	Bisht	SA	Supersonic-jet expansion (Jet)	emission	Suggestion of the origin of UV emission from the second most stable conformer	30
1995	Reva	Benzoic acid	MI	IR	*ν*C=O of monomer and dimer	32
1996	Denisov	Salicylic acid, 6-hydorxySA	Sol	UV-vis, emission	ESIPT in monomer and dimer	3
1996	Stepanian	Benzoic acid	MI	IR, Quantum Chemical Calculation (QCC)	*ν*C=O of monomer and dimer	20
1997	Denisov	SA	Sol	IR	*ν*C=O and *ν*O−H of monomer and dimer	4
1997	Lahmani	5-MethylSA, 5-MethoxySA	Sol, Jet	emission	Relation between emission and electron donating or withdrawing group	12
1997	Lahmani	SA-Acetic acid dimer, SA-Trifluoroacetic dimer	Jet	emission	Emission from hetero dimer	52

Table 1.1. History of studies on carboxylic acids (Continue).

					Potential energy curve of the S_1 state	
1998	Sobolewski	SA	-	QCC	Suggestion of visible-light emission from elongation of hydroxy group	31
1999	Fausto	Chloroacetic acid, Crotonic acid	MI	IR, QCC	Photoisomerization	41
2001	Yahagi	SA	Jet	IR-UV, QCC	Experimental support with Sobolewski's suggestion	22
2001	Fausto	Acrylic acid, Maleic acid	MI	IR, QCC	Photoisomerization, Photolysis	26
2003	Maçôas	Formic acid	MI	IR	Deutrium substituion for observation of photoisomerization, Observation of the overtone of νO−H	16
2003	Maçôas	Acetic acid	MI	IR, QCC	Photoisomerization, Hydrogen-atom tunneling	17
2003	El-Hakam	SA, 5-MethoxySA	Jet	IR-UV, emission	Relation between emission mechanism and substitution effect	19
2003	Southern	Anthranilic acid	Jet	IR-UV, emission, QCC	Elongation of N−H bond similar to the case of SA	25
2005	Szczepaniak	PA N-oxide	MI	IR	Lower-frequency shift of νO−H Mixing with νC=O and δO−H	21
2007	Nishino	2-Chlorobenzoic acid	MI	IR	Photoisomerization, Hydrogen-atom tunneling	42
2008	Khriachtchev	Formic acid	MI	IR	Photoisomerization, Hydrogen-atom tunneling	15
2008	Nishino	2-Chloropropionic acid	MI	IR	Photoisomerization	43

Table 1.1. History of studies on carboxylic acids (Continue).

2009	Pozdnyakov	SA, 5-AminoSA	Aq	UV-vis, emission	Relation between emission and ionization depending on pH	5
2010	Paul	5-ChloroSA	Sol	UV-vis, emission, QCC	Relation between emission wavelength and addition of acid or base	6
2010	Paul	3,5-DichloroSA	Sol	UV-vis, emission, QCC	Relation between emission wavelength and addition of acid or base	7
2010	Amiri	Benzoic acid and its derivatives	MI	IR, QCC	Photoisomerization, Hydrogen-atom tunneling	33
2011	Paul	3,5,6-TrichloroSA	Sol	UV-vis, emission, QCC	Relation between emission wavelength and addition of acid or base	8
2011	Ito	Trifluoroacetic acid hydrates	MI	IR, QCC	IR spectra of mono and dihydrates due to hydration	29
2012	Paul	4-ChloroSA	Sol	UV-vis, emission, QCC	Relation between emission wavelength and addition of acid or base	9
2012	Maier	Oxalic acid	MI	IR, QCC	Photoisomerization	14
2013	Ito	Trifluoroacetic acid hydrates	-	QCC	Structural optimization of tetrahydrates	28
2014	Ratajczak	Acetic acid-Trimethylamine comoplex	MI	IR, QCC	Structure of complex	18

1.4. Objectives of this thesis

As described in the previous section, numerous studies have ever been done on conformations and photoreaction mechanisms of single molecules. However, compared to phenol derivatives and aliphatic CAs, aromatic CAs have not been paid attention. In the studies on 2-chlorobenzoic acid and methyl salicylate, the presence and the strength of the IMHB strongly affect photoreactions. Indeed, in the study on 2-chloropropionic acid, the dissociation of HCl is related to the IMHB. However, similar reactions have never been reported in aromatic CAs, as described in the previous section.

Aromatic CAs have a potential to form an IMHB at the *ortho* position. Unlike aliphatic CAs, the OH part acts as the hydrogen acceptor in aromatic CAs, and the similar dissociation can be expected. However, such a reaction has not been reported, nor the observation of the OH radical has. Furthermore, there are few studies on the conformational changes, and the stable existence of the *trans* conformer has not been reported yet. Thus, conformations of single molecules and their photoreaction mechanisms have scarcely been investigated, even though many aromatic CAs are used in nature and applied industrially. In particular, the presence and the strength of IMHB are important because it affects the stability of conformers and also induces a dissociation reaction. Therefore the author investigated photoreaction mechanisms of aromatic CAs with the IMHB by the low-temperature matrix-isolation IR spectroscopy to reveal fundamental functions of the carboxy group both as the hydrogen donor and the acceptors.

Chapter 2 shows principle of experimental and calculation methods, and their details performed in the present thesis.

Chapter 3 describes molecular structure and photoreaction mechanisms of salicylic acid (2-hydroxybenzoic acid), and found conformational changes and dissociation of a water molecule, forming a molecular cluster.

Chapter 4 describes molecular structure and photoreaction mechanisms of 3-chlorosalicylic acid (2-hydroxy-3-chlorobenzoic acid) and the effect of the chlorine-atom substitution on the relative stability of conformers and photoreaction mechanisms.

Chapter 5 describes molecular structure and photoreaction mechanisms of 2-pyridinecarboxylic acid and found the stable existence of the *trans* conformer by

IMHB of COOH···N in the pyridine ring. The author also found the UV-induced conformational changes and its reaction mechanisms.

As a conclusion, Chapter 6 summarizes the conformations and photoreaction mechanisms of aromatic carboxylic acids.

1.7. References

[1] H.C. Joshi, H.B. Tripathi, T.C. Pant, D.D. Pant, Chem. Phys. Lett. 173 (1990) 83.

[2] D.D. Pant, H. C. Joshi, P.B. Bisht, H.B. Tripathi, Chem. Phys. 185 (1994) 137.

[3] G.S. Denisov, N.S. Golubev, V.M. Schreiber, Sh.S. Shajakhmedov, A.V. Shurukhina, J. Mol. Struct. 381 (1996) 73.

[4] G.S. Denisov, N.S. Golubev, V.M. Schreiber, Sh.S. Shajakhmedov, A.V. Shurukhina, J. Mol. Struct. 436-437 (1997) 153.

[5] I.P. Pozdnyakov, A. Pigliucci, N. Tkachenko, V.F. Plyusnin, E. Vauthey, H. Lemmetyinen, J. Phys. Org. Chem. 22 (2009) 449.

[6] B.K. Paul, A. Samanta, N. Guchhait, Photochem. Phobiol. Sci. 9 (2010) 57.

[7] B.K. Paul, A. Samanta, N. Guchhait, J. Mol. Struct. 977 (2010) 78.

[8] B.K. Paul, A. Samanta, N. Guchhait, J. Fluoresc. 21 (2011) 1265.

[9] B.K. Paul, N. Guchhait, Chem. Phys. 403 (2012) 94.

[10] F. Rollet, C. Richard, J.-F. Pilichowski, B. Aboab, Org. Biomol. Chem. 2 (2004) 2253.

[11] M.L.Ţînţaş, A.P. Diac, A. Soran, A. Terec, I. Grosu, E. Bogdan, J. Mol. Struct. 1058 (2014) 106.

[12] F. Lahmani, A. Z.-Rentien, J. Phys. Chem. A 101 (1997) 6141.

[13] A. Weller, Naturwissenschaften 42 (1955) 175.

[14] G. Maier, J. Endres, H.P. Reisenauer, J. Mol. Struct. 1025 (2012) 2.

[15] L. Khriachtchev, J. Mol. Struct. 880 (2008) 14.

[16] E.M.S. Maçôas, J. Lundell, M. Pettersson, L. Khriachtchev, R. Fausto, M. Räsänen, J. Mol. Spectrosc. 219 (2003) 70.

[17] E.M.S. Maçôas, L. Khriachtchev, M. Pettersson, R. Fausto, M. Räsänen, J. Am. Chem. Soc. 125 (2003) 16188.

[18] H. Ratajczak, M. Wierzejewska, A.J. Barnes, A.M. Yaremko, S.V. Virko, Chem. Phys. 436-437 (2014) 17.

[19] E.A. El-Hakam, A. El-Nasr, A. Fujii, T. Ebata, N. Mikami, Chem. Phys. Lett. 376 (2003) 788.

[20] S.G. Stepanian, I.D. Reva, E.D. Radchenko, G.G. Sheina, Vib. Spectrosc. 11 (1996) 123.

[21] K. Szczepaniak, W.B. Person, D. Hadži, J. Phys. Chem. A 109 (2005) 6710.

[22] T. Yahagi, A. Fujii, T. Ebata, N. Mikami, J. Phys. Chem. A 105 (2001) 10673.

[23] G. Meijer, M.S. de Vries, H.E. Hunziker, H.R. Wendt, J. Phys. Chem. 94 (1990) 4394.

[24] I.D. Reva, A.M. Plokhotnichenko, E.D. Radchenko, G.G. Sheina, Y.P. Blagoi, Spectrochim. Acta 50A (1994) 1107.

[25] C.A. Southern, D.H. Levy, G.M. Florio, A. Longarte, T.S. Zwier, J. Phys. Chem. A 107 (2003) 4032.

[26] R. Fausto, E.M.S. Maçôas, J. Mol. Struct. 563-564 (2001) 27.

[27] A. Kulbida, A. Nosov, J. Mol. Struct. 265 (1992) 17.

[28] F. Ito, Comput. Theor. Chem. 1016 (2013) 48.

[29] F. Ito, Chem. Phys. 382 (2011) 52.

[30] P.B. Bisht, H. Petek, K. Yoshihara, U. Nagashima, J. Chem. Phys. 103 (1995) 5290.

[31] A.L. Sobolewski, W. Domcke, Chem. Phys. 232 (1998) 257.

[32] I.D. Reva, S.G. Stepanian, J. Mol. Struct. 349 (1995) 337.

[33] S. Amiri, H.P. Reisenauer, P.R. Schreiner, J. Am. Chem. Soc. 132 (2010) 15902.

[34] E.M.S. Maçôas, L. Khriachtchev, M. Pettersson, J. Juselius, R. Fausto, M. Räsänen, J. Chem. Phys. 119 (2003) 11765.

[35] E.M.S. Maçôas, L. Khriachtchev, M. Pettersson, J. Lundell, R. Fausto, M. Räsänen, Vib. Spectrosc. 34 (2004) 73.

[36] E.M.S. Maçôas, L. Khriachtchev, M. Pettersson, R. Fausto, M. Räsänen, J. Am. Chem. Soc. 125 (2003) 16188.

[37] E.M.S. Maçôas, L. Khriachtchev, M. Pettersson, R. Fausto, M. Räsänen, J. Chem. Phys. 121 (2004) 1331.

[38] E.M.S. Maçôas, L. Khriachtchev, M. Pettersson, R. Fausto, M. Räsänen, J. Phys. Chem. A 109 (2005) 3617.

[39] E.M.S. Maçôas, L. Khriachtchev, M. Pettersson, R. Fausto, M. Räsänen, Phys. Chem. Chem. Phys. 7 (2005) 743.

[40] J. Nieminen, M. Pettersson, R. Räsänen, J. Phys. Chem. 97 (1993) 10925.

[41] R. Fausto, E.M.S. Maçôas, A. Kulbida, J. Mol. Struct. 480-481 (1999) 83.

[42] S. Nishino, M. Nakata, J. Phys. Chem. A 111 (2007) 7041.

[43] S. Nishino, M. Nakata, J. Mol. Struct. 875 (2008) 520.

[44] A. Halasa, L. Lapinski, I. Reva, H. Rostkowska, R. Fausto, M.J. Nowak, J. Phys.

Chem. A 118 (2014) 5626.
[45] A. Borba, A. G.-Zavaglia, R. Fausto, J. Chem. Phys. 141 (2014) 154306.
[46] I. Reva, C.M. Nunes, M. Biczysko, R. Fausto, J. Phys. Chem. A *in press* (dx.doi.org/10.1021/jp509578c).
[47] A. Kulbida, R. Fausto, J. Chem. Soc. Faraday Trans. 89 (1993) 4257.
[48] C.K. Nandi, A.K. Samanta, T. Chakraborty, Chem. Phys. Lett. 416 (2005) 261.
[49] A. Halasa, L. Lapinski, I. Reva, H. Rostkowska, R. Fausto, M.J. Nowak, J. Phys. Chem. A in press DOI: 10.1021/jp512302s.
[50] A. Kulbida, M.N. Ramos, M. Räsänen, J. Nieminen, O. Schrems, R. Fausto, J. Chem. Soc. Faraday Trans. 91 (1995) 1571.
[51] R. Fausto, A. Kulbida, O. Schrems, J. Chem. Soc. Faraday Trans. 91 (1995) 3755.
[52] F. Lahmani, A. Z.-Rentien, Chem. Phys. Lett. 271 (1997) 6.
[53] L. Evangelisti, P. Ecija, E.J. Cocinero, F. Castano, A. Lesarri, W. Caminati, R. Meyer. J. Phys. Chem. Lett. 3 (2012) 3770.
[54] Z. Smedarchina, A. Fernandez-Ramos, W. Siebrand, J. Chem. Phys. 122 (2005) 134309.
[55] R. More, M. Scholz, G. Busse, L. Busse, C. Paulmann, M. Tolkiehn, S. Techert, Phys. Chem. Chem. Phys. 14 (2012) 10187.
[56] C.S. Tautermann, A.F. Voegele, K.R. Liedl, J. Chem. Phys. 120 (2004) 631.
[57] Y. Shigeta, H. Ushiyama, K. Takatsuka, J. Mol. Struct. 615 (2002) 267.
[58] S. Ghoshal, M.K. Harza, J. Phys. Chem. A 118 (2014) 4620.
[59] S. Kudoh, M. Takayanagi, M. Nakata, J. Photochem. Photobiol. A Chem. 123 (1999) 25.
[60] S. Kudoh, M. Takayanagi, M. Nakata, Chem. Phys. Lett. 308 (1999) 403.
[61] S. Kudoh, M. Takayanagi, M. Nakata, Chem. Phys. Lett. 322 (2000) 363.
[62] N. Akai, S. Kudoh, M. Takayanagi, M. Nakata, Chem. Phys. Lett. 356 (2002) 133.
[63] M. Nagaya, M. Nakata, J. Phys. Chem. A 111 (2007) 6256.
[64] T. Itoh, N. Tanaka, H. Nishikiori, T. Fujii, Chem. Phys. Lett. 514 (2011) 247.
[65] N. Nagashima, S. Kudoh, M. Takayanagi, M. Nakata, J. Phys. Chem. A 105 (2001) 10832.
[66] L. Duarte, R. Fausto, I. Reva, Phys. Chem. Chem. Phys. 16 (2014) 16919.
[67] C. Zhang, M. Chen, J. Mol. Struct. 1037 (2013) 144.

[68] K. Ujike, S. Kudoh, M. Nakata, Chem. Phys. Lett. 396 (2004) 288.
[69] K. Ujike, S. Kudoh, M. Nakata, Chem. Phys. Lett. 409 (2005) 52.
[70] E. Orton, M.A. Morgan, G.C. Pimentel, J. Phys. Chem. 94 (1990) 7936.
[71] S. Iizumi, N. Akai, M. Nakata, J. Mol. Struct. 1025 (2014) 43.
[72] R.J. MacMahon, O.L. Chapman, J. Am. Chem. Soc. 109 (1987) 683.
[73] J. Morawietz, W. Sander, M. Träubel, J. Org. Chem. 60 (1995) 6368.
[74] B.M. Giuliano, I. Reva, L. Lapinski, R. Fausto, J. Chem. Phys. 136 (2012) 024505.
[75] N. Tanaka, H. Fujiwara, H. Ogawa, H. Nishikiori, J. Mol. Struct. 1025 (2012) 48.
[76] M. Sekine, H. Sekiya, M. Nakata, J. Phys. Chem. A 116 (2012) 8980.
[77] M. Sekine, Y. Nagai, H. Sekiya, M. Nakata, Chem. Phys. Lett. 490 (2010) 46.
[78] M. Sekine, Y. Nagai, H. Sekiya, M. Nakata, J. Phys. Chem. A 113 (2009) 8286.
[79] S. Nanbu, M. Sekine, M. Nakata, J. Mol. Struct. 1025 (2012) 69.
[80] S. Nanbu, M. Sekine, M. Nakata, J. Phys. Chem. A 115 (2011) 9911.
[81] N. Akai, S. Kudoh, M. Takayanagi, M. Nakata, J. Photochem. Photobiol. A 146 (2001) 49.
[82] N. Akai, S. Kudoh, M. Takayanagi, M. Nakata, Chem. Phys. Lett. 363 (2002) 591.
[83] A. Destexhe, J. Smets, L. Adamowicz, G. Maes, J. Phys. Chem. 98 (1994) 1506.
[84] M.J. Nowak, J. Fulara, L. Lapinski, J. Mol. Struct. 175 (1988) 91.
[85] M. Szczesniak, M.J. Nowak, K. Szczepaniak, J. Mol. Struct. 115 (1984) 221.
[86] L. Lapinski, J. Fulara, M.J. Nowak, Spectrochimica Acta A 46 (1990) 61.
[87] N. Akai, K. Ohno, M. Aida, Chem. Phys. Lett. 413 (2005) 306.
[88] L. Lapinski, J. Fulara, R. Czerminski, M.J. Nowak, Spectrochimica Acta A 46 (1990) 1087.
[89] S. Iizumi, N. Akai, M. Nakata, J. Mol. Struct. 1037 (2014) 29.
[90] L.G. Arnaut, S.J. Formosinho, J. Photochem. Photobiol. A 75 (1993) 1.
[91] S.J. Formosinho, L.G. Arnaut, J. Photochem. Photobiol. A 75 (1993) 21.
[92] A. Douhal, F. Lahmani, A.H. Zewail, Chem. Phys. 207 (1996) 477.
[93] C. Colominas, F.J. Luque, M. Oronzco, J. Am. Chem. Soc. 118 (1996) 6811.
[94] M.J. Nowak, L. Lapinski, J. Fulara, Spectrochim. Acta A 45 (1989) 229.
[95] R. Wysokiński, K. Helios, L. Lapinski, M.J. Nowak, D. Michalska, Vib. Spectrosc. 64 (2013) 108.
[96] O.L. Chapman, C.L. McIntosh, J. Pacansky, J. Am. Chem. Soc. 95 (1973) 244.

[97] G. Quinkert, Pure Appl. Chem. 33 (1973) 285.
[98] J. Griffiths, H. Hart, J. Am. Chem. Soc. 90 (1968) 5296.
[99] L. Lapinski, H. Rostkowska, A. Khvorostov, R. Fausto, M.J. Nowak, J. Phys. Chem. A 107 (2003) 5913.
[100] R.G.S. Pong, J.S. Shirk, J. Am. Chem. Soc. 95 (1973) 248.
[101] O.L. Chapman, J.D. Lassila, J. Am. Chem. Soc. 90 (1968) 2449.
[102] A. Krantz, J. Am. Chem. Soc. 96 (1974) 4992.
[103] J. Griffiths, H. Hart, J. Am. Chem. Soc. 90 (1968) 3297.
[104] D.R. Peterman, R.G. Daniel, R.J. Horwitz, J.A. Guest, Chem. Phys. Lett. 236 (1995) 564.
[105] S.S. Hunnicutt, L.D. Waits, J.A. Guest, J. Phys. Chem. 95 (1991) 562.
[106] S.S. Hunnicutt, L.D. Waits, J.A. Guest, J. Phys. Chem. 93 (1989) 5188.
[107] P. Ausloos, E.W.R. Steacie, Can. J. Chem. 33 (1955) 1530.
[108] J.C. Owrutsky, A.P. Baronavski, J. Chem. Phys. 111 (1999) 7329.
[109] D.L. Singleton, G. Paraskevopoulos, R.S. Irwin, J. Phys. Chem. 94 (1990) 695.
[110] E.M.S. Maçôas, L. Khriachtchev, R. Fausto, M. Räsänen, J. Phys. Chem. A 108 (2004) 3380.
[111] R. W. Matthews, J. Catal. 111 (1988) 264.
[112] J. Sabate, M.A. Anderson, H. Kikkawa, Q. Xu, S. Cervera-March, C.G. Hill Jr., J. Catal. 134 (1992) 36.
[113] J. Sabate, M.A. Anderson, H. Kikkawa, M. Edwards, C.G. Hill Jr., J. Catal. 127 (1991) 167.
[114] C.K. Scheck, F.H. Frimmel, Wat. Res. 29 (1995) 2346.

Chapter 2: Experimental and Calculation

2.1. Principle of matrix-isolation technique

Matrix-isolation technique was developed by Pimentel's and Porter's groups [1−2]. In this technique, gaseous sample is diluted by large amount of inert gas, and cooled by liquid nitrogen at 77 K. Recently, the mixed gaseous sample is deposited onto a plate cooled at several kelvins by a closed-cycle helium refrigerator. Spectral measurement combined with this matrix-isolation technique gives narrower bandwidths than that with conventional methods such as KBr disk method, because both intermolecular interactions and thermal fluctuation are suppressed due to isolation by inert molecules and low temperature, respectively.

Population ratio of conformers in the matrix corresponds to that in the gas phase at deposition temperature, because the mixed gas freezes immediately after deposition without thermal isomerization. In contrast, photoproducts by light irradiation are kept under low temperature. Thus unstable species such as radicals and reaction intermediates may exist stably and be identified, which is one of the purposes to apply this technique.

2.2. Principle of quantum chemical calculation

Because IR bands measured with matrix-isolation infrared (IR) spectroscopy are so narrow that the assignment of bands and the identification of the molecular structure are often done with an aid of quantum chemical calculation.

The author used the Gaussian 09W program package for the quantum chemical calculation [3]. Geometrical optimization and vibrational analysis are performed by density-functional-theory (DFT) method because this method requires low calculation cost and short calculation time. In the DFT method, energy terms (kinetic energy of electron, Coulomb energy, exchange energy and correlation energy) are defined as functionals of the electron density, which is proposed by Hohenberg and Kohn [4]. Geometrical optimization is performed by determining the electron density so that the total energy becomes the minimum.

The Hartree-Fock equation is expressed as follows:

$$\left(-\frac{1}{2}\nabla^2 - \sum_{A=1}^{M}\frac{Z_A}{r_A} + \sum_{j=1}^{n}\left(J_j - K_j\right)\right)\psi_i(\boldsymbol{r}) = \varepsilon_i\psi_i(\boldsymbol{r}) \quad (1.1)$$

the first and second terms in the left part represent operators of kinetic energy and attractive force of electrons. *Jj* and *Kj* in the third term represent the repulsive Coulomb and exchange operators, respectively. ψ_i and ε_i are the *i*th molecular orbital and its orbital energy,

In contrast, the corresponding equation in the DFT method is called Kohn-Sham equation [5], which is expressed as follows:

$$\left(-\frac{1}{2}\nabla^2 - \sum_{A=1}^{M}\frac{Z_A}{r_A} + \int\frac{\rho(r')}{|r-r'|}d\boldsymbol{r} + V_{XC}(\boldsymbol{r})\right)\psi_i(\boldsymbol{r}) = \varepsilon_i\psi_i(\boldsymbol{r}) \quad (1.2)$$

while the first and the second terms are same as those in equation (1.1), the third term is different, and there is the fourth term. The third term represents the repulsive Coulomb operator, and the fourth represents the exchange and correlation operator. ψ_i and ε_i represent the Kohn-Sham orbital and the corresponding orbital energy, respectively. The electron density, $\rho(\boldsymbol{r})$, is expressed as follows:

$$\rho(\boldsymbol{r}) = \sum_{i=1}^{n}\psi_i(\boldsymbol{r})^*\psi_i(\boldsymbol{r}) \quad (1.3)$$

if V_{xc} was given and the equation (1.2) could be solved, the electron energy was obtained accurately using $\rho(\boldsymbol{r})$ obtained from equation (1.3). However, V_{xc} can not be obtained practically, so is treated approximately. This is why the DFT method requires low calculation cost compared to the molecular orbital method.

While the DFT method is useful to estimate various molecular properties, there are some weak points: calculation of a transition state is not very accurate and the energy barrier between two structures tends to be underestimated. Furthermore, it is difficult to express van der Waals interaction originating from dispersion force. Nevertheless, because various experimental values can be reproduced with low calculation cost by the DFT method, it is quite useful as well as ab initio calculations.

Since electron distribution is not uniform in a molecular system, functionals based on generalized gradient approximation have been used. For example, B3LYP is one of the most popular functionals, which contains Becke's three-parameter hybrid density

functional in combination with Lee-Yang-Parr correlation functional [6−7].

The molecular orbital, ψ_i is expressed by a linear combination of basis functions:

$$\psi_i(\boldsymbol{r}) = \sum_{\mu=1}^{N} C_{\mu i}\varphi_u(\boldsymbol{r}) \quad (1.4)$$

where $C_{\mu i}$ is a coefficient, which is the weight of the contributions of the *i*th basis function. $\boldsymbol{r}$ is an electron coordinate, and *N* is the total number of basis functions.

The molecular orbital, ψ_i is also expressed by the linear combinations of atomic orbitals, which is called LCAO-MO (Linear Combinations of Atomic Orbitals-Molecular Orbital). Thus each AO has its basis functions. A set of basis functions is called a basis set. For example, STO-3G is a typical minimum basis set, and each AO is expressed by one Slater type orbital (STO), which is approximated by a linear combination of three Gaussian type orbitals (3G). Such an approximation is called contraction, and the Gaussian functions used for contraction is called primitive Gaussian.

Since STO-3G does not give accurate calculation results, more than one contracted Gaussian type orbitals CGTO) are used to express valence orbitals to consider expansion and contraction of orbitals, which are called split valence basis set such as double-zeta (DZ) and triple-zeta (TZ) basis sets. 6-31G is one of the DZ basis sets, and means that the inner-shell orbitals were expressed by one CTGO composed of six primitive Gaussians, and the valence orbitals were expressed by two CTGO composed of three and one primitive Gaussians, respectively.

Since electron distribution is actually not spherically-symmetric, 6-31G basis set does not give accurate calculation results. To solve this problem, additional polarization functions are required. For example, a basis set containing *d*-type polarization functions for atoms except H atoms, is written as 6-31G(d) or 6-31G*. If *p*-type polarization functions for H atoms is added to 6-31G*, it is written as 6-31G(d,p) or 6-31G**.

In calculation containing long and weak bonds such as van der Waals and hydrogen bonds, 6-31G** basis set is not appropriate to use. In this case, diffuse functions are needed as well as polarization functions. A diffuse function broadens the electron distribution. Thus in calculating an anion molecule or an electronic excited state, the diffuse functions should also be used. Basis functions are composed of Gaussian

functions expressed by $\exp(-\alpha r^2)$. The diffuse function has a small value of α, which means the broadening of the electron distribution.

A basis set with a diffuse function has a symbol of + before G, such as 6-31+G. In the same way of the polarization functions, 6-31+G means addition of a diffuse function to atoms except H atoms, and 6-31++G means addition of diffuse functions to atoms including H atoms.

2.3. Experimental apparatus and samples

A diagram of the matrix-isolation apparatus with an FT-IR spectrophotometer was shown in Fig. 2.1. Vacuum pressure in the vacuum chamber was kept under 10^{-4} Pa by a turbo-molecular pump (Mitsubishi Jukogyo, PT-300) and a rotary pump (EDWARDS, RV12). The CsI plate in the center of the vacuum chamber was cooled by closed-cycle helium refrigerator (Iwatani, CW303) at 20 K for deposition and at 10 K for measurement.

A small amount of powder sample is placed in the nozzle with heating system (Fig. 2.2(a)) or in a U-shaped glass tube (Fig. 2.2(b)) connected to the stainless steel pipe of 1/8 inch diameter with the sealed valve (Swagelok, SS-2H). Argon gas (Taiyo Toyo Sanso, 99.9999%) was flowed over the sample and the mixed gas was obtained. The mixed gas passed through the nozzle was deposited onto the CsI plate. The flow rate of the argon gas is adjusted with the needle valve (Swagelok, SS-SS2-VH).

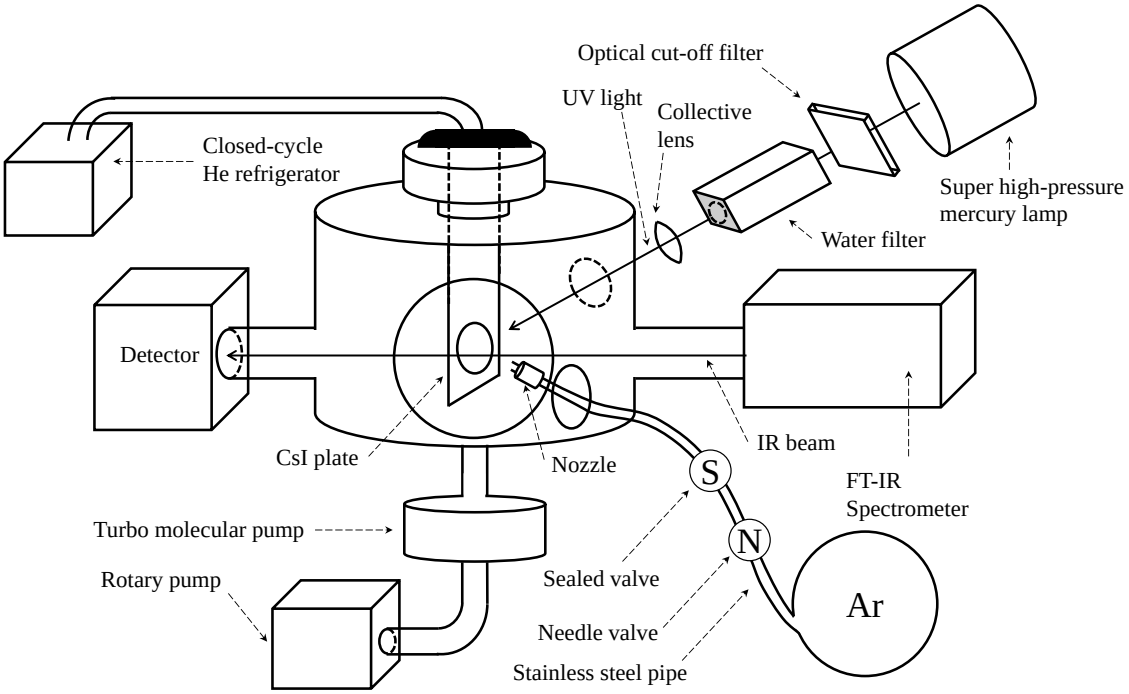

Fig. 2.1. Diagram of matrix-isolation apparatus with FT-IR spectrophotometer.

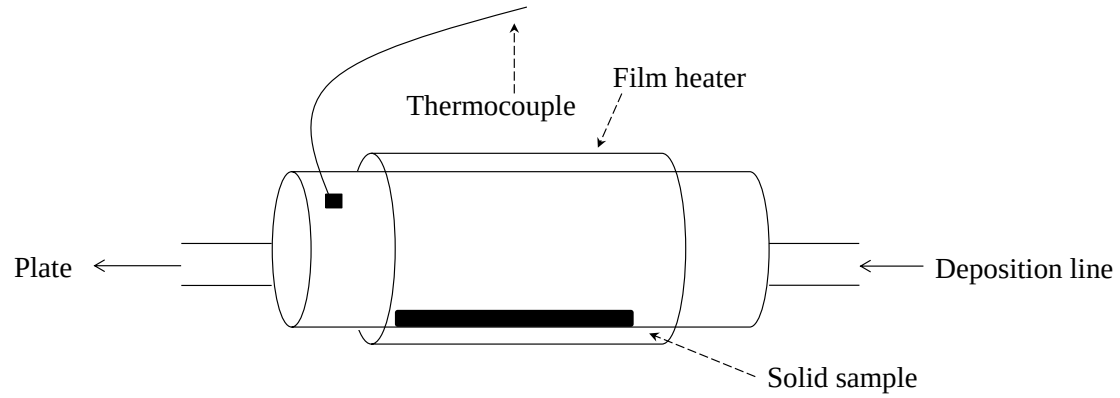

(a)

(b)

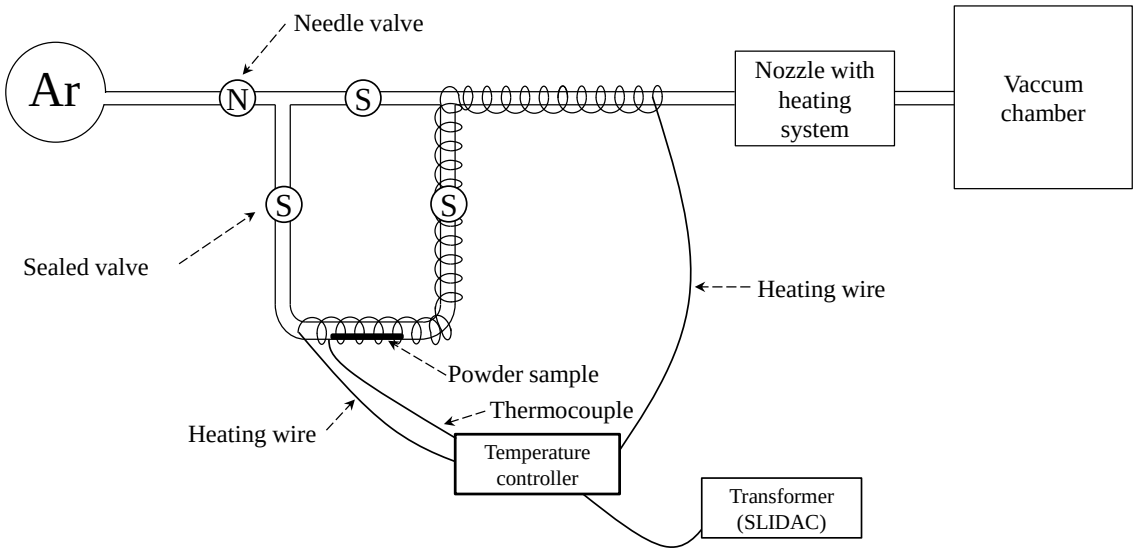

Fig. 2.2. Apparatus for heating system: (a) the nozzle and (b) U-shaped glass tube.

IR spectra were measured with an FTIR spectrometer (JEOL, JIR-WINSPEC50). The IR beam of the spectrometer was introduced into the matrix sample through a KBr window and detected with a liquid-nitrogen cooled MCT placed on the opposite side of the vacuum chamber. The spectral resolution was 0.5 cm^{-1}, and the number of accumulation was 64. Radiation coming from a super high-pressure mercury lamp (Ushio, BA-H500) was used to induce photoreaction. A water filter was placed between the lamp and the quartz window of the vacuum chamber to remove thermal reaction. Irradiation wavelength was selected by a short-wavelength cutoff optical filter.

The vacuum chamber combined with an UV-vis spectrometer (JASCO, V-550) was shown schematically in Fig. 2.3(a), (b) and (c). Vacuum pressure in the vacuum chamber was kept under 10^{-4} Pa by an oil-diffusion pump (DIAVAC, DPF-4Z) and a rotary pump (EDWARDS, E2W8). The quartz plate in the center of the vacuum chamber was cooled by closed-cycle helium refrigerator (Iwatani, CA101) at 20 K for deposition and at 10 K for measurement. The spectral resolution was 0.5 nm and the scanning speed was 100 nm/ min. When the electronic absorption spectra were measured, the movable matrix chamber was placed in the measurement room in the spectrometer. Because the vacuum chamber is too big, the measurement room can not be kept dark. Thus, all the measurements were performed in a dark room. When the matrix was irradiated by UV light, the chamber was placed out of the spectrometer.

Salicylic acid (Wako, purity > 99.5%), 3-chlorosalicylic acid (Sigma-Aldrich, purity > 98%) and picolinic acid (Wako, purity > 98%) were used after vacuum distillation to remove impurities. All the three samples were while solid, and the vapor pressures of them were insufficient to premix with pure argon. Thus a small amount of 3-chlorosalicylic acid was placed in the nozzle, and that of salicylic acid and picolinic acid was placed in the U-shaped glass tube. To obtain sufficient vapor pressure, salicylic acid and 3-chlorosalicylic acid was heated at 303 and 308 K, respectively. Since the vapor pressure of picolinic acid was sufficient under the vacuum pressure, picolinic acid was not heated, and kept at room temperature.

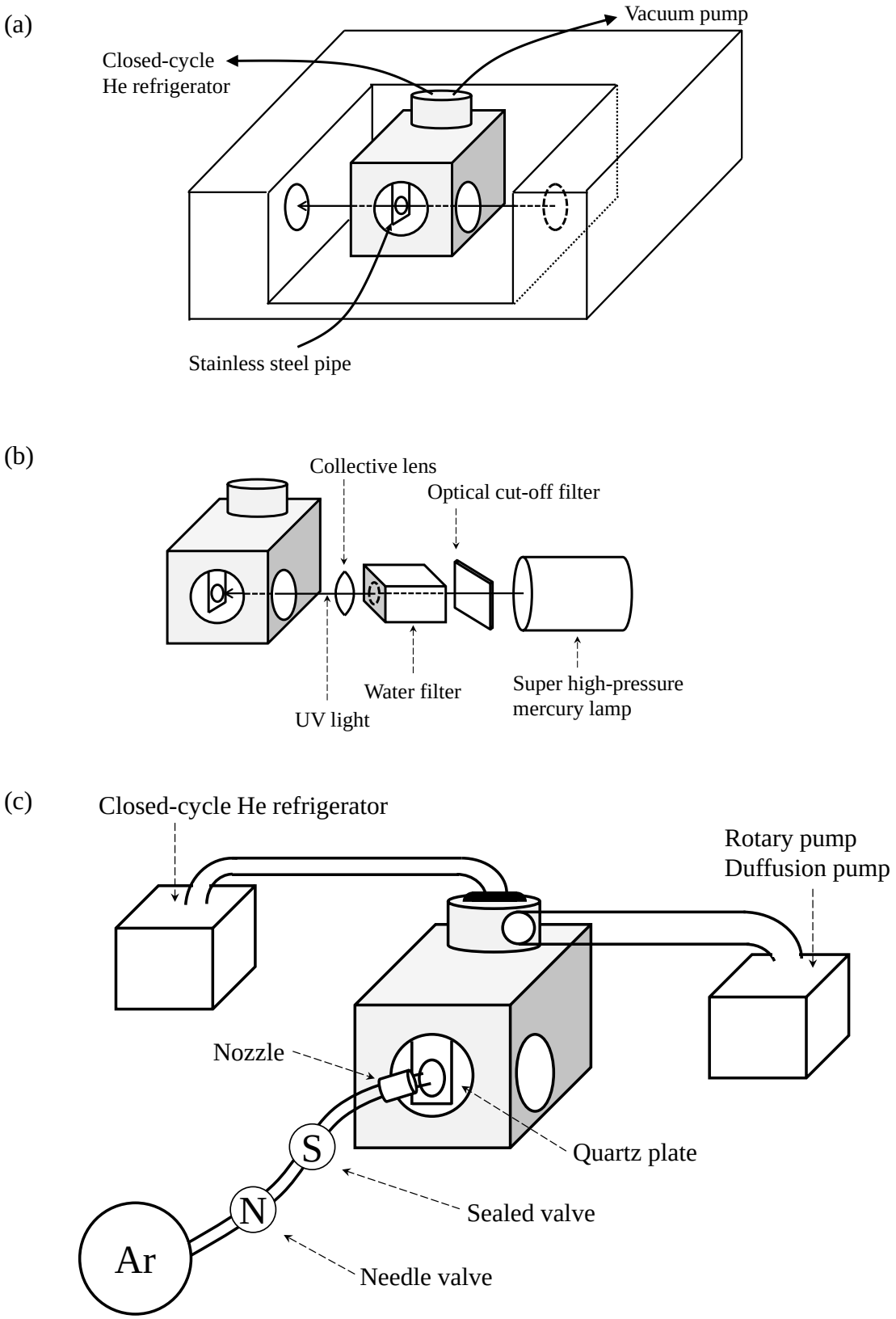

Fig. 2.3. Diagram of matrix-isolation apparatus with UV-vis spectrophotometer.

2.4. Calculation method

The GAUSSIAN 09W program was used to perform quantum chemical calculations of Density-Functional-Theory (DFT), Time-Dependent DFT (TD-DFT). The 6-31++G** basis sets were used. The Becke's three-parameter hybrid density functional in combination with Lee-Yang-Parr correlation functional (B3LYP), was used to optimize the geometrical structures. Single-point energy, optimized geometry and vibrational analysis were calculated by the DFT method, while electronic vertical transient energies were calculated by the TD-DFT method. CIS method was used to optimize the geometrical structures in the first electronic excited state. QST2 method was used to calculate the energy barrier between two structures. IRC calculation was performed to draw the potential energy curve between two structures.

2.5. References

[1] I. Norman, G. Porter, Nature 174 (1954) 508.

[2] E.D. Becker, G.C. Pimentel, J. Chem. Phys. 25 (1956) 224.

[3] Gaussian 09, Revision D.01, M. J. Frisch, G. W. Trucks, H. B. Schlegel, G. E. Scuseria, M. A. Robb, J. R. Cheeseman, G. Scalmani, V. Barone, B. Mennucci, G. A. Petersson, H. Nakatsuji, M. Caricato, X. Li, H. P. Hratchian, A. F. Izmaylov, J. Bloino, G. Zheng, J. L. Sonnenberg, M. Hada, M. Ehara, K. Toyota, R. Fukuda, J. Hasegawa, M. Ishida, T. Nakajima, Y. Honda, O. Kitao, H. Nakai, T. Vreven, J. A. Montgomery, Jr., J. E. Peralta, F. Ogliaro, M. Bearpark, J. J. Heyd, E. Brothers, K. N. Kudin, V. N. Staroverov, R. Kobayashi, J. Normand, K. Raghavachari, A. Rendell, J. C. Burant, S. S. Iyengar, J. Tomasi, M. Cossi, N. Rega, J. M. Millam, M. Klene, J. E. Knox, J. B. Cross, V. Bakken, C. Adamo, J. Jaramillo, R. Gomperts, R. E. Stratmann, O. Yazyev, A. J. Austin, R. Cammi, C. Pomelli, J. W. Ochterski, R. L. Martin, K. Morokuma, V. G. Zakrzewski, G. A. Voth, P. Salvador, J. J. Dannenberg, S. Dapprich, A. D. Daniels, Ö. Farkas, J. B. Foresman, J. V. Ortiz, J. Cioslowski, and D. J. Fox, Gaussian, Inc., Wallingford CT, 2009.

[4] P. Hohenberg, W. Kohn, Phys. Rev, B 136 (1964) 864.

[5] W. Kohn, L.S. Sham, Phys. Rev. A 140 (1965) 1133.

[6] A.D. Becke, J. Phys. Chem. 98 (1993) 5648.

[7] C. Lee, W. Yang, R.G. Parr, Phys. Rev. B 37 (1988) 785.

Chapter 3: Photoreaction of Salicylic Acid

Abstract

Photoreaction pathways of salicylic acid have been investigated by the low-temperature matrix-isolation infrared spectroscopy with an aid of the density-functional-theory calculations. Only the most stable E form existed in an argon matrix. The second stable R form and the fourth stable H form were produced by UV irradiation (λ > 290 nm). Ketoketene–water complex was yielded from R form by dissociation of the H and OH parts interacting through intramolecular hydrogen bonding upon prolonged UV irradiation.

3.1. Introduction

Salicylic acid (SA, hereafter) is one of the benzoic acid derivatives, having a hydroxy group at the *ortho* position. Since the carboxy and the hydroxy groups act as the hydrogen acceptor and the donor respectively, SA has an intramolecular hydrogen bond (IMHB, hereafter) of C=O···HO−Ph, and the effect of the IMHB on its photoreaction has been investigated. In 1955, Weller reported dual emission of SA in solution upon UV irradiation, and suggested tautomerization, where the H atom in the hydroxy group migrates to the C=O part in E form and keto form is produced, as shown in Scheme 3.1. [1−3]. Weller assumed that both E form and keto form have their potential minima both in the electronic ground and the excited states, S_0 and S_1, respectively. Since the longer-wavelength emission at 440 nm is Stokes shifted by more than 10,000 cm^{-1} in contrast to the other emission at 335 nm, this dual emission attracted much attention.

Thereafter, further studies on the photoreaction mechanisms of SA have been done in solution. However, since no spectral evidence of keto form was found, it was assumed that keto form has no potential minimum on the potential energy curve (PEC, hereafter) in the S_0 state. In other words, it was suggested that there is only one minimum at E form on the PEC in the S_0 state, and the keto form goes back to E form with no barrier, indicating the entire reaction mechanisms are cyclic, as shown in Scheme 3.2.

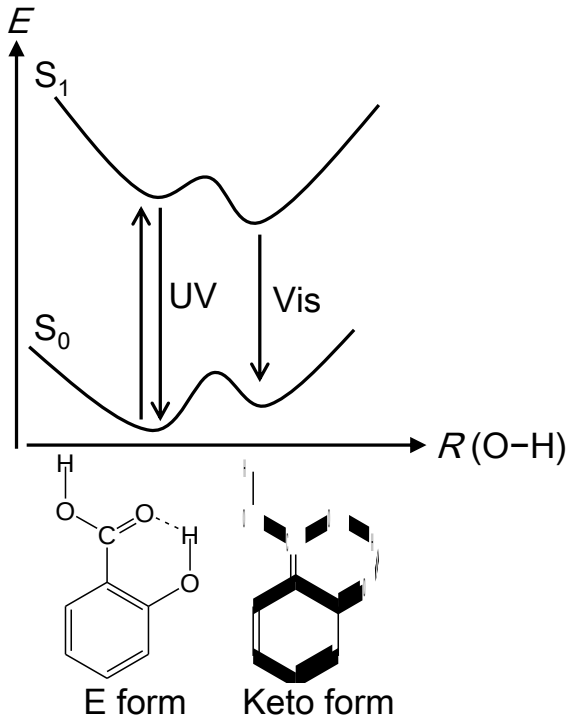

Scheme 3.1. Potential energy curve of salicylic acid proposed by Weller.

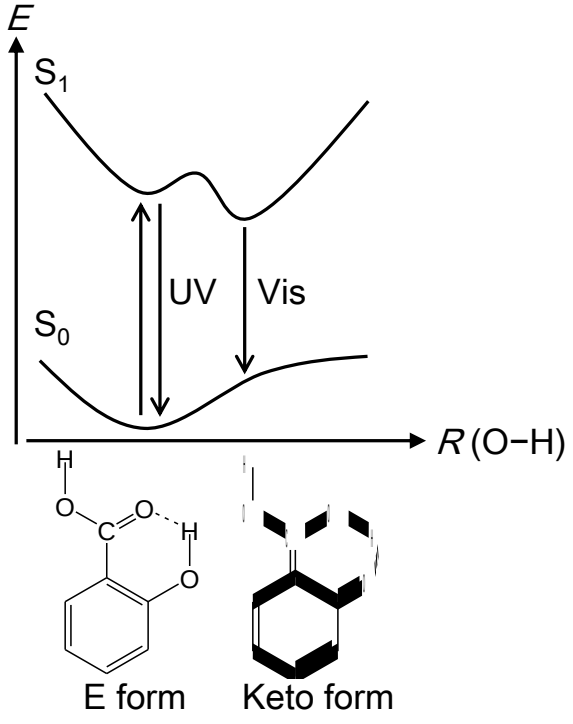

Scheme 3.2. Revised potential energy curve of salicylic acid.

To suppress intermolecular interactions with solvent molecules, Bisht et al. investigated origins of the dual emission in supersonic-jet expansion, and found the presence of another conformer named R form (Scheme 3.3) [4]. They suggested that the UV- and visible-light emissions originate from R form and keto form respectively, but the extent of the hydrogen-atom transfer is rather small. This proposition was supported by theoretical studies to draw the PECs of E form both in the S_0 and S_1 states [5,6]. Sobolewski et al. reported the PECs of E form shown in Scheme 3.3, where there is a local minimum neither at E form nor keto form but between them on the PEC in the S_1 state calculated at CASPT2 level, while only E form has a minimum on the PEC in the S_0 state. Thus, they concluded that the optimized structure, where the O−H bond in the hydroxy group is elongated in the S_1 state, is the origin of the visible-light emission, and keto form is not produced from E form. The photoreaction mechanisms shown in Scheme 3.3 were further supported experimentally. Yahagi et al. measured the O−H stretching bands both in the S_0 and S_1 states in supersonic-jet expansion with IR-UV and UV-IR double resonance spectroscopy respectively [7], and reported the two O−H stretching bands both of E form and R form in the S_0 state. In contrast, in the S_1 state, while the two bands of R form are observed, only one band of the carboxy group is observed in E form, but not that of the hydroxy group. This result indicates that the O−H bond in the hydroxy group is elongated in the

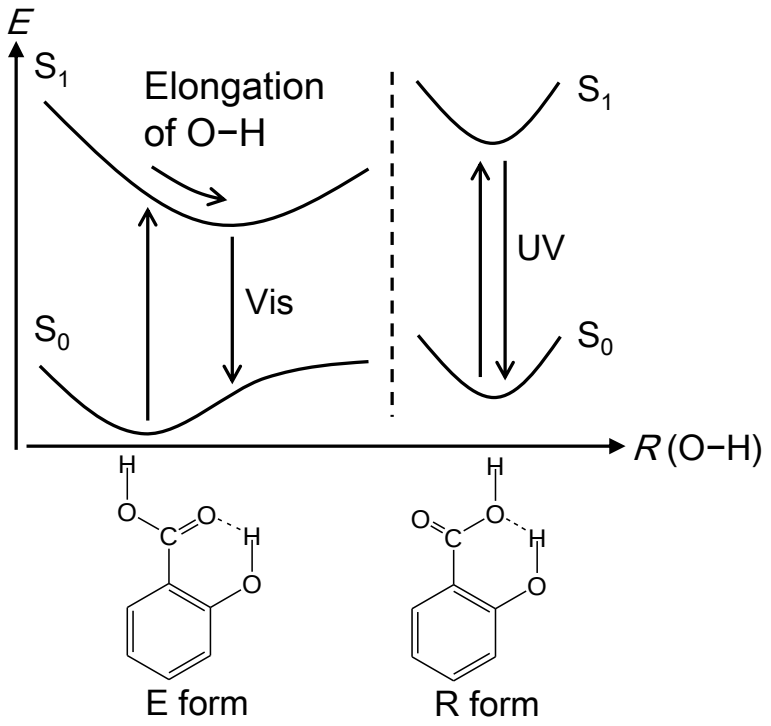

Scheme 3.3. Dual-emission mechanisms of salicylic acid proposed by Sobolewski et al.

S_1 state due to the IMHB of C=O···HO−Ph. According to their calculation, the elongated O−H stretching band is estimated to appear at 1902 cm^{-1}, which is below their measurement limit, 2400 cm^{-1}. Therefore, both experimental and theoretical results support the photoreaction mechanisms shown in Scheme 3.3.

The above discussions on the dual emission of SA appeal the importance of the C=O part as the hydrogen acceptor as well as the importance of understanding PECs both in the S_0 and S_1 states. However, the effect of the IMHB of C−O···HO−Ph in R form on its photoreaction has not been investigated at all. Since SA can be regarded as one of the hydrogen-bonding phenol derivatives, dissociation of the hydrogen-bonding parts may occur. Such a reaction has been reported in 2-chlorophenol and its derivatives, where a hydrogen halide dissociates to produce a ketene compound via a ketocarbene by the Wolff rearrangement [8−12]. Moreover, the author assumed that the *trans* conformer, H form (Fig. 3.1) may be produced by UV irradiation and may exist stably in an argon matrix due to the stabilization by the IMHB between COOH···OH−Ph. In this case, the carboxy group is the hydrogen donor. In spite of various studies on stabilization of the *trans* conformer by IMHB, there are few reports, where the *trans* conformer can exist stably, which is described in Chapter 1. Therefore it is important to investigate not only a further photoreaction starting from R form but also the light-induced conformational changes of SA. However, such a theoretical or experimental study has not been reported despite of the fact that the difference between E form and R form is only an internal rotation around the Ph−COOH bond. One of the reasons is that the less stable conformer, R form can not be observed in solution at room temperature with IR spectroscopy [13] probably due to destabilization by the interaction with solvent molecules or due to the back reaction. Another reason is that observation of a photoproduct is difficult in supersonic-jet expansion. Thus investigation of photoreaction mechanisms of SA with the low-temperature matrix-isolation IR spectroscopy may reveal the functions of the IMHB formed in the carboxy group, which is similarly pointed out

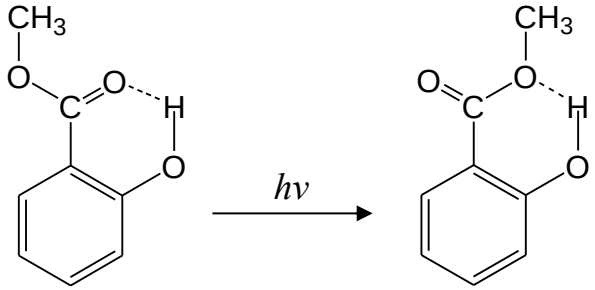

Scheme 3.4. Photoisomerization of methylsalicylate.

in methyl salicylate reported by Orton et al. shown in Scheme 3.4 [14].

In the present study, the author has determined the conformational changes of SA induced by UV irradiation, and also found the production of a ketene compound, leading to the whole UV-induced reaction pathways of SA. The experimental method is the low-temperature matrix-isolation IR spectroscopy, whereas the theoretical one is the density-functional-theory (DFT) method. This combined method, which makes it possible to compare observed IR spectra with calculated ones in the whole region, is known to be one of the most effective ways to distinguish slight differences due to conformational changes among reactants, intermediates and products, as shown in recent papers and references cited therein [8−12,15,16].

3.2. Results and discussion

3.2.1. Calculation results of SA monomer

Since SA has three rotational axes, one C−C and two C−O bonds, eight conformers can be considered. Seven among possible eight conformers of SA were optimized by the DFT calculations. The calculated relative energies of them are given in Fig. 3.1 after the correction of zero-point vibrational energy. The optimization for the far right conformer on the upper row was performed, but not successful probably because of repulsion of the two H atoms. The four conformers stabilized by IMHBs are abbreviated as E, R, O and H forms. It is possible to explain the order of the relative energies as follows: the *trans* conformers around the OC−OH bond on the right side are less stable than the *cis* on the left side because of repulsion between the lone pairs of the two O atoms in the carboxy group except for H form. Similar explanation is reported in detail in previous papers on 2-chlorobenzoic acid [15] and 2-chloropropionic acid [17]. The three conformers in the lower row except H form are destabilized by repulsion between the lone pairs of the two O atoms in the carboxy and hydroxy groups. Among the four conformers on the left side, the two conformers on the upper row, E form and R form, are more stabilized by the IMHB between the carboxy and hydroxy groups as shown in Fig. 3.1, where IMHBs are denoted by broken lines. Since the IMHB of E form originates, in-plane, from an sp^2 hybrid orbital, it is stronger than that of R form originating, out-of-plane, from an sp^3 hybrid orbital. As a result, E form is more stable than R form. This is supported by comparison with the bond lengths of the optimized

geometrical parameters listed in Table 3.1.

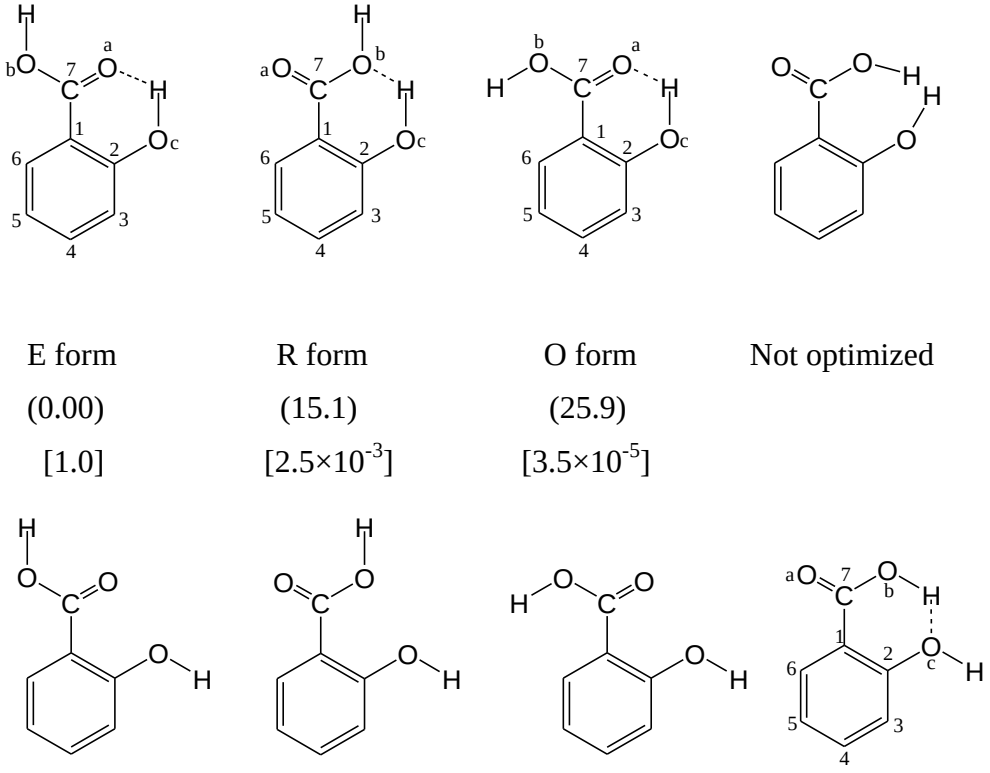

E form (0.00) [1.0]

R form (15.1) [2.5×10^{-3}]

O form (25.9) [3.5×10^{-5}]

Not optimized

(45.7)

(43.6)

(70.7)

H form (39.6) [1.5×10^{-7}]

Fig. 3.1. Eight possible conformers and numbering atoms of SA monomer. The numbers in parentheses represent relative energies in kJ mol^{-1} obtained at the DFT/B3LYP/6-31++G** level. The numbers in square brackets represent population ratios according to the Boltzmann distribution law at the deposition temperature of 303 K.

Table 3.1. Optimized geometry of E, R, O and H forms. [a,b]

Parameters [c]	E	R	O	H
$r(C_7{=}O_a)$	1.2340	1.2142	1.2275	1.2127
$r(C_7{-}O_b)$	1.3502	1.3783	1.3508	1.3494
$r(O_b{-}H)$	0.9719	0.9720	0.9669	0.9744
$r(C_1{-}C_7)$	1.4642	1.4759	1.4786	1.5085
$r(C_2{-}O_c)$	1.3450	1.3535	1.3408	1.3798
$r(O_c{-}H)$	0.9858	0.9729	0.9902	0.9661
$r(C_1{-}C_2)$	1.4203	1.4182	1.4231	1.4077
$r(C_2{-}C_3)$	1.4048	1.4047	1.4067	1.3969
$r(C_3{-}C_4)$	1.3882	1.3881	1.3862	1.3939
$r(C_4{-}C_5)$	1.4060	1.4043	1.4054	1.3981
$r(C_5{-}C_6)$	1.3862	1.3855	1.3863	1.3916
$r(C_6{-}C_1)$	1.4108	1.4114	1.4112	1.4047
$r(O\cdots H)$	1.7478	1.8095	1.6933	1.7903
$\Theta O_aC_7O_b$	120.55	120.11	117.58	119.20
ΘC_7O_bH	106.85	107.19	111.81	111.20
$\Theta O_aC_7C_1$	124.41	126.19	122.81	121.68
ΘHO_cC_2	107.95	109.88	107.46	111.24
$\Theta O_cC_2C_1$	122.86	124.73	122.84	118.36
$\Theta C_2C_1C_7$	118.83	124.71	118.12	125.64

[a] Calculated at the DFT/B3LYP/6-31++G** level.

[b] Units of r and Θ are Å and deg, respectively.

[c] Numbering of atoms is given in Fig. 3.1.

Since the bond lengths of C=O, $r(C_7{=}O_a)$ in E form and O form were 1.2340 and 1.2275 Å respectively, which are longer than that in H form (1.2127 Å), it was found that there is an IMHB with the H atom in the hydroxy group in E form and O form. In the same way, the value of $r(O_c{-}H_\beta)$ were 0.9858 and 0.9902 Å in E form and O form respectively, which are larger than that in H form (0.9661 Å). The value of $r(O_c{-}H_\beta)$ in R form was 0.9729 Å, which is larger than that of H form but smaller than those in E form and O form. This indicates the IMHB in R form are not as strong as those in E form or O form, which can be confirmed by comparing the value of $r(O_a{\cdots}H_\beta)$ in E, O and R forms. The value of $r(O_a{\cdots}H_\beta)$, is smaller than the corresponding length in R form by 0.062 Å, whereas $r(O_c{-}H)$ in E form is longer than that in R form by 0.013 Å. Similar results and discussion are given by the calculation at the DFT/B3LYP/6-31G** level [7]. Note that the geometry of keto form was not optimized in our calculations, meaning that it is not located at the minimum of the PEC in the S_0 state.

The energy difference between E form and R form (15.1 kJ mol^{-1}) is a little lower than the value obtained at DFT/B3LYP/6-31G** level (16.36 kJ mol^{-1}) in the previous study [7]. This is due to the difference of the basis sets. Electron distributions are widely spread both in E form and R form due to the IMHB. Thus, the author used 6-31++G** as the basis set, which contains diffuse functions both at H atom and O atom.

H form has an IMHB between the H atom and the O atom in the carboxy and hydroxy groups, respectively. This was confirmed by the facts that the value of $r(O_b{-}H_\alpha)$ in H form (0.9744 Å) is larger than those in E, R and O forms (0.9719, 0.9720 and 0.9669 Å, respectively), and that the value of $r(C_2{-}O_c)$ in H form (1.3798 Å) is larger than those in E, R and O forms (1.3450, 1.3535 and 1.3408 Å, respectively).

IMHB has an effect on the calculated wavenumbers obtained by the DFT calculations. For example, $\nu C_7{=}O_a$ of E form and O form appeared at 1683 and 1704 cm^{-1}, which are lower than those of R form and H form (1744 and 1755 cm^{-1}, respectively). This result indicates that the low electron density at the C=O part due to IMHB, and that the IMHB between Ph−OH···O=C is stronger than that between Ph−OH···OH. As well as the C=O stretching mode, $\nu O_c{-}H_\beta$ of E form and O form (3284 and 3204 cm^{-1}) appeared lower than that of R form (3512 cm^{-1}). This fact originates from the low electron density at $O_c{-}H_\beta$ due to the strong IMHB with the C=O part in the carboxy group. In E, R and O forms, while the $O_c{-}H_\beta$ bond is hydrogen

bonded with the C=O or C−O part, the O_b-H_α bond was not hydrogen bonded. Thus, νO_b-H_α appeared higher than νO_c-H_β by the DFT calculations.

The estimated population ratios of a conformer over E form at deposition temperature (303 K) according to the Boltzmann distribution law are shown in Fig. 3.1. The obtained value of the second most stable conformer, R form was only 2.5×10^{-3}. Thus, the author can expect only E form will exist in an argon matrix after deposition.

3.2.2. Calculation results of SA dimer

It is known that SA is present as a dimer with intermolecular hydrogen bonds between the two carboxy groups in solution or in solid phase. To confirm only monomeric SA is present in an argon matrix, the comparison of the matrix IR spectrum with the one obtained by the conventional KBr disk method is required. For the assignment of the latter, the author also optimized the SA dimer by the DFT calculations as well as the monomer.

Two optimized geometrical structures of SA dimer have been reported: EE form and RR form composed of two E form and R form, respectively. In addition to these two dimers, the author also optimized ER form composed of one E form and one R form. The optimized structures and the calculated relative energies of EE, ER and RR forms are shown in Fig. 3.2.

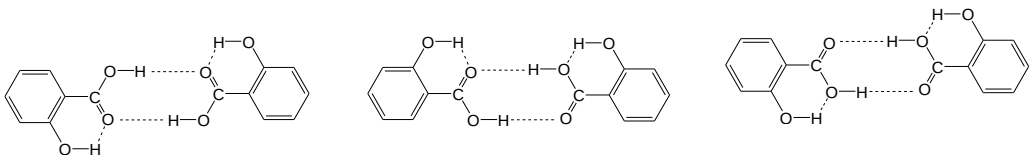

EE form (0.00) ER form (8.86) RR form (16.25)

Fig. 3.2. Three possible conformers of SA dimer. The numbers in parentheses represent relative energies in kJ mol^{-1} obtained at the DFT/B3LYP/6-31++G** level.

Each dimer has a pair of carboxy and a pair of hydroxy groups, and both of them

have symmetric and anti-symmetric stretching modes, respectively. Thus there are four O−H stretching modes. Among them, the symmetric modes of EE form and RR form are IR inactive because it does not change the dipole moment. As expected, the calculated intensities of them obtained by the DFT calculations are 10^{-4} times as weak as those of the anti-symmetric mode. Thus, only the anti-symmetric stretching mode was strong in EE form and RR form. In contrast, in ER form, the intensity of the O−H symmetric stretching mode was 1/60 times as weak as that of the anti-symmetric one, but was still as strong as that of the C=O stretching mode of R form composing ER form. The reason why only ER form shows the strong symmetric stretching mode in the carboxy group is dimerization of different monomers, E form and R form, resulting in the asymmetric structure. The wavenumber of the C=O stretching mode of EE form was calculated to be 28 cm^{-1} lowered than that of RR form, because only EE form has the IMHB of the C=O part with the hydroxy group. The presence of IMHB also has an effect on the relative energy differences: EE form is the most stable, and RR form is the least, which is consistent with the previous study calculated at DFT/B3LYP/6-31G** level [7].

3.2.3. IR spectrum of SA with KBr disk method

An IR spectrum with KBr disk method is shown in Fig. 3.3(a). Several broad bands appeared in the region of the O−H stretching modes. The wavenumbers and intensities of bands in the fingerprint region were also different from those measured in an argon matrix, which will be described in the following section. The observed IR spectrum was reproduced by the calculated spectral pattern of EE form (Fig. 3.3(b)), but not the other dimers or monomers. It was also found that ER form does not exist because only one band appears in the C=O stretching region. Therefore the author concluded that only EE form are present in the solid phase. The intensities of some observed bands were not reproduced well by the calculated bands. This is because the intermolecular interaction is not considered by the DFT calculations, while it can not be ignored in the solid phase. This conclusion is consistent with the results measured with low-temperature NMR spectroscopy reported previously [18].

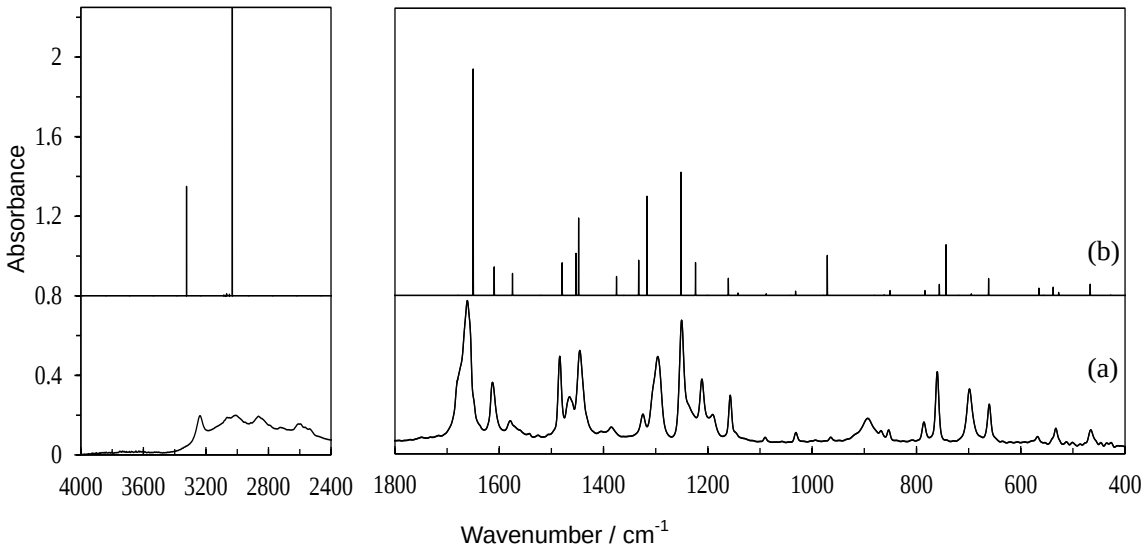

Fig. 3.3. IR spectra of SA measured by KBr disk method. (a) Observed spectrum; (b) calculated spectral pattern of EE form obtained at DFT/B3LYP/6-31++G** level, where a linear scaling formula of $0.9894–1.04\times10^{5}\ \nu_{calcd}$ was used.

3.2.4. IR spectrum of SA in a low-temperature argon matrix

An IR spectrum of SA in an argon matrix measured after deposition is shown in Fig. 3.4(a). In the C=O stretching region, a sharp band appeared at 1706 cm^{-1}, while one sharp and one broad bands appeared in the O−H stretching region. The broad O−H stretching band indicates its vibrational mode is related to the IMHB. The author assumed only the most stable conformer, E form exists in an argon matrix after deposition because only one and two bands appeared in the C=O and O−H stretching regions, respectively.

By comparison with the calculated spectral patterns of all the seven conformers, most of the observed bands were assigned to E form. The observed and calculated wavenumbers and the relative intensities of E form are summarized in Table 3.2. Some of the observed bands were found to be split by the Fermi resonance and/or matrix effects, and some calculated bands are slightly far from the corresponding observed ones as well as other multi-substituted derivatives of benzene and pyridine [8,9,12,16,19]. The band at 3562 cm^{-1} corresponds to the calculated value of the free

$\nu O_b{-}H_\alpha$, 3577 cm^{-1}. The band in the range between 3100 and 3300 cm^{-1} corresponds to the $\nu O_c{-}H_\beta$, which is broadened and weakened by the IMHB of Ph−OH···O=C in the carboxy group. The band at 1706 cm^{-1} corresponds to the calculated value of the C=O stretching mode, 1683 cm^{-1}, which shows a lower-frequency shift due to the IMHB by ~50 cm^{-1} from non-hydrogen-bonding C=O stretching modes such as benzoic acid [20,21]. The weak band at 1720 cm^{-1} may be a combination mode of the bands at 645 and 1075 cm^{-1}.

Yahagi et al. observed the O−H stretching mode of E form in supersonic-jet expansion with IR-UV double resonance spectroscopy [7]. Comparing the author's result with theirs, both $\nu O_b{-}H_\alpha$ and $\nu O_c{-}H_\beta$ in the present study appeared lower by 30 cm^{-1} than their study. These lower-wavenumber shifts are explained by the difference of the carrier gas: while helium was used in Ref. [7], argon was used in the present study, which can interact with SA. In another previous study [13], bands assigned to both E form and a dimer were observed in CCl_4 solution, where $\nu O_b{-}H_\alpha$, $\nu O_c{-}H_\beta$ and νC=O of E form appeared at 3540, 3200 and 1697 cm^{-1} respectively, which are lower than the ones in the present study probably due to intermolecular interaction. Since no IR band was observed around 1660 cm^{-1} assigned to EE form, it was found that gaseous sample of SA was well diluted by argon gas, and SA are isolated as a monomer in an argon matrix. Expecting to obtain an IR band of EE form, the author tried to heat the sample at more than 303 K and mixed with less argon gas to increase the mixing ratio of SA over argon. However, when the sample is heated at higher than 305 K, a sharp band appeared at 2135 cm^{-1} assignable to carbon monoxide, indicating SA is thermally decomposed.

Note that R form has been reported as a minor species besides the major E form in SA and some derivatives. For example, Yahagi et al. investigated the conformation of SA in supersonic-jet expansion by IR-UV double resonance spectroscopy [7] and detected the O−H stretching bands at 3585 and 3530 cm^{-1}. The author tried to find the bands of R form in our observed spectrum, but it was unsuccessful. In addition, no free C=O stretching band of R form was observed around 1760 cm^{-1}, leading to the conclusion that R form is undetectable in a low-temperature argon matrix. The author's result seems to be reasonable because the population ratio of R form over the most stable E form is estimated to be 2.5×10^{-3} according to the Boltzmann distribution law at 303 K, using the relative energies shown in Fig. 3.1, whereas the sample temperature

in their experiment was 360 K and the population ratio is estimated to be 6.5×10^{-3}. One possibility to explain the inconsistency between the author's result and that of Ref. [7] is that the sensitivity of double resonance spectroscopic technique is so high that they could observe the O−H stretching bands of R form, but not ones of other modes.

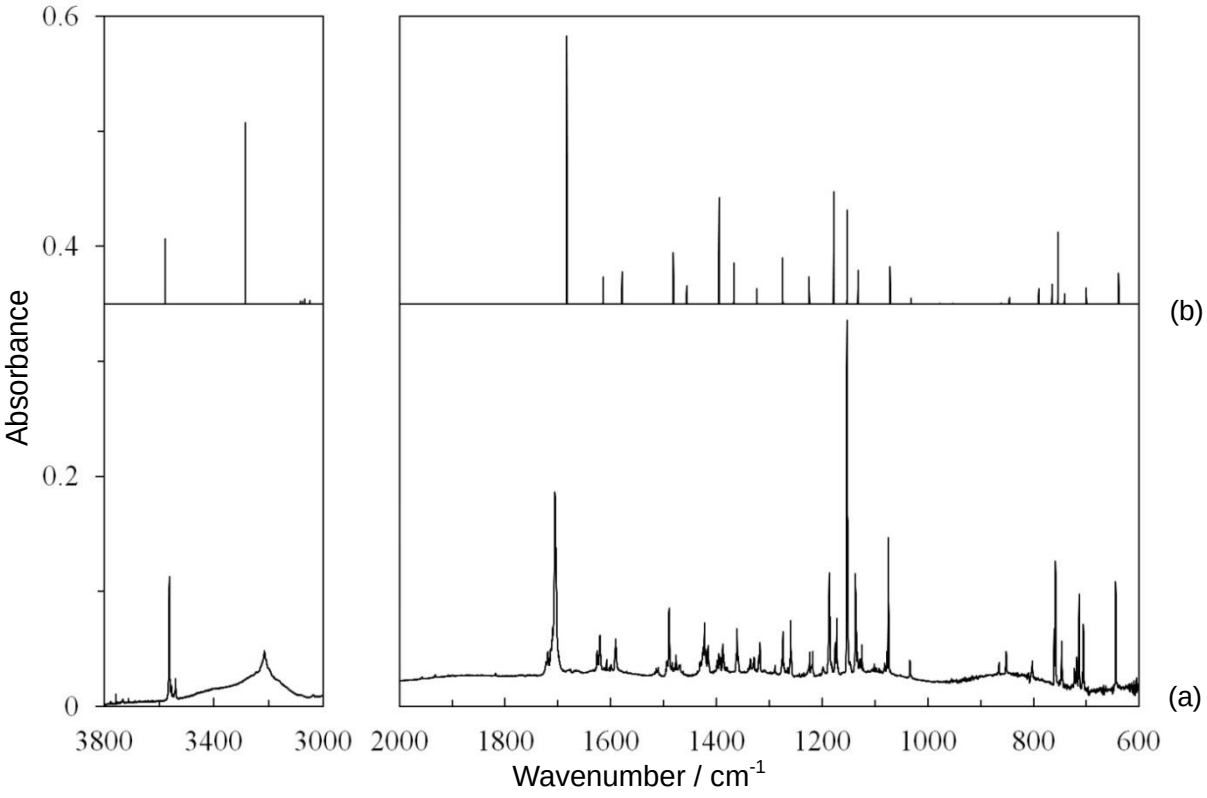

Fig. 3.4. IR spectra of SA in an argon matrix after deposition. (a) The observed spectrum after deposition; (b) the spectral pattern of E form calculated at the DFT/B3LYP/6-31++G** level, where a linear scaling formula of $0.9894–1.04\times10^{5}\ \nu_{calcd}$ was used.

Table 3.2. Observed and calculated wavenumbers and relative intensities of E form. [a]

Obsd.		Calcd. [b]	
ν / cm^{-1}	Int. [c]	ν / cm^{-1}	Int. [d]
3562,3554, 3539	s	3577	24.5
3215	m	3284	68.0
1706	s	1683	100
1626, 1620	w	1614	10.0
1591	w	1579	12.0
1490, 1984	m	1482	19.1
1477, 1468	w	1456	6.6
1423, 1417, 1415, 1399, 1395, 1388	m	1395	39.8
1361	m	1367	15.1
1335, 1328, 1317	w	1323	5.8
1274, 1260	m	1275	17.4
1224, 1218	w	1225	10.5
1187, 1175, 1172	m	1178	41.4
1153	vs	1153	35.4
1137, 1125	m	1132	12.5
1077, 1075	m	1071	14.2
802	w	790	5.0
761	m	765	7.2
758	m	753	30.2
722, 719, 713, 706	m	700	5.7
645	m	639	11.5

[a] Vibrational modes with intensities of less than 5.0 are omitted.

[b] Calculated at the DFT/B3LYP/6-31++G** level. A linear scaling formula of $0.9894-1.04 \times 10^{-5}\ \nu_{calcd}$ is used.

[c] Letters of vs, s, m, and w, denote very strong, strong, medium, and weak intensities, respectively.

[d] Relative intensities.

3.2.5. UV-vis spectrum of SA in a low-temperature argon matrix

To determine irradiation wavelength to the matrix sample, an UV-vis absorption spectrum of SA in an argon matrix after deposition was measured to determine the irradiation wavelength to E form. The obtained spectrum is shown in Fig. 3.5. A band peaking at 309 nm due to the ππ* transition was observed. Thus the author chose the wavelength of λ > 290 nm to induce photoreaction efficiently.

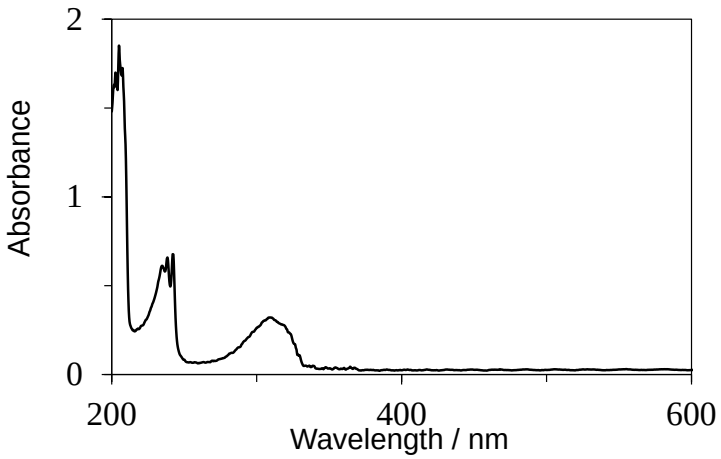

Fig. 3.5. UV-vis spectrum of SA in an argon matrix.

3.2.6. Conformational changes upon UV irradiation

When the matrix sample was exposed to UV light (λ > 290 nm), IR spectral changes were observed. The difference spectra between the spectra measured after minus before the UV irradiation are shown in Fig. 3.6, where the decreasing and increasing bands represent the reactant, E form, and photoproducts, respectively. The bands at 3560 cm^{-1}, which is disturbed with the decreasing band of E form, and at 3505 cm^{-1} appeared only at the early stage of the irradiation in Fig. 3.6(b). They disappeared at 120-min irradiation in Fig. 3.6(c), whereas the bands at 3633 and 3455 cm^{-1} continued increasing upon the prolonged UV irradiation. These findings imply that two kinds of species were produced by the UV irradiation. To distinguish the photoproducts, the author compared the observed spectra with the calculated spectral patterns of four relatively stable

conformers. As a result, it was found that the increasing bands were assignable to R form and H form. Pure observed IR spectra of R form and H form were extracted from the spectra measured at different irradiation times by canceling the bands of E form computationally, and were compared with the calculated spectral patterns of R form and H form in Fig. 3.7(a) and (b), respectively.

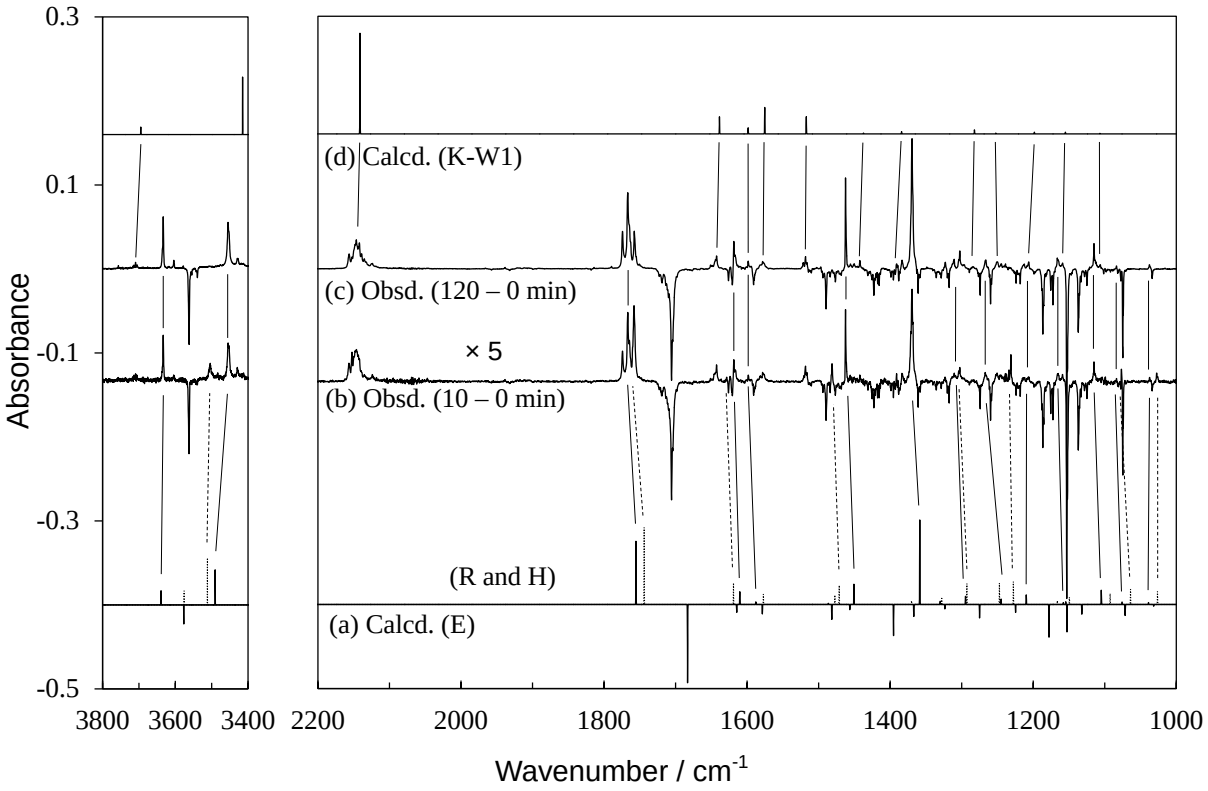

Fig. 3.6. IR spectral changes of SA by UV irradiation (λ > 290 nm): (a) Calculated spectral patterns of E form (lower side), R form (upper side, dotted line) and H form (upper side, solid line); (b) and (c) observed difference spectra between the spectra measured after minus before the UV irradiation for 10 and 120 min, respectively; (d) calculated spectral pattern of K−W1. The absorbance of the observed spectrum (b) is multiplied by 5. Spectral patterns were calculated at the DFT/6-31++G** level, where a linear scaling formula of $0.9894-1.04 \times 10^{-5}\, \nu_{calcd}$ was used.

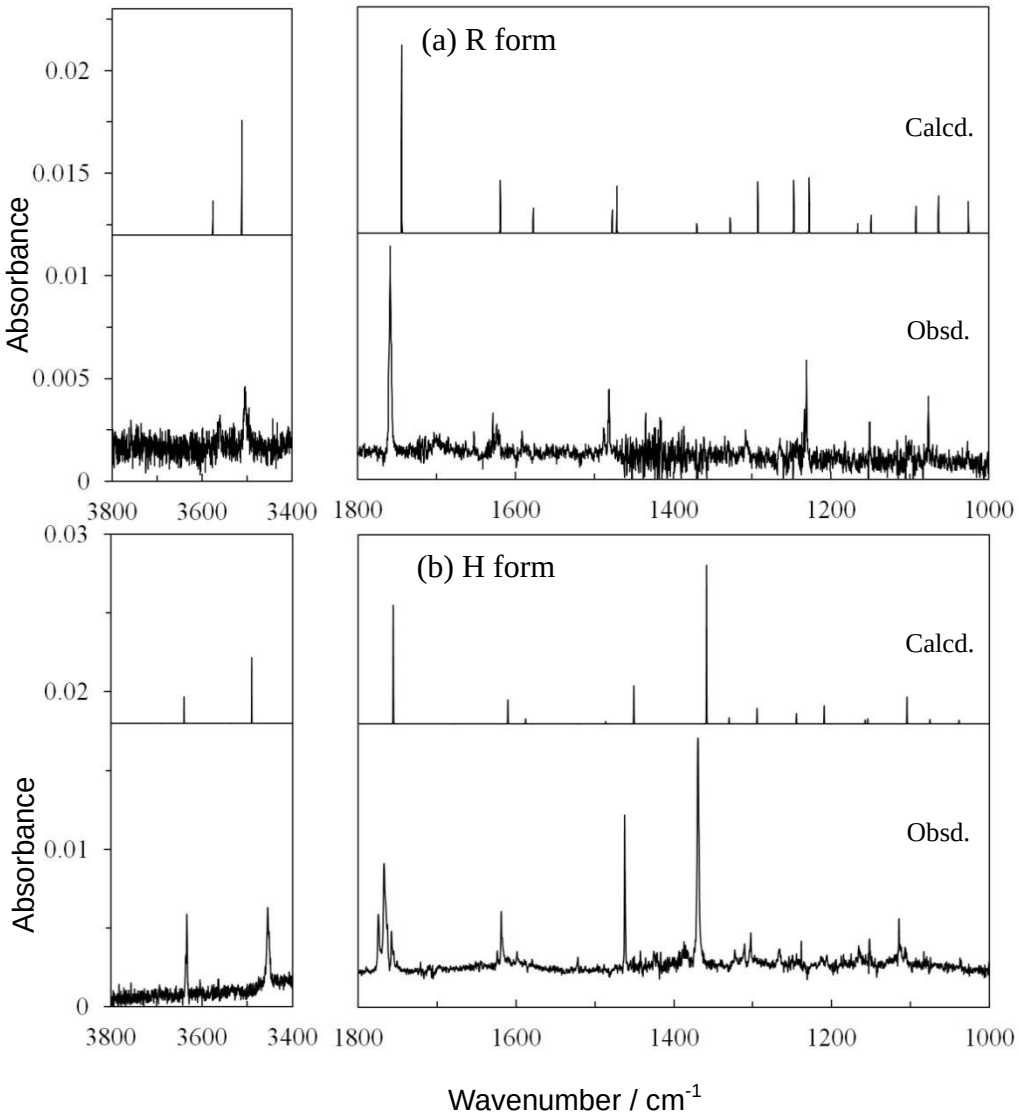

Fig. 3.7. IR spectra of photoproduced conformers of SA: (a) An observed spectrum obtained from difference spectra of (5−0 min) minus (10−5 min) and a calculated spectral pattern of R form; (b) an observed spectrum obtained from a difference spectrum of (100−80 min) and a calculated spectral pattern of H form. The bands of E form were subtracted computationally using a spectrum measured after deposition. Spectral patterns were calculated at the DFT/B3LYP/6-31++G** level, where a linear scaling formula of 0.9894−1.04 $\times 10^{-5}$ ν_{calcd} were used.

The both observed spectra were reproduced by their calculated spectral patterns satisfactorily. The wavenumbers of the O−H stretching modes of R form reported by Yahagi, 3585 and 3530 cm^{-1}, are 25 cm^{-1} higher than the corresponding values of our observation, 3560 and 3505 cm^{-1}. Since their wavenumbers of E form, 3585 and 3248 cm^{-1}, are also systematically higher than ours, 3562 and 3215 cm^{-1}, the wavenumber difference in the O−H stretching region may reflect the interaction due to argon atoms surrounding the conformers.

The band of the C=O stretching mode of H form splits at 1774, 1767 and 1758 cm^{-1} due to the Fermi resonance, similarly to the results obtained in other aromatic compounds [22−24]. They continued increasing like the O−H stretching bands at 3633 and 3455 cm^{-1}. On the other hand, the C=O stretching mode of R form appearing at 1758 cm^{-1} increased and then decreased like the bands at 3560 and 3505 cm^{-1}. The present study provides the first report of H form, which is the fourth stable conformer of SA. The observed and calculated wavenumbers and the relative intensities of R form and H form are summarized in Table 3.3. No IR spectra for the third stable conformer with an IMHB, O form, were detected, although the barrier height from O form to E form was estimated to be ~25 kJ mol^{-1} by the DFT calculation. The author assumes that O form immediately returns to the most stable conformer, E form through hydrogen-atom tunneling around OC−OH bond even if it is produced in the low-temperature argon matrix upon UV irradiation, similarly to formic acid and acetic acid [25−26].

Table 3.3. Observed and calculated wavenumbers and relative intensities of R form and H form.

R form				H form			
Obsd.		Calcd. [a]		Obsd.		Calcd. [a]	
ν / cm^{-1}	Int. [b]	ν / cm^{-1}	Int. [c]	ν / cm^{-1}	Int. [b]	ν / cm^{-1}	Int. [c]
3560	w	3576	18.2	3633	m	3639	16.7
3505	m	3512	61.1	3455	m	3490	41.5
1758	vs	1744	100	1774, 1767, 1758	s	1755	74.8
1628	m	1619	28.0	1618	m	1610	15.1
1591	w	1577	13.3	1598	w	1588	3.1
1488	w	1477	12.2	1497	vw	1486	1.4
1481	m	1471	24.9	1462	s	1451	24.0
−	−	1370	4.9	1369	s	1359	100
1335	vw	1328	8.1	1349	vw	1330	3.9
1308	w	1293	27.1	1302, 1310, 1323	w	1295	9.8
1265	w	1247	27.8	1266	w	1245	6.5
1231	s	1228	29.4	1206	w	1210	11.4
1171	vw	1166	5.0	1166	w	1158	2.4
1151	w	1149	9.5	1159	w	1154	3.2
1098	vw	1092	14.1	1115	m	1105	17.0
1077	m	1064	19.6	1084	w	1076	2.8
1027	w	1026	16.8	1038	w	1039	2.3

[a] Calculated at the DFT/B3LYP/6-31++G** level. A linear scaling formula of $0.9894 - 1.04 \times 10^{-5}\ \nu_{calcd}$ is used.

[b] Letters of vs, s, m, w, and vw denote very strong, strong, medium, weak and very weak intensities, respectively.

[c] Relative intensities.

3.2.7. Dissociation of a water molecule to produce ketoketene by UV irradiation

Some bands of photoproducts appearing in Fig. 3.6(c) are assignable to neither R form nor H form. One of them is the band around 2150 cm^{-1}, which is characteristic to the C=C=O stretching mode, suggesting that a ketene compound was produced by the UV irradiation besides the productions of R form and H form.

Since the IR bands of R form detected at the UV irradiation time of 10 min in Fig. 3.6(b) disappeared at 120 min in Fig. 3.6(c), it seems to be reasonable that the ketene compound was produced from R form. If the OH part in the carboxy group of R form is dissociated with its IMHB partner, the H atom in the hydroxy group, a biradical is produced with a water molecule as shown in Scheme 3.5(a). This biradical is so unstable that it immediately changes to a ketoketene compound, 6-(oxomethylene)cyclohexa-2,4-dienone (K, hereafter), by reconfiguration of electrons. The dissociated water molecule may locate in a matrix cage and interact with K. Thus, another expected photoproduct is a ketoketene-water complex (K-W, hereafter). The author performed the DFT calculations to optimize the geometry of K-W, resulting in at least two kinds of complexes shown in Fig. 3.8. The complex K-W1 is planar and more stable than the non-planar complex K-W2 by 4.3 kJ mol^{-1}. The optimized geometrical parameters of K-W1 and K-W2 are listed in Table 3.4.

(a)

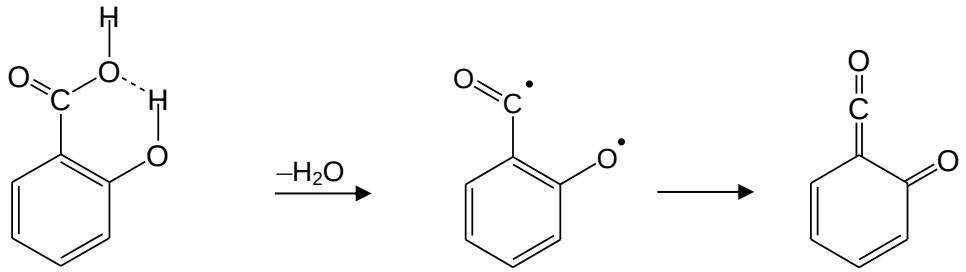

R form Ketoketene

(b)

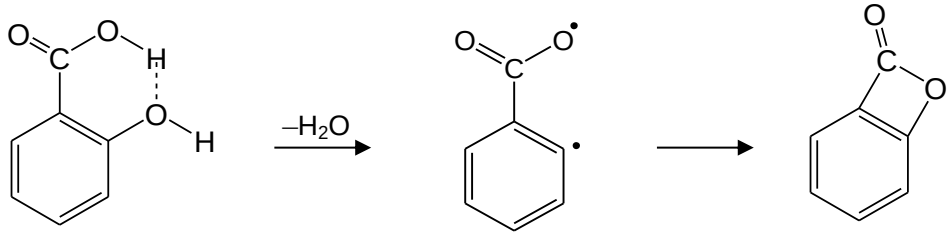

H form OBO

Scheme 3.5. Possible reaction pathways starting from (a) R form and (b) H form.

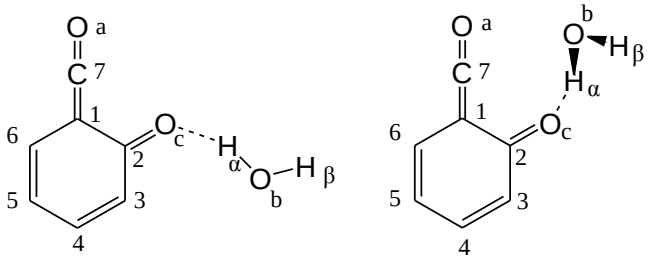

K-W1 K-W2

(0.0) (4.3)

Fig. 3.8. Optimized structures of ketoketene-water complexes. The numbers in parentheses represent relative energies in kJ mol^{-1} calculated at the DFT/B3LYP/6-31++G** level.

Table 3.4. Optimized geometry of K-W. [a,b]

Parameters [c]	K-W1	K-W2
$r(C_7-O_a)$	1.1549	1.1512
$r(C_1-C_7)$	1.3477	1.3535
$r(C_2-O_c)$	1.2452	1.2455
$r(C_1-C_2)$	1.4885	1.4857
$r(C_2-C_3)$	1.4536	1.4525
$r(C_3-C_4)$	1.3653	1.3660
$r(C_4-C_5)$	1.4391	1.4360
$r(C_5-C_6)$	1.3605	1.3621
$r(C_6-C_1)$	1.4470	1.4462
$r(O_b-H_\alpha)$	0.9788	0.9778
$r(O_b-H_\beta)$	0.9637	0.9638
$r(O_c\cdots H_\alpha)$	1.8650	1.8506
$\Theta(O_aC_7C_1)$	179.42	177.27
$\Theta(C_7C_1C_2)$	115.83	118.29
$\Theta(C_1C_2O_c)$	121.49	123.03
$\Theta(C_1C_2C_3)$	114.06	113.75
$\Theta(C_2C_3C_4)$	121.51	122.15
$\Theta(C_3C_4C_5)$	122.85	122.48
$\Theta(C_4C_5C_6)$	120.13	119.87
$\Theta(C_5C_6C_1)$	118.84	119.32
$\Theta(C_2O_cH_\alpha)$	114.20	119.80

[a] Calculated at the DFT/B3LYP/6-31++G** level.

[b] Units of r and Θ are Å and deg, respectively.

[c] Numbering of atoms is given in Fig. 3.8.

Since the calculated wavenumbers of K-W1 are consistent with the corresponding values of K-W2 within ~10 cm^{-1}, as shown in Table 3.5, the author compared the observed bands in Fig. 3.6(c) with the calculated spectral pattern of K-W1 in Fig. 3.6(d). The H−O−H bending mode of the dissociated water molecule was calculated to be 1575 cm^{-1}, which is consistent with the observed value, 1578 cm^{-1}. The asymmetric O−H stretching mode of the water appeared at 3709 cm^{-1}, which is weak and shifted toward lower-wavenumber side due to the intermolecular interaction with the ketoketene. The symmetric O−H stretching mode was not clearly observed probably because of the intermolecular hydrogen bond. Thus, the author assumes that K-W was produced by UV irradiation. The observed and calculated wavenumbers and the relative intensities are summarized in Table 3.5. The production of the K-W complex was supported by the TD-DFT calculations. The HOMO and LUMO of R form were shown in Fig. 3.9. A node was found at C_7−O_b, indicating the cleavage of this bond can be expected.

It is reported by Chapman et al. [27] that K was obtained by decomposition of phthaloyl peroxide. The author's observed wavenumbers are slightly inconsistent with their observations due to the coordination of the water molecule. It is noted that the intensity of the C=C=O stretching mode observed at 120 min is smaller than that at 10 min, implying that K is dissociated upon the prolonged UV irradiation, similarly to the other ketene compounds [8−11].

One may claim the possibility that K may be produced from H form by dissociation of the H atom in the carboxy group and the hydroxy group bonded to the benzene ring, which are interacting with each other through the IMHB. However, the biradical produced from H form is unable to change to K. Instead of it, an oxabicyclo compound, 7-oxabicyclo[4,2,0]octa-1,3,5-trien-8-one (OBO, hereafter), is formed (Scheme 3.5(b)), which was identified as a by-product in flash photolysis of phthaloyl peroxide by Chapman et al. [27]. In their study, one of the characteristic bands of OBO appeared at 1904 cm^{-1}. The author performed the DFT calculation of OBO and found that the C=O stretching mode was calculated to be 1894 cm^{-1} using the linear scaling formula, being consistent with their observed band. However, in the present study, no band was observed in this region in Fig. 3.6(c), indicating OBO was not produced from SA by the UV irradiation. Therefore, the author concluded that the K-W complex is produced from R form and that the IMHB plays an important role in dissociation of a water molecule.

Table 3.5. Observed and calculated wavenumbers and relative intensities of K-W.

Obsd.		Calcd. [a]			
		K-W1		K-W2	
ν / cm^{-1}	Int. [b]	ν / cm^{-1}	Int. [c]	ν / cm^{-1}	Int. [c]
3705	w	3695	7.5	3696	7.8
2146	s	2141	100	2152	100
1643	m	1639	17	1637	23.9
1598	w	1598	6.1	1588	0.3
1578	w	1575	26.2	1572	26.8
1518	m	1517	17.1	1515	17.4
1442	w	1437	0.8	1436	1.2
1389	w	1384	2.3	1380	1.8
1283	vw	1282	4.0	1280	3.3
1250	vw	1252	0.9	1244	2.9
1206	w	1198	1.7	1186	1.7
1159	vw	1155	1.7	1151	1.9
1106	vw	1107	0.5	1107	0.5

[a] Calculated at the DFT/B3LYP/6-31++G** level. A linear scaling formula of $0.9894-1.04\times10^{-5}\ \nu_{calcd}$ is used.

[b] Letters of s, m, w, and vw denote strong, medium, weak, and very weak intensities, respectively.

[c] Relative intensities.

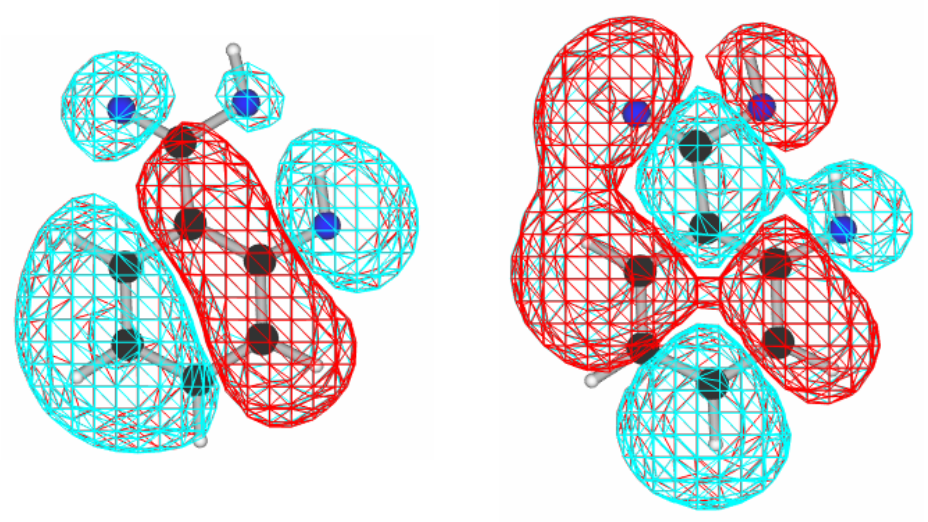

HOMO LUMO

Fig. 3.9. HOMO and LUMO of R form calculated at TD-DFT/B3LYP/6-31++G** level.

3.2.8. Photoreaction mechanisms of SA

To determine the photoreaction pathways, the author investigated the IR absorbance changes of the photoproducts against the UV irradiation time, which is shown in Fig. 3.10.

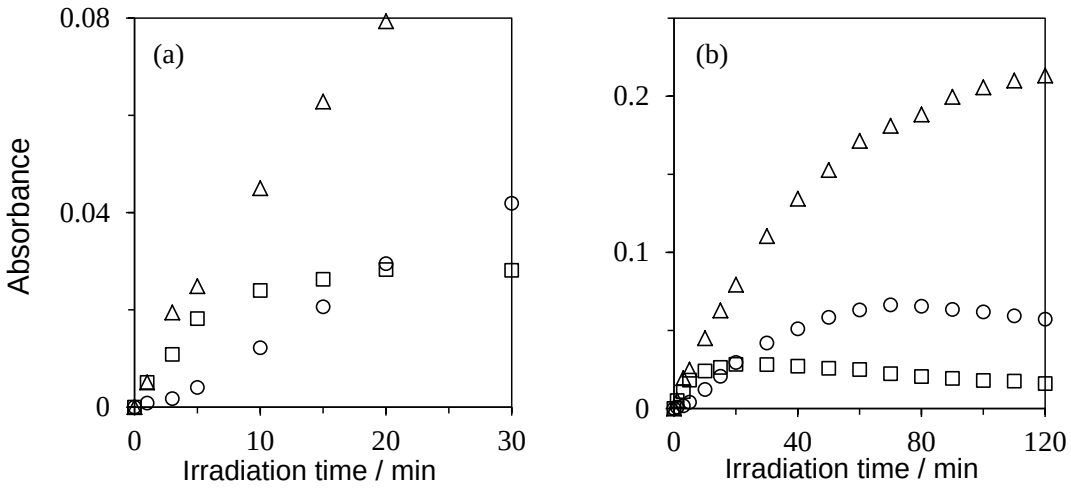

Fig. 3.10. Absorbance changes against irradiation time from the start to (a) 30 min and (b) 120 min. Symbols of (△), (□), and (○) represent the IR bands of H form (3455 cm^{-1}), R form (3505 cm^{-1}), and K-W complex (1643 cm^{-1}), respectively.

Since both plots of R form and H form had no induction period, it was found that they are produced from E form directly. In contrast, the plot of the K-W complex had an induction period, indicating it is not produced from E form directly. The K-W complex seems to be produced from R form because the plot of R form had its maximum at 20 min, and started decreasing upon the prolonged irradiation, indicating R form is a reaction intermediate to produce the K-W complex. The production of the K-W complex from H form does not likely occur because the plot of H form never decreased upon the prolonged irradiation shown in Fig. 3.10(b). The plot of the K-W complex started decreasing at 70 min, suggesting it was decomposed. Decomposition of a ketene compound was studied in 3-hydroxy-2,4-cyclopentadiene-1-ylidenemethanone

produced from 4-chlororesorcinol, where dissociation of CO part from the ketenyl group occurred. In the present study, a new band at 2135 cm^{-1}, which is assignable to CO increased upon the prolonged irradiation. Thus the author assumes the same reaction occurred in the case of the K-W complex.

From the perspective of conformations, production of the K-W complex from R form is convincing. The dissociating part, OH and H in the carboxy and hydroxy groups are close to each other and hydrogen bonding in R form, while they are away from each other, and not hydrogen bonding neither in E form nor H form. In other words, the dissociation of H_2O can be achieved in one-step reaction in R form, but it requires more than one step in the case of E form and H form; dissociation of the OH part in the carboxy group, migration of the OH radical and the following dissociation of the H atom in the hydroxy group. These reactions seem to hardly occur in an argon matrix because OH radical is not small enough to migrate.

3.3. Summary

In the present study, the conformations of SA at the potential minima in the S_0 state were determined by a comparison of the IR spectra measured by the low-temperature matrix-isolation method with the calculated spectral patterns obtained by the DFT method. Only the most stable E form with IMHB of Ph−OH···O=C in the carboxy group existed in the argon matrix. The second stable R form with Ph−OH···OH in the carboxy group and the fourth stable H form with COOH···OH−Ph were produced by UV irradiation (λ > 290 nm). The third stable O form with Ph−OH···O=C in the carboxy group was assumed to return immediately to E form even if it was produced upon UV irradiation. Ketoketene-water complex was yielded from R form by dissociation of a water molecule from the IMHB part of Ph−OH···OH in the carboxy group upon prolonged UV irradiation. The whole photoreaction pathways are summarized in Scheme 3.6.

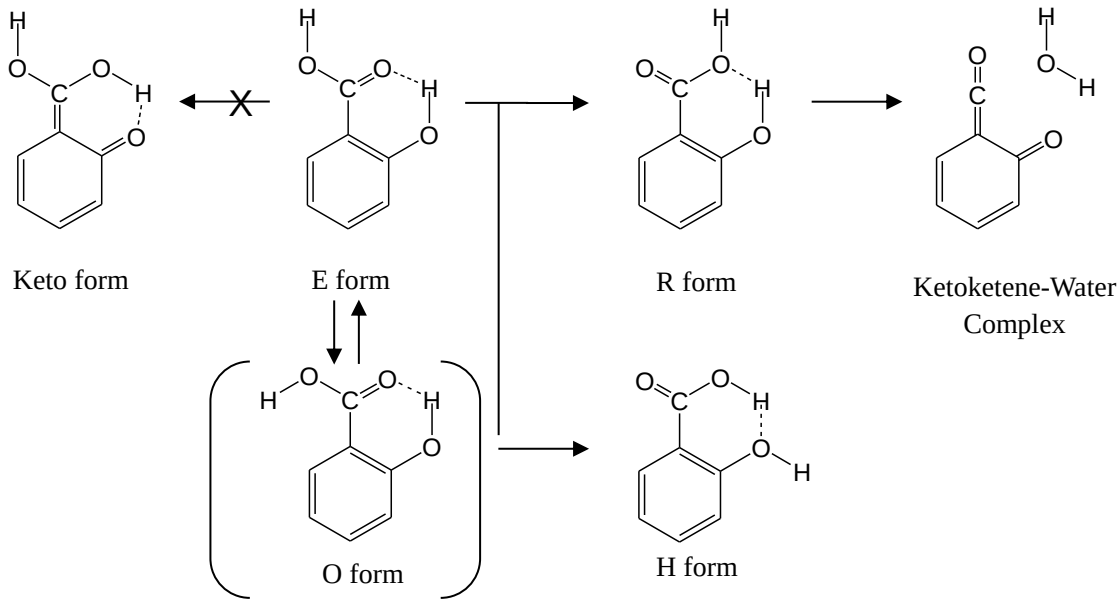

Scheme 3.6. Photoreaction pathways of salicylic acid.

3.4. References

[1] A. Weller, Naturwissenschaften 42 (1955) 175.

[2] A. Weller, Z. Elektrochem. 60 (1956) 1144.

[3] A. Weller, Prog. React. Kinet. 1 (1961) 187.

[4] P.B. Bisht, H. Petek, K. Yoshihara, U. Nagashima, J. Chem. Phys. 103 (1995) 5290.

[5] S. Nagaoka, U. Nagashima, Chem. Phys. 136 (1989) 153.

[6] A.L. Sobolewski, W. Domcke, Chem. Phys. 232 (1998) 257.

[7] T. Yahagi, A. Fujii, T. Ebata, N. Mikami, J. Phys. Chem. A 105 (2001) 10673.

[8] S. Nanbu, M. Sekine, M. Nakata, J. Mol. Struct. 1025 (2012) 43.

[9] N. Akai, S. Kudoh, M. Nakata, J. Photochem. Photobiol. A 169 (2005) 47.

[10] S. Nanbu, M. Sekine, M. Nakata, J. Phys. Chem. A 115 (2011) 9911.

[11] M. Nagaya, S. Iizumi, M. Sekine, M. Nakata, J. Mol. Struct. 1025 (2012) 53.

[12] M. Miyagawa, N. Akai, M. Nakata, Chem. Phys. Lett. 602 (2014) 52.

[13] G.S. Denisov, N.S. Golubev, V.M. Schreiber, Sh.S. Shajakhmedov, A.V. Shurukhina, J. Mol. Struct. 436 (1997) 153.

[14] E. Orton, M.A. Morgan, G.C. Pimentel, J. Phys. Chem. 94 (1990) 7936.

[15] S. Nishino, M. Nakata, J. Phys. Chem. A 111 (2007) 7041.

[16] M. Nagaya, M. Nakata, J. Phys. Chem. A 111 (2007) 6256.

[17] S. Nishino, M. Nakata, J. Mol. Struct. 875 (2008) 520.

[18] N.S. Golubev, G.S. Denisov, J. Mol. Struct. 270 (1992) 263.

[19] I. Reva, B.J.A.N. Almeida, L. Lapinski, R. Fausto, J. Mol. Struct. 1025 (2012) 74.

[20] I.D. Reva, S.G. Stepanian, J. Mol. Struct. 349 (1995) 337.

[21] S.G. Stepanian, I.D. Reva, E.D. Radchenko, G.G. Sheina, Vib. Spectrosc. 11 (1996) 123.

[22] A.Yu. Ivanov, S.G. Stepanian, L. Adamowicz, J. Mol. Struct. 1025 (2012) 92.

[23] M.J. Nowak, J. Mol. Struct. 193 (1989) 35.

[24] A. Les, L. Adamowicz, Spectrochim. Acta 48A (1992) 1385.

[25] M. Pettersson, J. Lundell, L. Khriachtchev, M. Rasanen, J. Am. Chem. Soc. 119 (1997) 11715.

[26] E.M.S. Macoas, L. Khriachtchev, M. Pettersson, R. Fausto, M. Rasanen, J. Am. Chem. Soc. 125 (2003) 16188.

[27] O.L. Chapman, C.L. MacIntosh, J. Pacansky, J. Am. Chem. Soc. 95 (1973) 4061.

Chapter 4: Photoreaction of 3-Chlorosalicylic Acid

Abstract

Photoreaction pathways of 3-chlorosalicylic acid have been investigated by the low-temperature matrix-isolation infrared spectroscopy with an aid of the density-functional-theory calculations. Only the most stable E form existed in an argon matrix. As well as salicylic acid, UV-induced conformational changes and production of ketoketene–water complex have occurred. It was implied that substitution of the Cl atom may induce another photoreaction pathway from Cl form to produce a 5-membered ring ketene compound.

4.1. Introduction

In the previous chapter, the author investigated photoreaction mechanisms of salicylic acid (SA, hereafter), and found the H atom in the hydroxy group dissociates with the OH part in the carboxy group to produce the water complex of 6-(oxomethylene)cyclohexa-2,4-dienone (K-W, hereafter). Focusing on the hydroxy group, SA can be regarded as a phenol derivative. The dissociation of the H atom has also been reported in halogenated phenols. For example, in 2-chlorophenol, dissociation of the H and Cl atoms occurs, and cyclopentadienylidenemethanone (CPYM, hereafter) is produced from the ketocarbene by Wolff rearrangement shown in Scheme 4.1 [1].

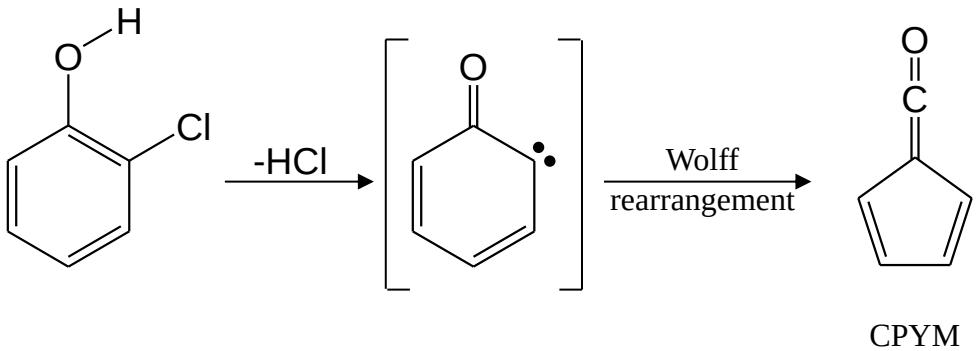

Scheme 4.1. Photoreaction of 2-chlorophenol.

Other studies also revealed the production of CPYM derivatives is related to intramolecular hydrogen bond (IMHB, hereafter) of H···X, where X is a halogen atom. Thus the author assumed that 3-chlorosalicylic acid (3-CSA, hereafter) may produce a CPYM derivative upon UV irradiation. Such a reaction seems to occur from Cl form (Fig. 4.1) corresponding to H form of SA, while no photoreaction occurs in H form of SA, as described in the previous chapter. On the other hand, it is also expected that the K-W derivative is produced from R form (Fig. 4.1), and which photoreaction occurs depends on the irradiation wavelength. The author calls those derivatives K-W and CPYM in short in the present study.

Since 3-CSA is one of the halogenated aromatic compounds, is used for fungicides, and is highly soluble in water, its decomposition was investigated over TiO_2 membranes upon UV irradiation [2,3]. On the other hand, even though there is no study on 3-CSA, the effect of chlorine-atom substitution on the dual emission has also been investigated in 4-CSA, 5-CSA, 3,5-diCSA and 3,5,6-triCSA by Paul et al. [4−7], similarly to that of SA described in section 3.1. Since the previous studies were performed in solution, the dual emission is assumed to originate from E form and keto form in the electronic excited state as well as slight spectral shifts due to the chlorine-atom substitution, pH and solvent polarity. However, the production of K-W or CPYM is not reported, probably because neither of them is too unstable to exist stably in solution. In other words, the effect of the chlorine-atom substitution on the photoreaction has not been revealed.

Unlike 4- and 5-CSAs, the chlorine-atom substitution into the third position of SA has an effect on the relative stability of each conformer due to the IMHB of Ph−OH···Cl. Since two conformations, *cis* and *trans*, around the three single bonds of Ph−COOH, C−OH and Ph−OH must be considered, eight stable conformers presented in Fig. 4.1 are possible. The relative energy of each conformer mainly depends on the following three factors: (1) Stabilization due to IMHB, (2) repulsion between lone pairs of the two O atoms in the carboxy group, and (3) steric hindrance between two H atoms in the carboxy group and the hydroxy group or the benzene ring. Thus it may be a complicated problem in relation to IMHB to clarify which conformer is the most stable, which conformers exist in the gas phase at room temperature, and which conformers are

produced upon UV irradiation. The geometrical structure and photoreaction of its parent molecule, salicylic acid (SA), have been investigated by many research groups [8−21], but neither experimental nor theoretical report on the conformation of 3-CSA has yet been published, except for the photodecomposition [2,3], because the conformation of 3-CSA is more complex than that of SA, originating from IMHB due to the Cl atom.

In the present study, the author has determined the conformation of the most stable conformer by comparison of the spectra measured by low-temperature matrix-isolation infrared (IR) spectroscopy with calculated spectral patterns obtained by the density-functional-theory (DFT) method. This combined method is known to be one of the most effective ways to determine the conformations of complex molecules such as multi-substituted aromatic and heterocyclic compounds correctly, as shown in recent papers [1,22−33]. The author has also identified the conformational changes and production of K-W, and the production of CPYM has also been implied.

4.2. Results and discussion

4.2.1. Calculation results of 3-CSA monomer

The calculated relative energies of eight conformers of 3-CSA are given in Fig. 4.1 after the correction of zero-point vibrational energies, where the four relatively stable conformers are abbreviated as E, R, O and Cl forms. Four conformers on the right side in Fig. 4.1 are less stable than four conformers on the left side because of repulsion between the lone pairs of the two O atoms in the carboxy group. Similar explanation is reported in detail in the previous papers on 2-chlorobenzoic acid [29] and 2-chloropropionic acid [34]. Among the four conformers on the left side, the two conformers on the upper row, E form and R form, are more stabilized by the IMHB of COOH···OH−Ph than by the IMHB of Ph−OH···Cl in the two conformers on the lower row, as shown in Fig. 4.1, where IMHBs are denoted by broken lines. Since the IMHB of E form originates, in plane, from an sp^2 hybrid orbital of the C=O part in the carboxy group, it is stronger than the IMHB of R form originating, out of plane, from an sp^3 hybrid orbital of the OH part. As a result, E form is the most stable conformer, whereas R form is the second stable one. This is supported by comparison of the bond lengths of the optimized geometrical parameters listed in Table 4.1, where the length of the IMHB in E form, $r(O_a\cdots H_\beta)$, is shorter than the corresponding length in R form, $r(O_b\cdots H_\beta)$, by

0.065 Å, whereas $r(O_c-H_\beta)$ in E form is longer than that in R form by 0.014 Å. A similar result was reported in the calculated results of SA obtained at the DFT/B3LYP/6-31G** level [21].

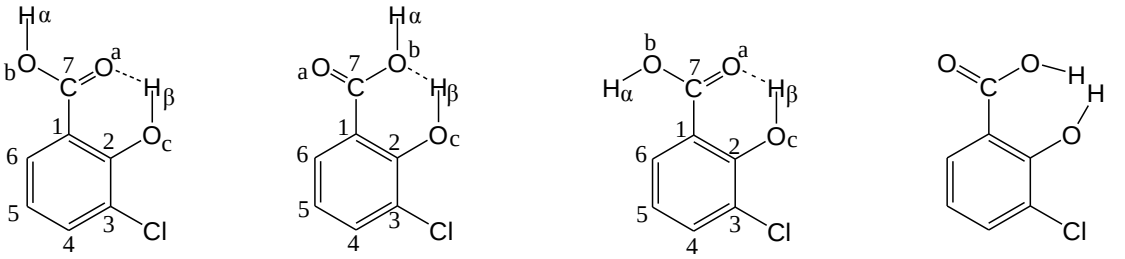

E form (0.00) [1]

R form (15.8) [2.1×10^{-3}]

O form (26.8) [2.9×10^{-5}]

(60.5)

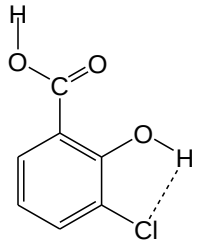

(33.8)

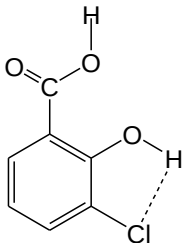

(31.2)

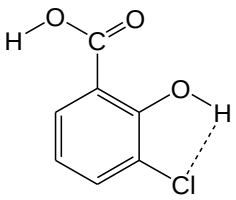

(59.2)

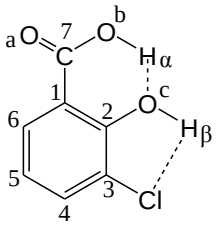

Cl form (28.4) [1.5×10^{-5}]

Fig. 4.1. Eight possible conformers of 3-CSA. The numbers in parentheses represent relative energies in kJ mol^{-1} obtained at the DFT/B3LYP/6-31++G** level. The numbers in square brackets represent population ratios according to the Boltzmann distribution law at the deposition temperature of 308 K.

Table 4.1. Optimized geometry of E, R, Cl and O forms [a,b].

parameters[c]	E form	R form	Cl form	O form
r(O···H)	1.7270	1.7917	1.7948	1.6693
r(C=O)	1.2333	1.2131	1.2120	1.2275
r(C_7−O_b)	1.3483	1.3765	1.3474	1.3483
r(O_b−H_α)	0.9720	0.9722	0.9743	0.9669
r(C_1−C_7)	1.4671	1.4792	1.5115	1.4814
r(C_2−O_c)	1.3377	1.3458	1.3673	1.3334
r(O_c−H_β)	0.9876	0.9736	0.9714	0.9929
r(C_3−Cl)	1.7474	1.7491	1.7625	1.7454
r(C_1−C_2)	1.4214	1.4196	1.4084	1.4242
r(C_2−C_3)	1.4108	1.4111	1.4023	1.4134
r(C_3−C_4)	1.3885	1.3887	1.3904	1.3871
r(C_4−C_5)	1.4026	1.4006	1.3967	1.4017
r(C_5−C_6)	1.3863	1.3857	1.3918	1.3861
r(C_6−C_1)	1.4083	1.4085	1.4027	1.4089
Θ($O_aC_7O_b$)	120.73	120.31	120.23	117.64
Θ($C_7O_bH_\alpha$)	106.99	107.41	111.42	112.04
Θ($O_aC_7C_1$)	124.39	125.88	121.35	122.75
Θ($H_\beta O_c C_2$)	107.71	109.70	110.37	107.20
Θ($O_cC_2C_1$)	123.01	124.81	119.32	122.96
Θ(ClC_3C_2)	119.05	119.02	118.15	118.89
Θ($C_2C_1C_7$)	118.25	124.15	124.91	117.61
Θ($C_6C_1C_7$)	121.52	116.10	116.62	123.14

[a] Calculated at the DFT/B3LPY/6-31++G** level.

[b] Units of r and Θ are Å and deg, respectively.

[c] Numbering of atoms is given in Fig. 4.1.

Among the four conformers on the right side, O form is the most stable one, because this conformer is stabilized by an IMHB originating from an sp^2 hybrid orbital of the C=O part in the carboxy group like E form. On the other hand, Cl form is stabilized by an IMHB originating from an sp^3 hybrid orbital of the O atom in the hydroxy group like R form. Therefore, Cl form could be less stable than O form, but should be stabilized by another IMHB of Ph−OH···Cl, leading to the conclusion that Cl form is as stable as O form. Comparing $r(O_c-H_\beta)$ of Cl form with that of R form, it was found that the hydroxy group forms an stronger IMHB with the C=O or C−O part in the carboxy group than Ph−Cl shown in Table 4.1. The stabilization energy due to the IMHB of Ph−OH···Cl was estimated to be about 11 kJ mol^{-1} according to the lower rows in Fig. 4.1 and Fig. 3.1 in the previous chapter. Hereafter the four conformers, E, R, O and Cl forms, are mainly considered in our analysis.

4.2.2. IR spectrum measured after deposition before UV irradiation

An IR spectrum of 3-CSA in an argon matrix measured after deposition is shown in Fig. 4.2. The population ratio of the second stable R form over the most stable E form is estimated to be 2.1×10^{-3} according to the Boltzmann distribution law at the deposition temperature of 308 K, using the relative energies shown in Fig. 4.1. Since the population ratios of the other forms are less than 2.1×10^{-3}, it is credible that all the IR spectral bands measured after deposition are assignable to E form.

By comparison with the calculated spectral patterns of all the eight conformers, most of the observed bands were assigned to E form, as expected from the estimated population ratios. The observed and calculated wavenumbers and the relative intensities of E form are summarized in Table 4.2.

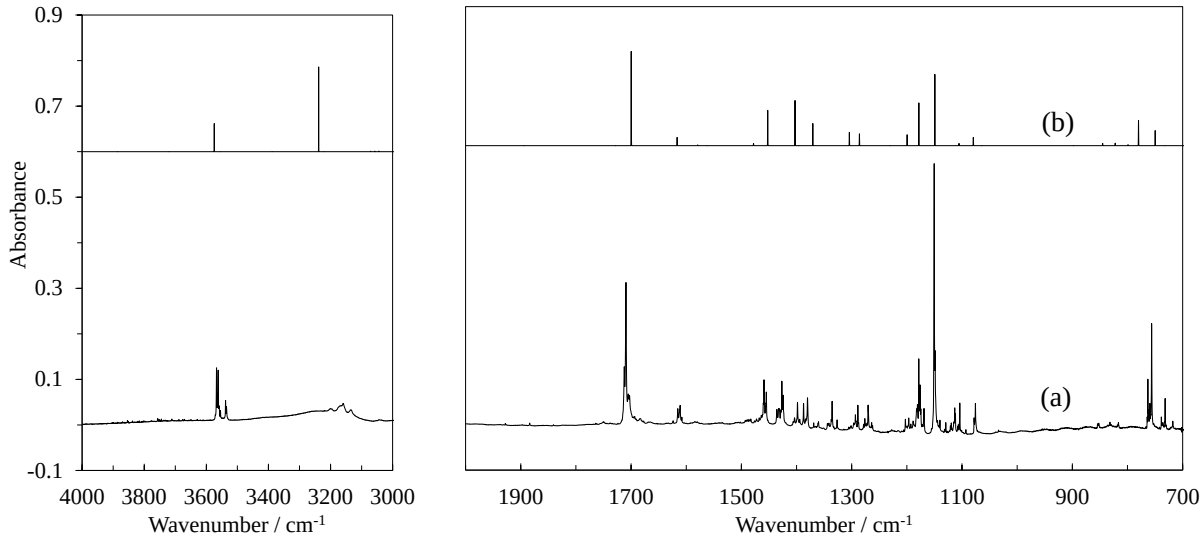

Fig. 4.2. IR spectra of 3-CSA: (a) An observed spectrum after deposition; (b) a spectral pattern of E form calculated at the DFT/B3LYP/6-31++G** level. A linear scaling formula of $0.9894-1.04\times10^{-5}\nu_{calcd}$ was used.

Table 4.2. Observed and calculated wavenumbers (in cm^{-1}) and their relative intensities of E form. [a]

Obsd.		Calcd.[b]	
v	Int.[c]	*v*	Int.[d]
3567, 3562, 3538, 3535	s	3576	30.4
3200,3159, 3134	m	3252	91.6
1712, 1709, 1705, 1703	s	1685	100
1615, 1611	w	1604	8.8
1484, 1483	vw	1469	1.2
1459, 1455	m	1443	37.5
1436, 1432, 1427, 1424	m	1395	48
1398, 1387, 1380	m	1363	23.5
1335, 1326	m	1298	14.1
1293, 1289, 1276, 1270,1264	m	1280	12.5
1203, 1196	w	1195	11.6
1181, 1178, 1176, 1169	s	1175	45.4
1150, 1149	vs	1146	75.7
1112, 1104	m	1103	2.4
1078, 1076	w	1077	8.7
851	vw	845	2.5
832	vw	823	2.7
816	vw	800	1.1
763, 759, 752	s	781	26.7
739, 732	w	751	16

[a] Vibrational modes with intensities of less than 1.0 are omitted.

[b] Calculated at the DFT/B3LYP/6-31++G** level. A linear scaling formula of $0.9894-1.04\times10^{-5}\nu_{calcd}$ was used.

[c] Letters of vs, s, m, w, and vw denote very strong, strong, medium, weak, and very weak intensities, respectively.

[d] Relative intensities.

Most of the observed bands are split by the Fermi resonance and/or matrix effects. Similar splits were observed in the IR spectra of multi-substituted phenols [1,25,35]. The bands appearing in the range between 3530 and 3570 cm^{-1} correspond to the calculated value of the free O−H stretching mode in the carboxy group, 3576 cm^{-1}. On the other hand, the bands in the range between 3130 and 3200 cm^{-1} correspond to the O−H stretching mode in the hydroxy group, which are broadened and weakened by the IMHB of Ph−OH···O=C. The bands appearing in the range between 1700 and 1715 cm^{-1} corresponds to the calculated value of the C=O stretching mode, 1685 cm^{-1}, which shows a low-wavenumber shift due to the IMHB of Ph−OH···O=C by ca. 50 cm^{-1} from normal free C=O stretching modes such as benzoic acid [36,37]. The observed bands in other regions also show splits, and some of them are located far from the corresponding calculated bands. For example, the band at 1335 cm^{-1} is far from the calculated band at 1298 cm^{-1} assigned to the $H_{\beta}O_cC_2$ bending mode. The author carried out the DFT calculation using various basis sets, but this inconsistency could not be removed. Similar inconsistency has often been found in multi-substituted derivatives of benzene and pyridine [4,33,38]. Thus the author mainly discusses about the spectral changes in the O−H and C=O stretching regions to identify conformers produced by UV irradiation, because they strongly reflect the differences in the conformations in relation to IMHB.

Note that SA and some derivatives have been reported to contain R form as a minor species in addition to the major E form [5−7,11,21,39,40]. For example, Paul *et al*. investigated 3,5,6-trichlorosalicylic acid in various solutions by UV-visible absorption spectroscopy [39] and found that E form and R form coexist and that their relative intensities depended on the polarity of solvents, even though E form is more stable than R form by 17.7 kJ mol^{-1} calculated at DFT/B3LYP/6-31G** level. In contrast to their report, the author has observed no free C=O stretching band around 1760 cm^{-1} as shown in Fig. 4.2, indicating that the population of R form is negligible in a low-temperature argon matrix with no stabilization due to solvents, as supported by the results on the calculated relative energy.

4.2.3. UV-vis spectrum of 3-CSA after deposition

An UV-vis absorption spectrum of 3-CSA after deposition was measured to determine the irradiation wavelength to E form. The obtained spectrum is shown in Fig.

4.3(a) with that of SA in Fig 4.3(b) for comparison. A band peaking at 316 nm due to ππ* transition was observed. Its tail on the longer-wavelength side was at 341 nm. The obtained transition energy of 3-CSA in the present study is smaller than that of SA described in the previous chapter by 716 cm^{-1} because of the electron-withdrawing effect of the Cl atom at the third position of the benzene ring.

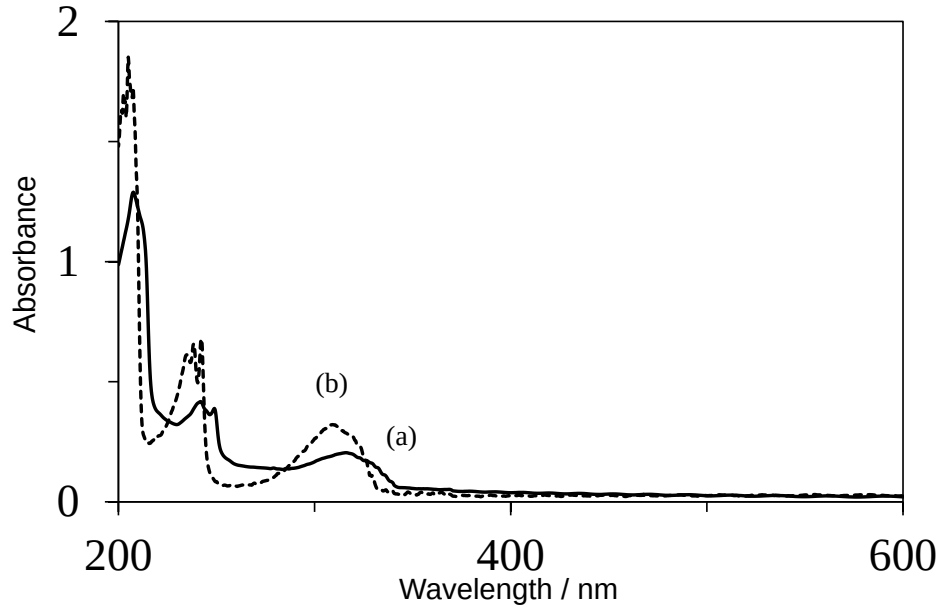

Fig. 4.3. UV-vis spectra of E form in an argon matrix: (a) 3-CSA (solid line); (b) SA (dotted line).

4.2.4. Isomerization from E form to R form and Cl form upon UV irradiation (λ > 330 nm)

When the matrix sample was exposed to UV light (λ > 330 nm), an IR spectral change was observed. The difference spectrum between the spectra measured after minus before the 300-min UV irradiation is shown in Fig. 4.4, where the decreasing and increasing bands represent the reactant, E form, and photoproducts, respectively. To

determine which conformer was produced upon the UV irradiation, the author compared the observed spectra with the calculated spectral patterns of four relatively stable conformers. As a result, it was found that the increasing bands were assignable to R form and Cl form. For example, two O−H stretching modes of Cl form appeared at 3464 and 3532 cm^{-1}, where the former is due to the IMHB of COOH···OH−Ph, and the latter is due to the IMHB of Ph−OH···Cl. Since the wavenumber of the former is lower than that of the latter, the IMHB due to the COOH···OH−Ph is stronger than that due to the Ph−OH···Cl. R form also has two O−H stretching modes. One is observed at 3486 cm^{-1}, which is assignable to the O−H stretching mode of the hydroxy group interacting with the OH part in the carboxy group. The O−H stretching mode for the OH part in the carboxy group is expected to appear around 3570 cm^{-1}, but it was not found because of overlapping with the corresponding decreasing band of E form. On the other hand, the C=O stretching modes of R form and Cl form, which are free from IMHB, were observed at 1764 and 1769 cm^{-1}, respectively. The calculated wavenumbers and the relative intensities of R form and Cl form are compared with the observed wavenumbers in Table 4.3. Note that no IR bands assignable to O form were observed because its strong C=O stretching band expected to appear at 1720 cm^{-1} by the DFT calculation was undetectable in the observed spectrum. By analogy with other carboxylic acid derivatives [23,24], O form may be changed to E form through hydrogen-atom tunneling even if produced upon UV irradiation.

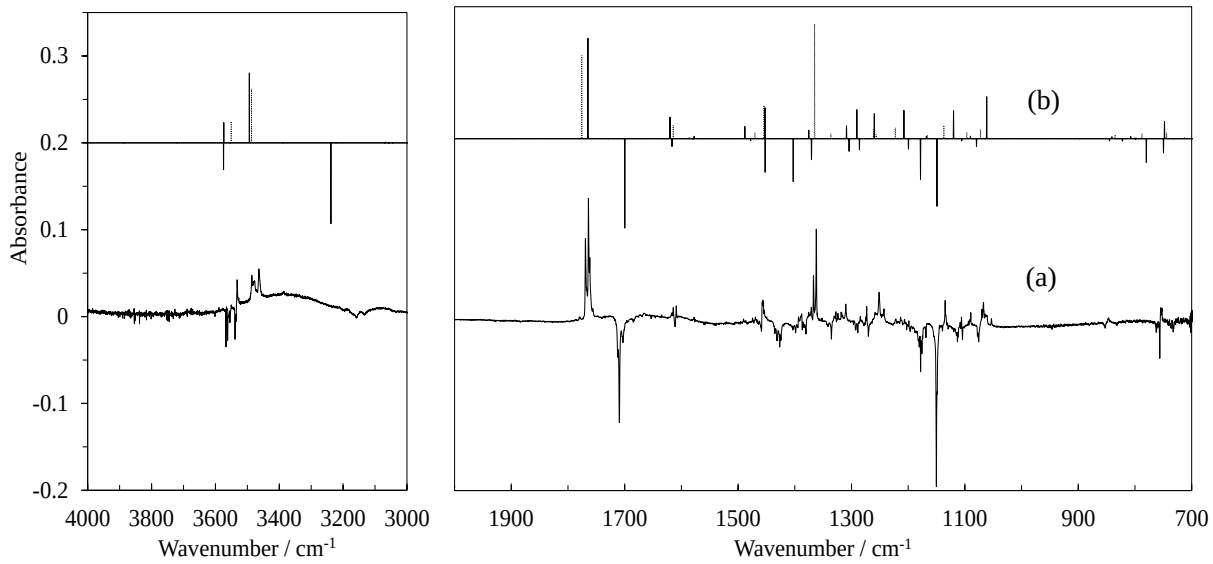

Fig. 4.4. IR spectral changes by UV irradiation (λ > 330 nm): (a) An observed difference spectrum between the spectra measured after minus before the UV irradiation; (b) spectral patterns of E form (lower side), R form (upper side, solid line) and Cl form (upper side, dotted line) calculated at the DFT/B3LYP/6-31++G** level. A linear scaling formula of $0.9894-1.04 \times 10^{-5}\, \nu_{calcd}$ was used.

Table 4.3. Observed and calculated wavenumbers (in cm^{-1}) and relative intensities of R and Cl forms.[a]

Obsd.			Calcd.[b]			
			R form		Cl form	
ν	Int.[c,e]		ν	Int.[d]	ν	Int.[d]
3565	w	↓	3575 (O_b-H_α)	20.4		
3532	w	↑			3553 (O_c-H_β)	18.9
3486	m	↓	3498 (O_c-H_β)	70.5		
3464	m	↑			3491 (O_b-H_α)	47.6
1769	s	↑			1758	72.5
1764	vs	↓	1748	100		
1614	m	↓	1607	21.5		

Table 4.3. Observed and calculated wavenumbers (in cm^{-1}) and relative intensities of R and Cl forms.[a] (Continue).

1609	m	↑			1602	11.7
1490	vw	↓	1478	12.2		
1474	w	↑			1461	5.5
1456	m	↑			1445	29.2
1455	m	↓	1444	30.9		
1375	w	↓	1368	8.5		
1367	m	↑			1358	100
1318, 1310	m	↓	1303	12.7		
1284	w	↓	1285	28.9		
1258	vw	↑			1256	8
1251	m	↓	1254	25		
1214, 1199	w	↓	1203	28.2		
1145	w	↑			1134	11.6
1135	m	↓	1117	27.8		
1106	m	↑			1094	5.5
1067	m	↓	1060	41.8	1070	8
755	w	↑			745	5.3
752	w	↓	749	17		

[a] Vibrational modes with intensity of less than 5.0 are omitted.

[b-d] See the caption of Table 4.2.

[e] Marks ↓ and ↑ represent decreasing and increasing upon 290-nm irradiation, respectively.

To produce R form from E form, the conformational change around Ph−COOH bond is required. On the other hand, to produce Cl form from E form, multi-conformational changes around Ph−COOH, CO−OH and Ph−OH are required. Thus, one may claim that Cl form could be produced from E form via R form. To solve the question whether Cl form is produced directly from E form or indirectly via R form, the author analyzed the IR absorbance changes against the irradiation time. The 1709, 1764 and 1769 cm^{-1} bands were chosen in the kinetic analysis for E, R and Cl forms, respectively. As shown in Fig. 4.5, the absorbance of the both photoproducts were found to increase immediately after the start of the UV irradiation with no induction period, implying that the both R form and Cl form were directly produced from E form upon the 330-nm irradiation. In addition, the absorbance of the photoproducts never decreased upon the prolonged irradiation, indicating that no other photoreaction occurred.

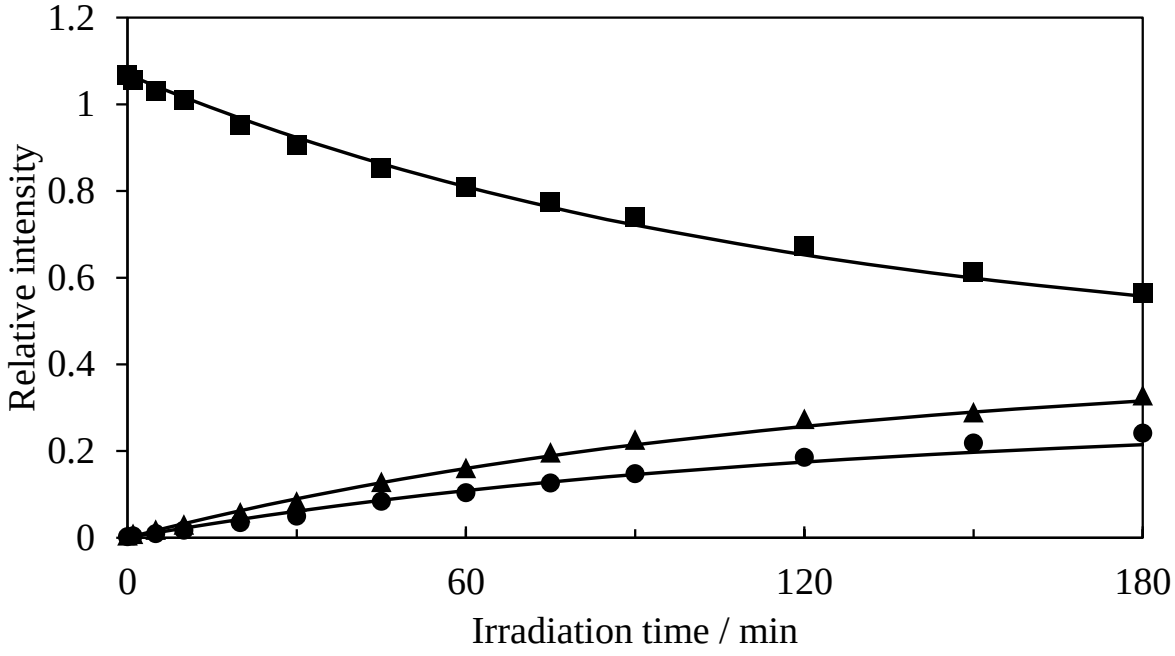

Fig. 4.5. Absorbance changes against irradiation time: Symbols of ■, ▲, and ● represent the IR bands of E (1709 cm^{-1}), R (1764 cm^{-1}), and Cl (1769 cm^{-1}) forms, respectively. Solid lines represent the calculated values of IR absorbance using the Eqs. (7) ~ (9).

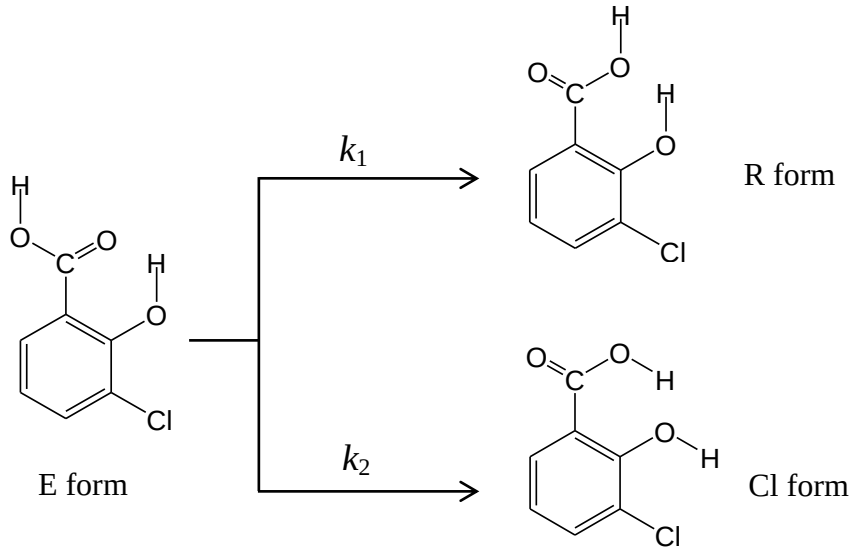

Scheme 4.2. Conformational changes of SA upon UV irradiation (λ > 330 nm).

To support the proposed reaction pathways, the author tried to determine the rate constants shown in Scheme 4.2 from the absorbance changes of the IR bands. The corresponding rate equations can be derived from a general kinetic theory as follows:

$$\frac{\mathrm{d}}{\mathrm{d}t}[\mathrm{E}] = -(k_1 + k_2)([\mathrm{E}] - [\mathrm{E}]_\infty) \quad (1)$$

$$\frac{\mathrm{d}}{\mathrm{d}t}[\mathrm{R}] = k_1([\mathrm{E}] - [\mathrm{E}]_\infty) \quad (2)$$

$$\frac{\mathrm{d}}{\mathrm{d}t}[\mathrm{Cl}] = k_2([\mathrm{E}] - [\mathrm{E}]_\infty) \quad (3)$$

where the concentrations of E, R and Cl forms in the matrix are denoted as [E], [R] and [Cl], respectively. The rate constants k_1 and k_2 are defined in Scheme 4.2. The term of $[\mathrm{E}]_\infty$ denotes the concentration of E form at the infinite time. By solving the differential equations (1) ~ (3), the following equations can be obtained using the concentration of E form at the start of UV irradiation, $[\mathrm{E}]_0$:

$$[\mathrm{E}] = ([\mathrm{E}]_0 - [\mathrm{E}]_\infty)\mathrm{e}^{-(k_1+k_2)t} + [\mathrm{E}]_\infty \quad (4)$$

$$[\mathrm{R}] = ([\mathrm{E}]_0 - [\mathrm{E}]_\infty)\frac{k_1}{-(k_1+k_2)}(\mathrm{e}^{-(k_1+k_2)t} - 1) \quad (5)$$

$$[\mathrm{Cl}] = ([\mathrm{E}]_0 - [\mathrm{E}]_\infty)\frac{k_2}{-(k_1+k_2)}(\mathrm{e}^{-(k_1+k_2)t} - 1) \quad (6)$$

Equations (4) ~ (6) are represented in terms of the corresponding IR absorbance A and the corresponding absorption coefficient ε instead of the concentrations, using the relationships, for example, $A^{\mathrm{E}} = [\mathrm{E}]\varepsilon^{\mathrm{E}}$,

$$A^{\mathrm{E}} = (A_0^{\mathrm{E}} - A_\infty^{\mathrm{E}})\mathrm{e}^{-(k_1+k_2)t} + A_\infty^{\mathrm{E}} \quad (7)$$

$$A^{\mathrm{R}} = (A_0^{\mathrm{E}} - A_\infty^{\mathrm{E}})\frac{k_1}{-(k_1+k_2)}\left(\mathrm{e}^{-(k_1+k_2)t} - 1\right)\frac{\varepsilon^{\mathrm{R}}}{\varepsilon^{\mathrm{E}}} \quad (8)$$

$$A^{\mathrm{Cl}} = (A_0^{\mathrm{E}} - A_\infty^{\mathrm{E}})\frac{k_2}{-(k_1+k_2)}\left(\mathrm{e}^{-(k_1+k_2)t} - 1\right)\frac{\varepsilon^{\mathrm{Cl}}}{\varepsilon^{\mathrm{E}}} \quad (9)$$

where the symbols of $A^{\mathrm{E}}{}_0$ and $A^{\mathrm{E}}{}_\infty$ represent the IR absorbance of E form at the start (0 min) and the last (300 min) irradiation times, which can be estimated from the observed spectra to be 1.069 and 0.4069, respectively.

In the least-squares fitting process to obtain the rate constants of k_1 and k_2 from the absorbance changes, the values of $\varepsilon^{\mathrm{R}} / \varepsilon^{\mathrm{E}}$ and $\varepsilon^{\mathrm{Cl}} / \varepsilon^{\mathrm{E}}$ are needed. Since the experimental values of ε were not available in the present study, the author assumed the ratios of ε using the values obtained by the DFT calculations to be 1.123 and 0.9311 for $\varepsilon^{\mathrm{R}} / \varepsilon^{\mathrm{E}}$ and $\varepsilon^{\mathrm{Cl}} / \varepsilon^{\mathrm{E}}$, respectively. Then the parameters k_1 and k_2 were determined to be 0.0046 ± 0.0003 and 0.0037 ± 0.0003 min^{-1}, respectively, where the uncertainty represents one standard deviation. The rate to produce R form was found to be slightly faster than the one to produce Cl form. The calculated IR absorbance values using these obtained values were drawn by solid lines in Fig. 4.5, which reproduced the observed IR absorbance changes satisfactorily. This finding strongly supports Scheme 4.2 for the photoreaction pathways of E form to R form and Cl form upon the UV irradiation (λ > 330 nm) and implies that an intermediate, an electronic excited state to produce R form and Cl form, is non-planar.

4.2.5. Isomerization from R form to Cl form upon UV irradiation (λ > 290 nm)

When the matrix sample was exposed to UV light (λ > 290 nm) following the

300-min UV irradiation (λ > 330 nm), another conformational change was found. The difference spectrum between the spectra measured after minus before 1-min UV irradiation is shown in Fig. 4.6(a) with the calculated spectral patterns of R form and Cl form (Fig. 4.6(b)). It is notable that no spectral change of the reactant, E form, was observed during this short irradiation period because most of E form had already been isomerized to R form or Cl form upon the 300-min preliminary irradiation (λ > 330 nm). The 3565 and 3486 cm^{-1} bands in the O−H stretching region and the 1764 cm^{-1} band in the C=O stretching region assigned to R form decreased, whereas the corresponding 3532, 3464 and 1769 cm^{-1} bands assigned to Cl form increased, indicating that the conformational changes around the OC−OH and Ph−OH single bonds occurred simultaneously upon the shorter-wavelength UV irradiation (λ > 290 nm).

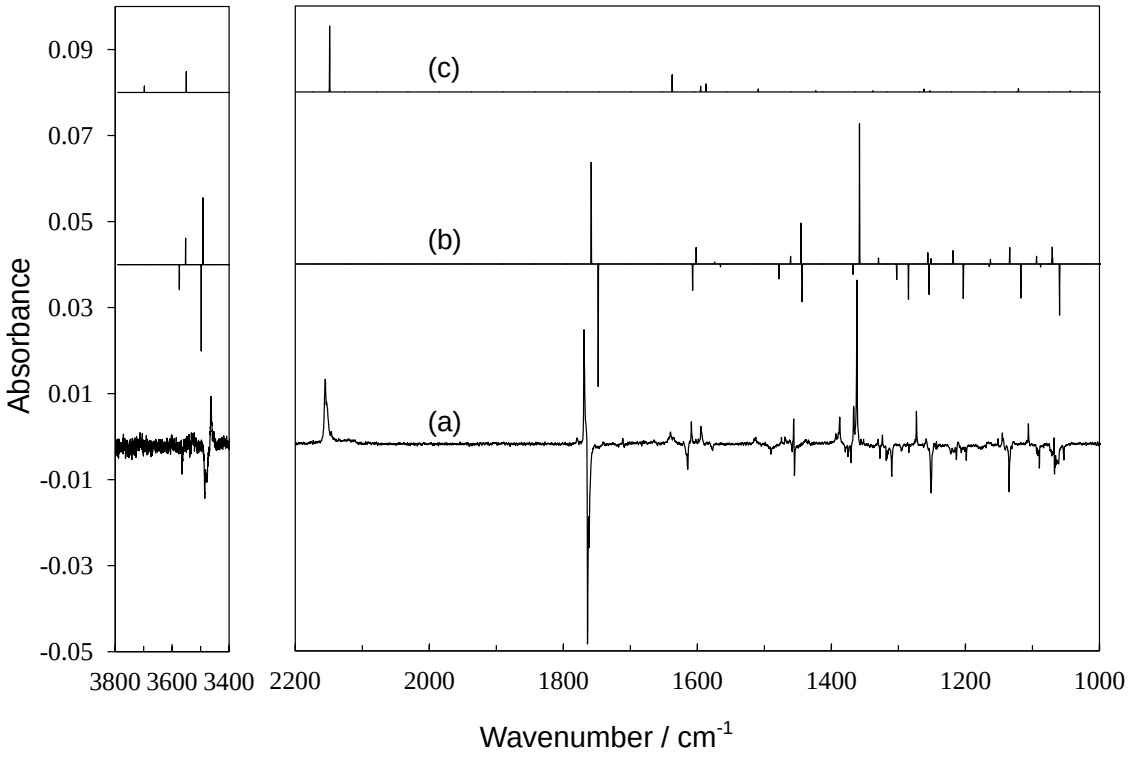

Fig. 4.6. IR spectral change by 1-min UV irradiation (λ > 290 nm) after 300-min UV irradiation (λ > 330 nm): (a) A difference spectrum between the spectra measured after minus before the UV irradiation; (b) calculated spectral patterns obtained at the DFT/B3LYP/6-31++G** level, where R and Cl forms are displayed in the lower and upper sides, respectively; (c) a calculated spectral pattern of K−W1. A linear scaling formula of $0.9894-1.04 \times 10^{-5}\, \nu_{\mathrm{calcd}}$ was used.

4.2.6. Production of the K-W complex upon UV irradiation (λ > 290 nm)

In Fig. 4.6(a), some unassigned bands are left unassigned to R form or Cl form for example 2155, 1640, 1596 and 1513 cm^{-1}. These bands appeared near those of K-W produced from SA. Thus, the author assumed the K-W complex was also produced from R form of 3-CSA. As well as K-W of SA, two kinds of K-W of 3-CSA were optimized by the DFT calculations shown in Fig. 4.7.

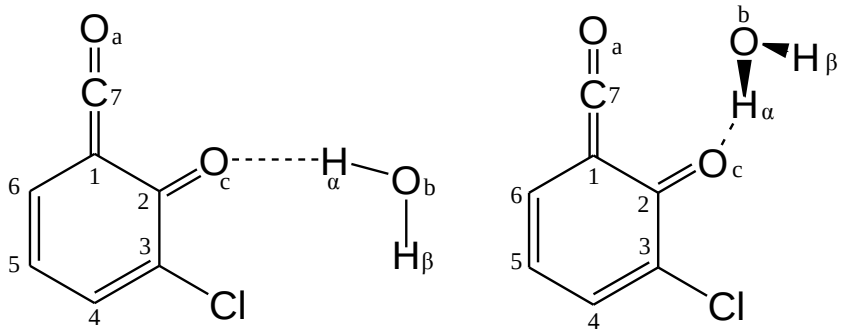

K-W1 (2.4)

K-W2 (0.0)

Fig. 4.7. Optimized structures of ketoketene-water complexes. The numbers in parentheses represent relative energies in kJ mol^{-1} calculated at the DFT/B3LYP/6-31++G** level.

The conformation of water molecule in K-W1 was different from that in K-W1 of SA probably due to the electronic repulsion of lone pairs of the Cl atom and the O atom of the water molecule. Unlike the case of SA, the planar K-W1 is less stable than the non-planar K-W2 by 2.4 kJ mol^{-1}. The author assumes that the repulsion between the lone pairs of the O atom in the C=O part and the substituted Cl atom affects the electron distribution of the O atom and the stabilization energy by the intermolecular hydrogen bond. The optimized geometrical parameters of K-W1 and K-W2 are listed in Table 4.4.

Tabele 4.4. Optimized geometry of K-W. [a,b]

Parameters [c]	K-W1	K-W2
$r(C_7-O_a)$	1.1526	1.1499
$r(C_1-C_7)$	1.3515	1.3560
$r(C_2-O_c)$	1.2354	1.2399
$r(C_1-C_2)$	1.4857	1.4814
$r(C_2-C_3)$	1.4655	1.4641
$r(C_3-C_4)$	1.3658	1.3670
$r(C_4-C_5)$	1.4351	1.4326
$r(C_5-C_6)$	1.3613	1.3624
$r(C_6-C_1)$	1.4437	1.4436
$r(O_b-H_\alpha)$	0.9719	0.9761
$r(O_b-H_\beta)$	0.9643	0.9640
$r(C_3-Cl)$	1.7423	1.7422
$r(O_c\cdots H_\alpha)$	1.9666	1.8826
$\Theta(O_aC_7C_1)$	179.95	176.90
$\Theta(C_7C_1C_2)$	115.04	117.26
$\Theta(C_1C_2O_c)$	121.93	123.10
$\Theta(C_1C_2C_3)$	112.75	112.79
$\Theta(C_2C_3C_4)$	122.33	122.52
$\Theta(C_3C_4C_5)$	122.31	122.15
$\Theta(C_4C_5C_6)$	120.45	120.27
$\Theta(C_5C_6C_1)$	118.56	118.85
$\Theta(C_2O_cH_\alpha)$	149.67	118.21

[a] Calculated at the DFT/B3LYP/6-31++G** level.

[b] Units of r and Θ are Å and deg, respectively.

[c] Numbering of atoms is given in Fig. 4.7.

The C=O stretching mode was calculated to be 1638 and 1629 cm^{-1} in K-W1 and K-W2, respectively. The O−H bending mode was also calculated to be 1587 and 1573 cm^{-1} in K-W1 and K-W2, respectively. Thus the author assumed that not K-W2 but K-W1 was produced by the UV irradiation (λ > 290 nm). The symmetric O−H stretching mode at 3550 cm^{-1} was not clearly observed probably because of the intermolecular hydrogen bond. The reason why the less stable K-W1 was observed may be argon atoms surrounding K-W. The author assumes that it is difficult for the water molecule to interact with K through out-of-plane intermolecular hydrogen bond in solid argon. The observed and calculated wavenumbers of K-W1 are summarized in Table 4.5.

Table 4.5. Observed and calculated wavenumbers (in cm^{-1}) and relative intensities of K−W1.[a]

Obsd.		Calcd.[b]	
v	Int.[c]	*v*	Int.[d]
3704	vw	3698	10.0
-	-	3550	31.7
2155	s	2149	100
1640	m	1638	26.3
1602	w	1596	8.8
1595	w	1587	12.4
1515, 1513	w	1510	4.7
1264	vw	1262	4.5
1126	vw	1121	5.5

[a] Vibrational modes with intensities of less than 4.0 are omitted.

[b-d] See the caption of Table 4.2.

4.2.7. Production of the CPYM-HCl complex upon UV irradiation (λ > 270 nm)

Since no IR bands assignable to H−Cl stretching mode were observed by UV irradiation (λ > 290 nm), it was indicated that the dissociation of HCl from Cl form or the following production of CPYM did not occur. To investigate whether H form can produce the CPYM, the author irradiated shorter-wavelength UV light (λ > 270 nm) following the 300-min UV irradiation (λ > 330 nm). The obtained difference spectra are shown in Fig. 4.8.

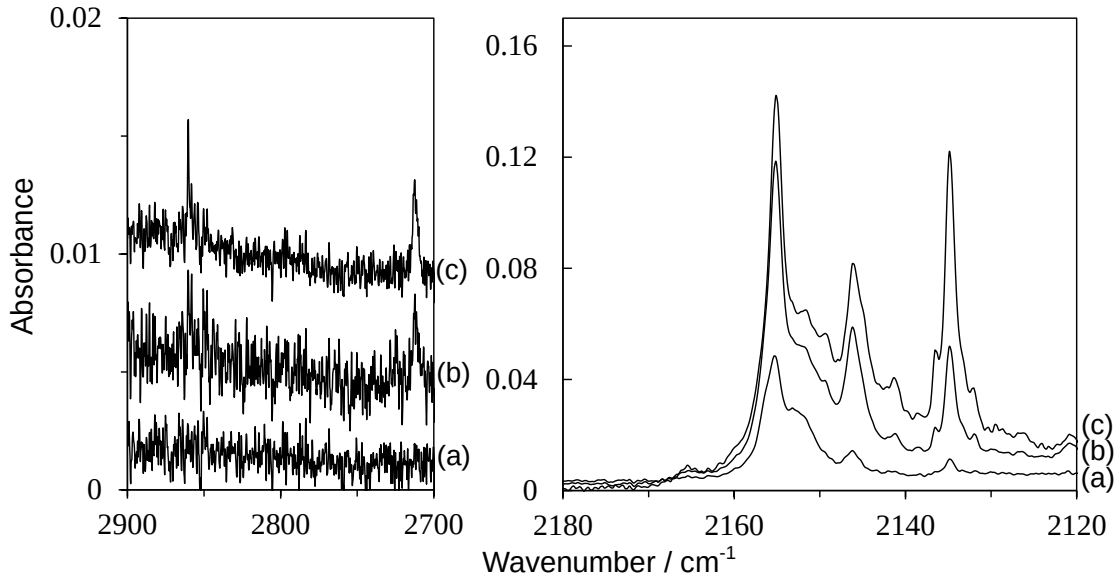

Fig. 4.8. IR spectral changes of SA by UV irradiation (λ > 270 nm) after 300-min UV irradiation (λ > 330 nm): (a) 1-0 min; (b) 10-0 min; (c) 40-0 min.

Both in the H−Cl and C=C=O stretching regions, new bands appeared. In the former region, new bands appeared at 2860 and 2713 cm^{-1}. According to the previous papers on 2-chlorophenol and its derivatives [1,26], the former band seems assigned to the CPYM-HCl having an intermolecular hydrogen bond of C=C=O···H−Cl. In contrast, the latter band has not been reported yet. Thus the author assumed a CPYM-HCl having an intermolecular hydrogen bond between COOH and HCl was produced upon the UV irradiation. In addition to 2155-cm^{-1} band assigned to K-W1, new bands also appeared

in the C=C=O stretching region. While the bands at 2142 and 2135 cm^{-1} are due to carbon monoxide dissociating from the C=C=O group, those at 2153, 2149 and 2146 cm^{-1} seem assignable to the C=C=O stretching modes. These facts imply the CPYM-HCl were produced upon the UV irradiation (λ > 270 nm).

The author performed the DFT calculations to optimize structures of the CPYM-HCl complex, which are shown in Fig. 4.9 together with the energy differences and the calculated wavenumbers of the C=C=O and the H−Cl stretching modes. *Cis* or *trans* means the conformation of the C=O and C=C bonds in the carboxy group and the five-membered ring, respectively. The symbols of a, b and c mean the hydrogen-bonding O atom numbering in Fig. 4.9. By comparison of the observed bands with the calculated ones, productions of *trans*-c or *cis*-c, *trans*-a and *trans*-b were implied. Unfortunately it was hard to assign the IR bands in the fingerprint region because of the bands of E form and R form appearing downward and those of Cl form and K-W1 appearing upward. However, production of the CPYM-HCl from Cl form was implied because the H−Cl and C=C=O stretching bands appeared upon the UV irradiation (λ > 270 nm).

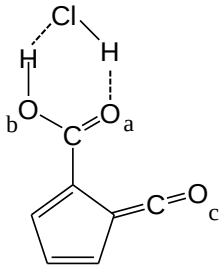

trans-a
(0.00)
[2153, 2350]

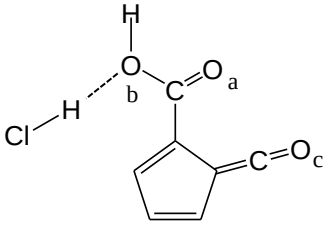

trans-b
(13.8)
[2160, 2729]

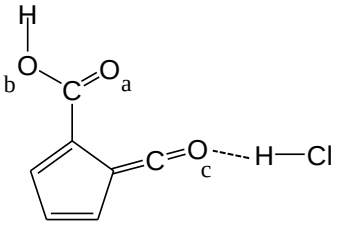

trans-c
(19.6)
[2149, 2870]

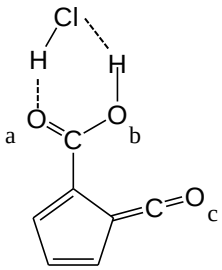

cis-a1
(4.63)
[2152, 2300]

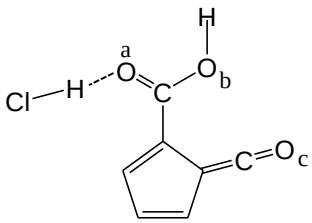

cis-a2
(6.94)
[2151, 2549]

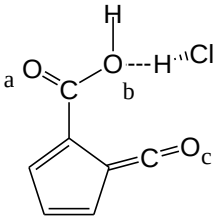

cis-b
(24.4)
[2160, 2738]

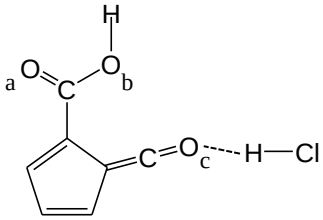

cis-c
(25.9)
[2149, 2871]

Fig. 4.9. Optimized structures of CPYM−HCl. The numbers in parentheses represent relative energies in kJ mol^{-1} obtained at the DFT/B3LYP/6-31++G** level. The numbers in bracket represent calculated wavenumbers of C=C=O and H−Cl stretching modes, where a linear scaling formula of 0.9894–1.04×10^{5}ν_{calcd} was used.

4.2.8. Enol-keto tautomerization

In SA [9,13] and its derivatives including 3,5-dichlorosalicylic acid [7] and 3,5,6-trichlorosalicylic acid [39], it is reported that the enol-keto tautomerization, so called excited-state intramolecular proton transfer (ESIPT), occurs upon UV irradiation [9−14,18,20,5−7,39−42]. These studies were carried out in solution or in supersonic jet expansion by fluorescence spectroscopy. No IR spectrum of keto form has been reported so far, implying that no potential local minimum at keto form is located on the ground state, which was confirmed by the DFT calculation [16,6,7,39,40]. In the present study on 3-CSA, the IR spectra of three enol forms, E, R and Cl forms, were observed in a low-temperature argon matrix, but not keto form. The author also tried to optimize the geometrical structure of keto form of 3-CSA by the DFT calculation, resulting in the conclusion that only enol forms can be optimized. Therefore the author assumes that keto form is not produced upon UV irradiation in a low-temperature argon matrix.

4.3. Summary

Conformations of 3-CSA were investigated by low-temperature matrix-isolation infrared spectroscopy. Only the most stable conformer, E form existed in the argon matrix. Cl form was produced upon UV irradiation (λ > 330 nm), in addition to R form with the IMHB of Ph−OH···OH in the carboxy group, the second stable conformer. The conformational change from R form to Cl form was induced by UV irradiation (λ > 290 nm) following the 300-min UV irradiation (λ > 330 nm). As well as SA, the K-W complex was produced from R form in 3-CSA. Since new bands appeared in the H−Cl and C=C=O stretching regions, production of CPYM-HCl complex from Cl form was also implied upon UV irradiation (λ > 270 nm). The whole reaction pathways are summarized in Scheme 4.3.

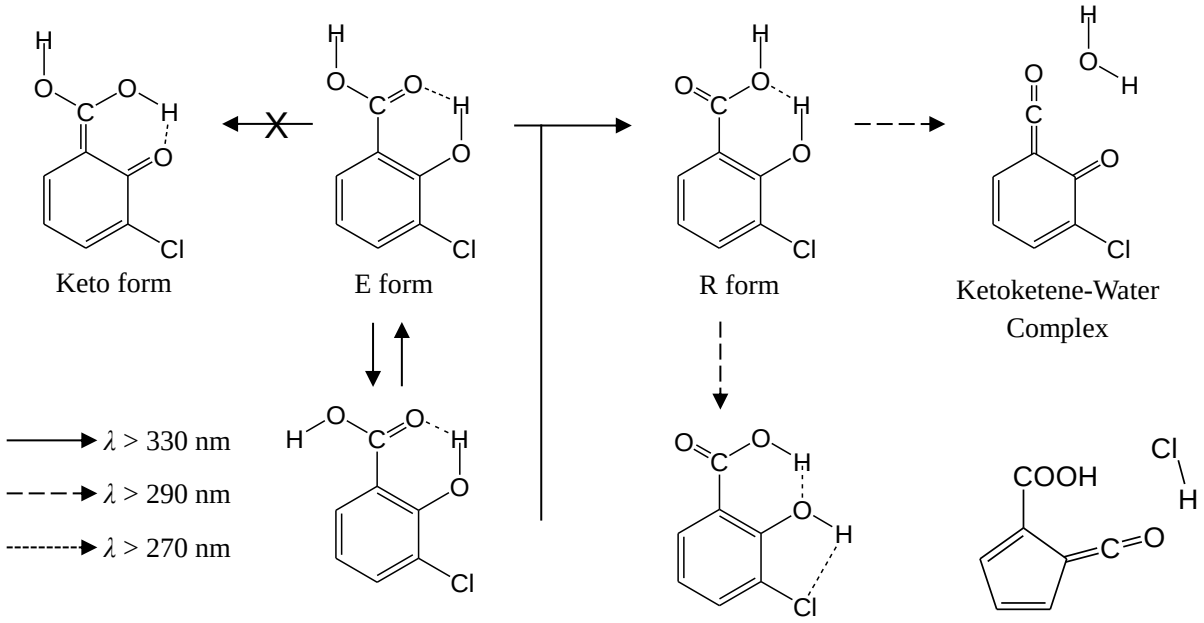

Scheme 4.3. Photoreaction pathways of 3-chlorosalicylic acid.

4.4. References

[1] N. Akai, S. Kudoh, M. Takayanagi, M. Nakata, J. Photochem. Photobiol. A 146 (2001) 49.

[2] J. Sabate, M.A. Anderson, H. Kikkawa, M. Edwards, C.G. Hill, Jr., J. Catal. 127 (1991) 167.

[3] J. Sabate, M.A. Anderson, H. Kikkawa, Q. Xu, S. C-March, C.G. Hill, Jr., J. Catal. 134 (1992) 36.

[4] B.K. Paul, A. Samanta, N. Guchhait, Photochem. Photobiol. Sci. 9 (2010) 57.

[5] B.K. Paul, A. Samanta, N. Guchhait, J. Mol. Struct. 977 (2010) 78.

[6] B.K. Paul, A. Samanta, N. Guchhait, J. Fluoresc. 21 (2011) 1265.

[7] B.K. Paul, N. Guchhait, Chem. Phys. 403 (2012) 94.

[8] M.J. Wojcik, Chem. Phys. Lett. 83 (1981) 503.

[9] H.C. Joshi, H.B. Tripathi, T.C. Pant, D.D. Pant, Chem. Phys. Lett. 173 (1990) 83.

[10] D.D. Pant, H.C. Joshi, P.B. Bisht, H.B. Tripathi, Chem. Phys. 185 (1994) 137.

[11] P.B. Bisht, H. Petek, K. Yoshihara, J. Chem. Phys. 103 (1995) 5290.

[12] G.S. Denisov, N.S. Golubev, V.M. Schreiber, Sh.S. Shajakhmedov, A.V. Shurukhina, J. Mol. Struct. 381 (1996) 73.

[13] G.S. Denisov, N.S. Golubev, V.M. Schreiber, Sh.S. Shajakhmedov, A.V. Shurukhina, J. Mol. Struct. 436-437 (1997) 153.

[14] F. Lahmani, A. Zehnacker-Rentien, Chem. Phys. Lett. 271 (1997) 6.

[15] A.L. Sobolewski, W. Domcke, Chem. Phys. 232 (1998) 257.

[16] I. Rodriguez-Santiago, M. Sodupe, A. Oliva, J. Bertran, J. Am. Chem. Soc. 121 (1999) 8882.

[17] S. Nagaoka, H. Teramae, U. Nagashima, Bull. Chem. Soc. Jpn. 82 (2009) 570.

[18] I.P. Pozdnyakov, A. Pigliucci, N. Tkachenko, V.F. Plyusnin, E. Vauthey, H. Lemmetyinen, J. Phys. Org. Chem. 22 (2009) 449.

[19] C. Chen, S.-F. Shyu, J. Mol. Struct. (Theochem) 536 (2001) 25.

[20] E.A. El-Hakam Abou El-Nasr, A. Fujii, T. Ebata, N. Mikami, Chem. Phys. Lett. 376 (2003) 788.

[21] T. Yahagi, A. Fujii, T. Ebata, N. Mikami, J. Phys. Chem. A 105 (2001) 10673.

[22] S. Nanbu, M. Sekine, M. Nakata, J. Mol. Struct. 1025 (2012) 69.

[23] N. Akai, S. Kudoh, M. Takayanagi, M. Nakata, Chem. Phys. Lett. 363 (2002) 591.

[24] N. Akai, S. Kudoh, M. Nakata, J. Photochem. Photobiol. A 169 (2005) 47.
[25] S. Nanbu, M. Sekine, M. Nakata, J. Phys. Chem. A 115 (2011) 9911.
[26] M. Nagaya, S. Iizumi, M. Sekine, M. Nakata, J. Mol. Struct. 1025 (2012) 53.
[27] N. Akai, S. Kudoh, M. Takayanagi, M. Nakata, Chem. Phys. Lett. 363 (2002) 591.
[28] N. Akai, S. Kudoh, M. Nakata, J. Phys. Chem. A 107 (2003) 3635.
[29] S. Nishino, M. Nakata, J. Phys. Chem. A 111 (2007) 7041.
[30] M. Nagaya, S. Kudoh, M. Nakata, Chem. Phys. Lett. 427 (2006) 67.
[31] M. Nagaya, S. Kudoh, M. Nakata, Chem. Phys. Lett. 432 (2006) 446.
[32] K. Ujike, S. Kudoh, M. Nakata, Chem. Phys. Lett. 409 (2005) 52.
[33] K. Ujike, S. Kudoh, M. Nakata, Chem. Phys. Lett. 396 (2004) 288.
[34] S. Nishino, M. Nakata, J. Mol. Struct. 875 (2008) 520.
[35] S.G. Stepanian, I.D. Reva, E.D. Radchenko, G.G. Sheina, Vib. Spectrosc. 11 (1996) 123.
[36] C. Zhang, M. Chen, J. Mol Struct. 1037 (2013) 144.
[37] A.Y. Ivanov, S.G. Stepanian, L. Adamowicz, J. Mol. Struct. 1025 (2012) 92.
[38] A.U. Acuna, F.Amat-Guerri, J. Calalan, F.Gonzalez-Tablas, J. Phys. Chem. 84 (1980) 629.
[39] A. Weller, Elektrochemistry 60 (1956) 1144.
[40] A. Weller, Prog. React. Kinet. 1 (1961) 187.
[41] L. Helmbrook, J.E. Kenny, B.E. Kohler, G.W. Scott, J. Phys. Chem. 87 (1083) 280.
[42] F. Lahmani, A. Zehnacker-Rentien, J. Phys. Chem. A 101 (1997) 6141.

Chapter 5: Photoreaction of 2-Pyridinecarboxylic Acid

Abstract

Conformational changes of 2-pyridinecarboxylic acid upon UV irradiation have been investigated by low-temperature matrix-isolation infrared spectroscopy. It is found that only one conformer having an intramolecular hydrogen bond of COOH···N in the pyridine ring exists in argon matrices after deposition before UV irradiation in contrast to a result in CCl_4 solution reported previously. The hydrogen bond is broken by UV irradiation, resulting in two less stable conformers; one increases immediately at the early irradiation time and the other increases slowly during the prolonged irradiation time. The conformations around the OC−OH and C−COOH bonds of the photoproducts are identified by assignments of IR bands measured in an argon matrix with an aid of the density-functional-theory calculation. Photoreaction pathways on the conformational changes are proposed and supported by a kinetic analysis using IR absorbance changes of the reactant and the photoproducts against the irradiation time.

5.1. Introduction

In chapter 1, the author described the difficulty to observe the *trans* conformation around the OC−OH bond in carboxylic acids, and the stabilization of the *trans* by the formation of an intramolecular hydrogen bond (IMHB, hereafter) [10]. Since the higher the energy barrier is, the lower the rate of the hydrogen-atom tunneling is, the potential energy curve of the *cis* and the *trans* conformers is important in relation to the stabilization energy by the IMHB. In chapter 3 and 4, the author found the photoproduction of *trans* conformer of salicylic and 3-chlorosalicylic acid, which exists stably due to the strong IMHB of COOH···OH−Ph. However, Cl form in 3-chlorosalicylic acid is still less stable than E form despite of the two IMHBs (Fig. 4.1). This fact indicates that the strength of IMHB is much affected by the hybrid orbital of the lone pair.

Unlike the benzene ring, the heterocyclic ring such as pyridine contains a lone pair of the hetero atom, which can form an IMHB with the H atom in the carboxy group. The author assumed such an IMHB may stabilize the *trans* conformer greatly if it

originates from the sp^2 hybrid orbital. In this point, 2-pyridinecarboxylic acid (Fig. 5.1) has a possibility that the *trans* conformation is the most stable due to the strong IMHB of COOH···N.

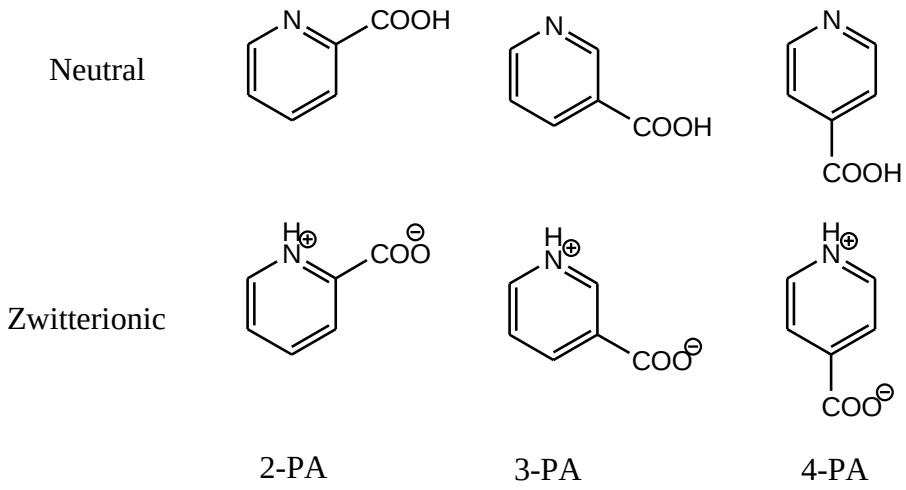

Fig. 5.1. Three structural isomers and their zwitterionic forms of PA.

Pyridinecarboxylic acids (PAs, hereafter) are used for food supplements and active agents in drugs as metal complexes and heterodimers with other carboxylic acids [11−14]. Since PA has a hydrogen donor in the carboxy group and a hydrogen acceptor of the lone pair at the N atom in the pyridine ring, it remains controversial whether they exist predominantly as a neutral form or a zwitterionic form in an isoelectric aqueous solution. As for 3-PA, where the carboxy group is bonded at the third position of the pyridine ring, it was once considered to be present predominantly as a neutral form [15,16], but it has later been concluded that PAs are predominantly present as a zwitterionic form [17−20].

In contrast to the results in aqueous solutions, PAs are expected to be present as a neutral form in non-polar solutions. If this is true, only 2-PA among the three neutral forms of PAs has a conformer named TT in Fig. 5.2, being stabilized by the IMHB of COOH···N in the pyridine ring. The former letter T denotes *trans* conformation of the O

atom in the C=O part against the N atom in the pyridine ring, while the latter T denotes *trans* conformation of the O−H part against the C=O part. Ōki et al. reported the infrared (IR) absorption bands of 2-PA in CCl_4 solution and identified a non-hydrogen-bonded conformer, named TC in Fig. 5.2, besides the hydrogen-bonded conformer TT [21]. However, the resolution of their observed assignments of the two C=O stretching bands to TT and TC in the CCl_4 solution did not seem to provide correct identification of the slight difference in the position of the H atom in the COOH group in view of the wide widths of the IR bands in the solution. In addition, the relative energy of the less stable conformer is estimated to be 15.3 kJ mol^{-1} higher than that of TT [22] by a quantum chemical calculation at the DFT/B3PW91/6-311++G** level, implying that the population of TC is so small that identification of TC is hard at room temperature judging from the Boltzmann distribution law.

The finding for 2-PA that the *trans* conformation around the OC−OH bond (TT) is more stable than the *cis* conformation (TC) totally contrasts with general carboxylic acids, because the *trans* conformation is destabilized by the repulsion of lone pairs in the two O atoms in the COOH group. For example, the less stable conformers, *trans*, in formic acid [23−25], acetic acid [23,26−27], propionic acid [23,28], and benzoic acid [29] are produced from the more stable conformers, *cis*, by IR radiation and return to *cis* in darkness through hydrogen-atom tunneling. Another example is reported that the *trans* conformer of 2-chlorobenzoic acid produced from the *cis* conformer by UV irradiation is unable to exist stably even in a low-temperature argon matrix in spite of the stabilization due to the IMHB of COOH···Cl [30]. It is assumed that the *trans* conformer immediately returns to the *cis* conformer through hydrogen-atom tunneling. Thus, it is required to confirm that the most stable conformer of 2-PA, where the C−Cl part of 2-chlorobenzoic acid is replaced by the N atom in the pyridine ring, is *trans* around the OC−OH bond in the carboxy group and that the *cis* conformer of 2-PA is negligible at room temperature.

In the present study, the author has investigated the conformation of 2-PA monomer using the low-temperature matrix-isolation IR spectroscopy. 2-PA has two possible conformations, *trans* and *cis*, around the C−COOH and OC−OH bonds, resulting in the four conformers shown in Fig. 5.2. To confirm that only TT exists stably at room temperature, the author has measured IR spectra of a low-temperature argon-matrix

sample and performed vibrational assignments with an aid of the density-functional-theory (DFT) calculation. In addition, the author has measured the IR spectra of less stable conformers produced from the most stable conformer by UV irradiation and determined their conformations around the C−COOH and OC−OH bonds by comparison of the observed spectra with the spectral patterns obtained by the DFT calculation. This combined technique is one of the most effective methods to stabilize less stable conformers with a small amount of population and distinguish slight differences due to conformational changes, as shown in recent papers and the references therein [31−36].

5.2. Results and discussion

5.2.1. Optimized geometrical structures of 2-PA by DFT calculations

The Four conformers of 2-PA shown in Fig. 5.2 were optimized by the DFT calculations. Among the four conformers, only CT is non-planar so as to avoid the steric hindrance between the two H atoms; one is in the O−H group and the other is bonded to the pyridine ring. The optimized geometrical parameters of the four conformers are listed in Table 5.1, where the numbering of carbon atoms is denoted in Fig. 5.2.

The calculated relative energies of the four conformers are listed in Fig. 5.2 after the correction of zero-point vibrational energy, showing that TT is the most stable conformer. This result is in contrast to the fact that general carboxylic acids prefer *cis* to *trans* conformation about the OC−OH bond in the carboxy group [11−17], as described in the previous section, implying that TT of 2-PA is strongly stabilized by the IMHB of COOH···N despite of the electronic repulsion between lone pairs of the two O atoms in the carboxy group. This is supported by comparison of the O−H bond length; the *r*(O−H) of TT is longer than that of other conformers by ~0.01 Å as shown in Table 5.1.

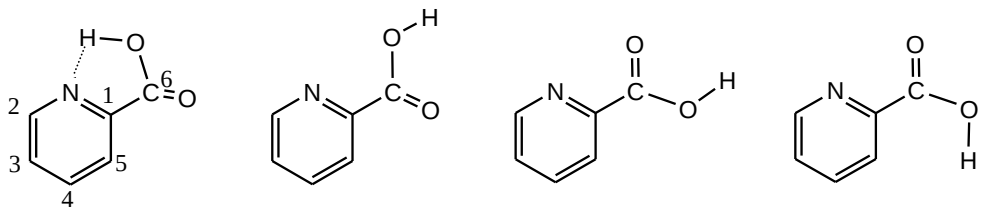

TT	TC	CC	CT
(0.00)	(12.4)	(17.9)	(47.7)
[1.0]	[6.6×10^{-3}]	[7.2×10^{-4}]	[4.4×10^{-9}]

Fig. 5.2. Four possible conformers of 2-PA and numbering of carbon atoms. The numbers in parentheses represent calculated relative energies in kJ mol-1. The numbers in square brackets represent population ratios according to the Boltzmann distribution law at the deposition temperature of 298 K using the calculated relative energies.

Table 5.1

Optimized geometry of four conformers of 2-PA.[a,b]

Parameters[c]	TT	TC	CC	CT
$r(C_1-N)$	1.342	1.341	1.341	1.340
$r(N-C_2)$	1.338	1.336	1.334	1.336
$r(C_2-C_3)$	1.398	1.399	1.400	1.400
$r(C_3-C_4)$	1.396	1.395	1.393	1.393
$r(C_4-C_5)$	1.395	1.394	1.396	1.396
$r(C_5-C_1)$	1.396	1.400	1.401	1.402
$r(C_1-C_6)$	1.510	1.501	1.504	1.514
$r(C_6=O)$	1.211	1.218	1.209	1.203
$r(C_6-O)$	1.343	1.346	1.363	1.365
$r(O-H)$	0.981	0.972	0.971	0.968
$r(N\cdots H)$	2.009	—	—	—
$\Theta(C_6-C_1-N)$	115.6	118.5	115.4	115.8
$\Theta(C_1-C_6=O)$	123.1	123.3	125.8	124.1
$\Theta(C_1-C_6-O)$	114.0	113.9	111.9	115.4
$\Theta(C_6-O-H)$	107.0	106.3	106.5	110.8
$\Theta(C_5-C_1-C_6)$	120.8	117.9	121.3	120.9
$\tau(H-O-C=O)$	180.0	0.0	0.0	−171.3
$\tau(H-O-C_6-C_1)$	0.0	180.0	180.0	10.5
$\tau(O=C_6-C_1-N)$	180.0	180.0	0.0	42.0
$\tau(O-C_6-C_1-N)$	0.0	0.0	180.0	−139.8

[a] Calculated at the DFT/B3LYP/6-31++G** level.

[b] The unit of bond length r is Å, and the units of bond angle Θ and torsional angle τ are degrees.

[c] Numbering of carbon atoms is given in Fig. 5.2.

5.2.2. IR spectrum after deposition before UV irradiation

An IR spectrum of 2-PA in an argon matrix measured after deposition is shown in Fig. 5.3(a). The population ratio of the second most stable conformer TC over TT is estimated to be 6.6×10^{-3} according to the Boltzmann distribution law at 298 K, using the calculated relative energies shown in Fig. 5.2. Thus the author can expect that all the IR bands measured after deposition are assignable to TT, but not to other conformers.

By comparison of the observed matrix spectrum with the calculated spectral patterns of the four conformers, the author has found that most of the observed bands are consistent with TT (Fig. 5.3(b)). The strongest band appearing at 1349 cm^{-1} is assigned to the C−O−H in-plane bending mode. The C=O stretching band splits into two peaks at 1773 and 1791 cm^{-1}, probably due to the Fermi resonance and/or the matrix effect. The band observed at 3339 cm^{-1} is relatively broad and shifts toward lower-wavenumber side from the corresponding calculated value, 3409 cm^{-1}, indicating that the effect due to the IMHB of COOH···N is strong. The largely splitting bands around 1400 cm^{-1} may be due to a combination mode of the bands appearing at 710 and 692 cm^{-1}, which are assigned to C−O−H out-of-plane and C−H out-of-plane bending modes, respectively. The observed and calculated wavenumbers and the relative intensities of TT are summarized in Table 5.2.

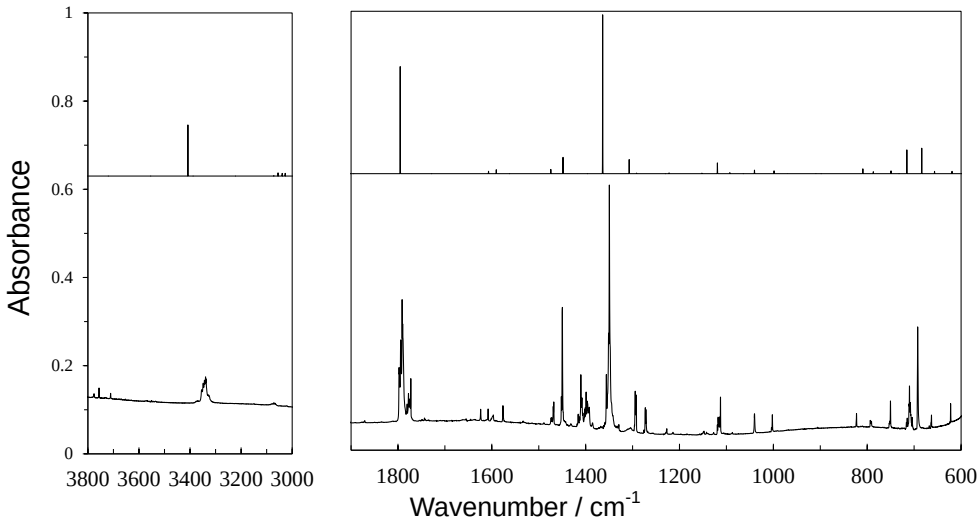

Fig. 5.3. IR spectra of 2-PA: (a) an observed spectrum after deposition; (b) a spectral pattern of TT calculated at the DFT/B3LYP/6-31++G** level. Scaling factors of 0.98 and 0.95 are used in the regions lower and higher than 2000 cm^{-1}, respectively. Bands with an asterisk are due to H_2O.

Table 5.2 Observed and calculated wavenumbers (in cm^{-1}) and relative intensities of TT.

Obsd.		Calcd.[a]	
v	Int.[b]	*v*	Int.[c]
3339	m	3409	32.0
1791, 1773	s	1795	67.4
1597	w	1607	1.6
1576	w	1591	2.5
1472, 1468	w	1474	2.7
1452, 1450	s	1448	10.3
1410, 1408, 1399, 1396	m	(692+710)	
1356, 1351, 1349	vs	1364	100.0
1294, 1292, 1273, 1272	m	1307	8.9
		1292	0.4
1227	w	1222	0.5

Table 5.2 Observed and calculated wavenumbers (in cm^{-1}) and relative intensities of TT (Continue).

1148	w	1152	0.3
1118, 1114	m	1119	6.8
1087	vw	1093	0.7
1040	w	1040	2.2
		1003	0.0
1002	w	999	1.8
		970	0.1
		909	0.1
823	w	809	3.0
794, 790	w	787	1.2
752, 750	m	749	1.8
715, 710, 704	m	716	15.0
692	s	684	16.1
663	w	657	1.5
622	m	619	1.5

[a] Calculated at the DFT/B3LYP/6-31++G** level. Scaling factors of 0.98 and 0.95 are used in the regions lower and higher than 2000 cm^{-1}, respectively.

[b] Letters of vs, s, m, w and vw denote very strong, strong, medium, weak, and very weak intensities, respectively.

[c] Relative intensities.

The observed matrix IR spectrum shows no trace of other conformers except for TT, leading to the conclusion that only TT exists in the gas phase at room temperature as expected from the relative population ratio described earlier. This finding is inconsistent with the result in CCl_4 solution reported by Ōki et al. [21]. They assigned a 3535-cm^{-1} band to TC, and also assigned two bands at 1783 and 1772 cm^{-1} in the C=O stretching region to TT and TC, respectively. One may claim that the latter two bands appear in Fig. 5.3(a). However, the observed matrix spectrum shows no band in the O−H stretching region except for the 3339 cm^{-1} band of TT.

It is known that the hydrogen-atom tunneling occurs in the COOH group of general carboxylic acids [11−17], from the less stable *trans* to the more stable *cis*. The author kept the matrix sample in darkness or annealed it from 10 to 27 K to confirm whether the hydrogen-atom tunneling occurs or not. However, no IR spectral change from TT to TC was observed, indicating neither hydrogen-atom tunneling nor thermal rotational isomerization around the OC−OH bond occurs in 2-PA. This is because TT is stabilized by the strong IMHB and the barrier height for isomerization from TT to TC becomes relatively high, 56.2 kJ mol^{-1}. The potential energy curve between TT and TC is drawn in Fig. 5.4(a). This finding is consistent with the proposition of Barnes, who claimed that thermal rotational isomerization around a single bond occurs at a matrix temperature lower than 27 K, if its barrier height is lower than 8 kJ mol^{-1}. The value of the barrier hight is also quite larger than that from the *cis* to the *trans* of benzoic acid derivatives, ca. 20 kJ mol^{-1} calculated at MP2/cc-pVDZ level [29], resulting in no hydrogen-atom tunneling in 2-PA.

One may claim that TC exists after the deposition but isomerizes to TT by thermal isomerization or hydrogen-atom tunneling. However, the barrier height for isomerization from TC to TT is calculated to be 43.8 kJ mol^{-1}, which is high enough for TC to exist stably in an argon matrix. Such a high barrier originates from the fact that the destabilization due to the electronic repulsion between the N and O atoms in the transition state. Furthermore, TC does not isomerize to TT by the hydrogen-atom tunneling, as described in the following section. Thus our observation leads to the conclusion that only TT existed in an argon matrix.

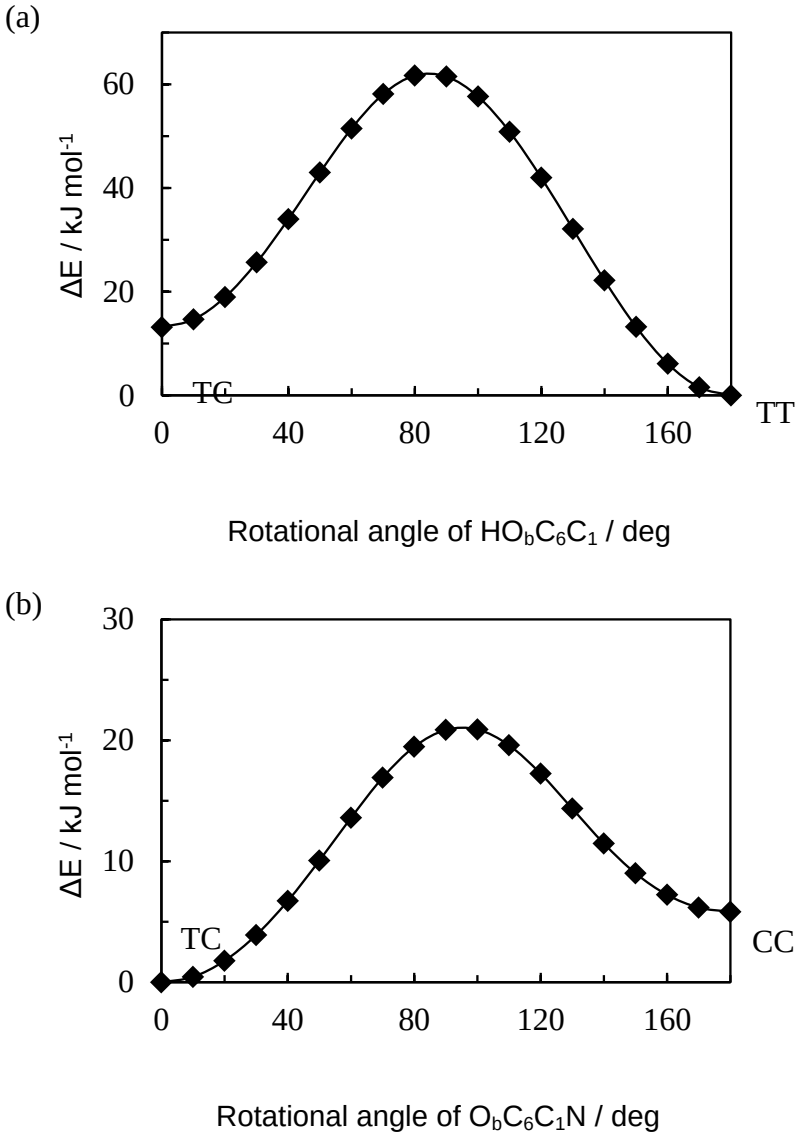

Fig. 5.4. Potential energy curves for isomerization (a) between TT and TC, and (b) between TC and CC by IRC calculation at the DFT/B3LYP/6-31++G** level.

5.2.3. Conformational changes of 2-PA upon UV irradiation

When the matrix sample was exposed to UV light without optical filters, IR spectral changes were observed. The difference spectra between those measured after minus before the UV irradiation for 5 and 100 min are shown in Figs. 5.5(a) and (b), respectively, where the decreasing and increasing bands represent the reactant, TT, and its photoproducts, respectively. A new band at 3562 cm^{-1} in the O−H stretching region appears upon 5-min irradiation (Fig. 5.5(a)), the wavenumber of which is higher than that of TT, indicating that the new conformer has no IMHB of COOH···N unlike TT. A new band splitting at 1750 and 1754 cm^{-1} appears in the C=O stretching region. The wavenumber is lower than that of TT, implying that it is influenced by the IMHB of C=O···HC in the pyridine ring. To determine which conformer is produced upon the UV irradiation, the author compared the observed spectrum with the calculated spectral patterns of TC, CC and CT. As a result, most of the increasing bands in Fig. 5.5(a) were found to be assignable to TC, which has the IMHB of C=O···HC in the pyridine ring. The influence of this IMHB is supported by the calculation result that the bond length of $r(C_6{=}O)$ and the bond angle of $\Theta(C_5{-}C_1{-}C_6)$ of TC are is longer and smaller than the corresponding values of other conformers, as shown in Table 5.1.

It is noteworthy that the 3562-cm^{-1} band in the O−H stretching and the 1750- and 1754-cm^{-1} bands in the C=O stretching modes are close to the 3535- and 1772-cm^{-1} bands in CCl_4 solution reported by Ōki et al. [21]. If their assignments are valid, the stabilization due to the interaction between 2-PA and CCl_4 may enable the existence of TC in the solution at room temperature, although TC never exists in the gas phase and in the argon matrices before UV irradiation.

Some additional new bands appear during the prolonged 100-min irradiation, which are denoted by arrows in Fig. 5.5(b). The O−H stretching mode of the new photoproduct, appearing at 3571 cm^{-1}, is 9 or 232 cm^{-1} higher than that of TC or TT, respectively. This finding suggests that the new conformer has no IMHB of COOH···N like TC. The C=O stretching band appears at 1796 and 1780 cm^{-1}, which is close to that of TT but far from that of TC by 40−30 cm^{-1}, suggesting that the new conformer has no IMHB between C=O···HC unlike TC. In fact, the bands appearing newly are reproduced by the calculated spectral pattern of CC, denoted by broken lines in Fig. 5.5(c). The observed

and calculated wavenumbers and the relative intensities of TC and CC are summarized in Table 5.3.

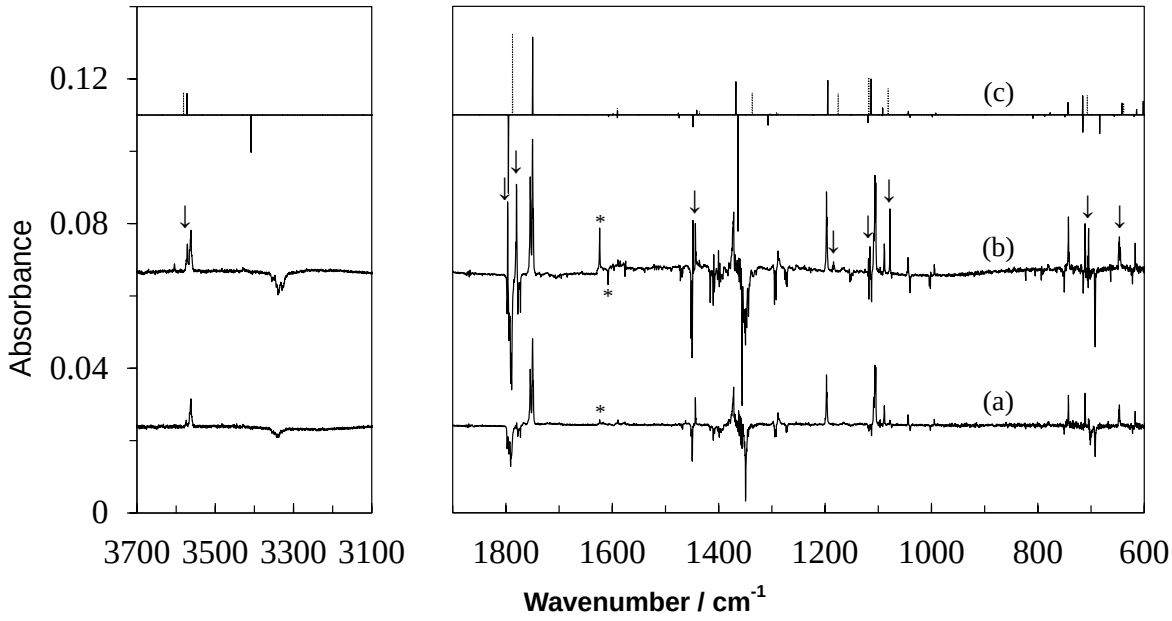

Fig. 5.5. IR spectral changes of 2-PA upon UV irradiation without optical filters: (a) and (b) observed difference spectra between the spectra measured after minus before the UV irradiation for 5 and 100 min, respectively; (c) spectral patterns of TT (lower side), TC (upper side, solid line) and CC (upper side, dotted line) calculated at the DFT/B3LYP/6-31++G** level. Scaling factors of 0.98 and 0.95 are used in the regions lower and higher than 2000 cm^{-1}, respectively. Bands with an asterisk are due to H_2O. Bands with an arrow in (b) are assigned to CC.

Table 5.3 Observed and calculated wavenumbers (in cm^{-1}) and relative intensities of TC and CC.

TC				CC			
Obsd.[a]		Calcd.[b]		Obsd.[c]		Calcd.[b]	
v	Int.[d]	*v*	Int.[e]	*v*	Int.[d]	*v*	Int.[e]
3562	s	3573	27.8	3571	m	3581	27.9
1754,1750	vs	1750	100.0	1796,1780	vs	1788	100.0
		1599	1.6			1597	0.4

Table 5.3 Observed and calculated wavenumbers (in cm^{-1}) and relative intensities of TC and CC (Continue).

1589	w	1590	5.2	1585	w	1591	8.1
1474	w	1476	2.5	1448	m	1476	0.2
1444	m	1441	6.1			1436	4.1
1372,1374	s	1368	42.7	1339	w	1337	27.2
		1304	0.2			1304	1.2
1288,1286	w	1289	1.3	1295	w	1291	3.4
1197	s	1195	44.3	1184	w	1176	26.0
		1151	0.5			1156	0.3
1106,1105	s	1114	46.1	1116	m	1118	45.9
1089	m	1092	9.1	1078	s	1082	32.3
1044	w	1044	4.4	1046	w	1046	1.9
995	w	992	2.5	1001	w	991	1.8
		972	0.2			972	0.1
		910	0.2			908	0.1
		821	0.7			822	0.7
780	w	777	2.9			771	1.4
742	m	744	16.0	741	w	743	10.2
711	m	716	24.7	705	m	707	24.0
647	m	642	15.2	645	w	639	14.5
619	m	615	7.1			614	3.1

[a] Increasing during the early irradiation period and decreasing upon the shorter-wavelength cut-off UV irradiation (λ > 270 nm).

[b] Calculated at the DFT/B3LYP/6-31++G** level. Scaling factors of 0.98 and 0.95 are used in the regions lower and higher than 2000 cm^{-1}, respectively.

[c] Increasing during the prolonged irradiation period and being constant upon the shorter-wavelength cut-off UV irradiation (λ > 270 nm).

[d] Letters of vs, s, m and w denote very strong, strong, medium, and weak intensities, respectively.

[e] Relative intensities.

When the matrix sample was exposed to shorter-wavelength cut-off UV light (λ > 270 nm) following the 100-min UV irradiation without optical filters, a back reaction from TC to TT was observed. The difference spectrum between the spectra measured after minus before the UV irradiation (λ > 270 nm, 30 min) is shown in Fig. 5.6(a) with the calculated spectral patterns of TC and TT (Fig. 5.6(b)). For example, the intensity of the band at 3562 cm^{-1} in the O−H stretching region and those at 1750 and 1754 cm^{-1} in the C=O stretching region of TC decrease, whereas the intensities of corresponding bands at 3339, 1773 and 1791 cm^{-1} of TT increase. Thus the author concludes that the back reaction from TC to TT occurs and confirms that the vibrational assignments of TC and CC summarized in Table 5.3 are correct. Since the bands of CC do not change upon the UV irradiation with λ > 270 nm, the author proposes Scheme 5.1 as the photoreaction pathways of 2-PA.

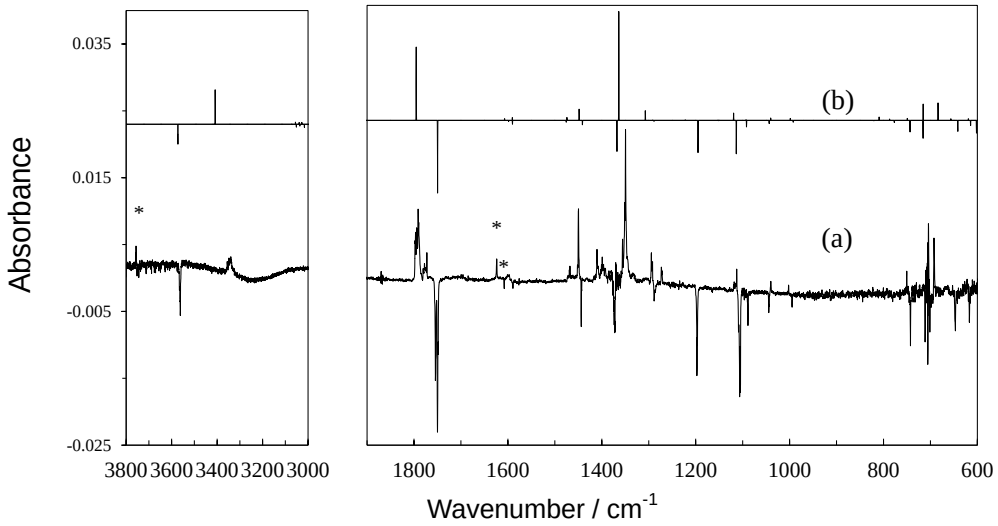

Fig. 5.6. IR spectral changes of 2-PA by 30-min UV irradiation (λ > 270 nm) after 100-min UV pre-irradiation without optical filters: (a) observed difference spectrum between the spectra measured after minus before the UV irradiation; (b) spectral patterns of TC (lower side) and TT (upper side) calculated at the DFT/B3LYP/6-31++G** level. Scaling factors of 0.98 and 0.95 are used in the regions lower and higher than 2000 cm^{-1}, respectively. Bands with an asterisk are due to H_2O.

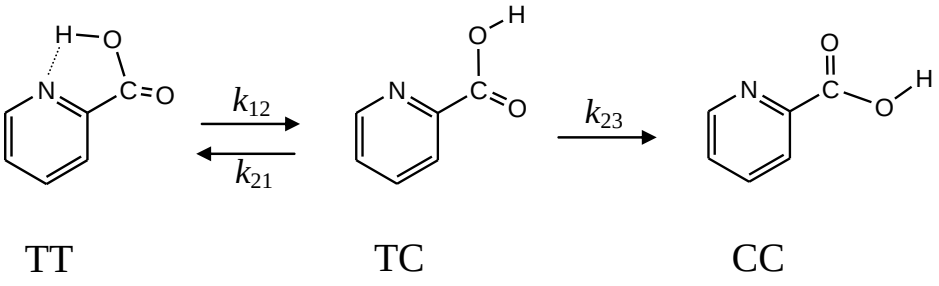

Scheme 5.1. Photoreaction pathways of 2-PA.

5.2.4. Kinetic analysis

To confirm the reaction pathways shown in Scheme 5.1, the author examined the absorbance changes of IR bands against the UV irradiation time. If Scheme 5.1 is true, the corresponding rate equations can be derived from a general kinetic theory as follows [37]:

$$\frac{\mathrm{d}}{\mathrm{d}t}[\mathrm{TT}] = -k_{12}[\mathrm{TT}] + k_{21}[\mathrm{TC}] \quad (1)$$

$$\frac{\mathrm{d}}{\mathrm{d}t}[\mathrm{TC}] = k_{12}[\mathrm{TT}] - k_{21}[\mathrm{TC}] - k_{23}[\mathrm{TC}] \quad (2)$$

$$\frac{\mathrm{d}}{\mathrm{d}t}[\mathrm{CC}] = k_{23}[\mathrm{TC}] \quad (3)$$

where the concentrations of TT, TC and CC in the argon matrix are denoted as [TT], [TC] and [CC], respectively. The rate constants k_{12}, k_{21} and k_{23} are defined in Scheme 5.1. By solving the differential equations (1) − (3), the concentration of each conformer can be obtained using the concentration of TT at the start of UV irradiation, $[\mathrm{TT}]_0$, as follows:

$$[\mathrm{TT}] = [\mathrm{TT}]_0 \left(\frac{k_{12}(p-k_{23})}{p(p-q)} \mathrm{e}^{-pt} + \frac{k_{12}(k_{23}-q)}{q(p-q)} \mathrm{e}^{-qt} \right) \quad (4)$$

$$[\mathrm{TC}] = [\mathrm{TT}]_0 \left(-\frac{k_{12}}{p-q} \mathrm{e}^{-pt} + \frac{k_{12}}{p-q} \mathrm{e}^{-qt} \right) \quad (5)$$

$$[\mathrm{CC}] = [\mathrm{TT}]_0 \left(\frac{k_{12}k_{23}}{pq} + \frac{k_{12}k_{23}}{p(p-q)} \mathrm{e}^{-pt} - \frac{k_{12}k_{23}}{q(p-q)} \mathrm{e}^{-qt} \right) \quad (6)$$

where p and q are defined as follows:

$$p = \frac{1}{2}\left\{ k_{12} + k_{21} + k_{23} + [(k_{12} + k_{21} + k_{23})^2 - 4k_{12}k_{23}]^{\frac{1}{2}} \right\} \quad (7)$$

$$q = \frac{1}{2}\left\{ k_{12} + k_{21} + k_{23} - [(k_{12} + k_{21} + k_{23})^2 - 4k_{12}k_{23}]^{\frac{1}{2}} \right\} \quad (8)$$

Each IR-absorption band area, A, is proportional to the corresponding concentration. The proportional constant is the absorption coefficient, ε, and then, for example, the IR-absorption band are of TT, A_{TT}, is equal to [TT]ε_{TT}. Thus, equations (4) – (6) are replaced by the following equations (9) – (11):

$$A_{TT} = A_{TT0}\left(\frac{k_{12}(p-k_{23})}{p(p-q)}e^{-pt} + \frac{k_{12}(k_{23}-q)}{q(p-q)}e^{-qt}\right) \quad (9)$$

$$A_{TC} = A_{TT0}\left(-\frac{k_{12}}{p-q}e^{-pt} + \frac{k_{12}}{p-q}e^{-qt}\right)\frac{\varepsilon_{TC}}{\varepsilon_{TT}} \quad (10)$$

$$A_{CC} = A_{TT0}\left(\frac{k_{12}k_{23}}{pq} + \frac{k_{12}k_{23}}{p(p-q)}e^{-pt} - \frac{k_{12}k_{23}}{q(p-q)}e^{-qt}\right)\frac{\varepsilon_{CC}}{\varepsilon_{TT}} \quad (11)$$

where the symbol of A_{TT0} represents the IR-absorbance band area of TT at the start of irradiation.

The time evolution of IR-absorbance band area with no optical filters is plotted in Fig. 5.7, where the 3339, 3562 and 3571-cm^{-1} bands are chosen for TT, TC and CC, respectively. The value of A_{TT0} can be obtained from a spectrum before irradiation after deposition to be 0.9906. The parameters of k_{12}, k_{21}, k_{23}, $\varepsilon_{TC}/\varepsilon_{TT}$ and $\varepsilon_{CC}/\varepsilon_{TT}$ are determined from the absorbance changes by the least-squares fitting process to be 0.0083 ± 0.0003 min^{-1}, 0.133 ± 0.005 min^{-1}, 0.0042 ± 0.0004 min^{-1}, 0.78 ± 0.02, and 1.04 ± 0.09, respectively. The calculated values of $\varepsilon_{TC}/\varepsilon_{TT}$ and $\varepsilon_{CC}/\varepsilon_{TT}$ obtained by the DFT method, 0.58 and 0.61, are slightly different from the corresponding observed values, probably because of the influence of the IMHB in the calculation. The ratio of $\varepsilon_{TC}/\varepsilon_{TT}$ is reported to be 0.12 by Ōki et al. [21], which is clearly inconsistent with the corresponding value in the author's study, 0.78, probably because of the intermolecular interaction between 2-PA and CCl_4.

Only 7.7% of TT reacts during the 100-min UV irradiation, because the rate constant for the back reaction from TC to TT, k_{21}, is ~16 times larger than that of the forward reaction from TT to TC, k_{12}. The calculated values are found to reproduce the observed IR-absorbance time evolution satisfactorily. One may claim that the observed values of CC are slightly inconsistent with the corresponding calculated values at the early irradiation stage. This finding suggests the direct conformational change from TT to CC disregarded in this kinetic analysis, but its amount is negligible. Therefore the

author concludes that the photoreactions shown in Scheme 5.1 mainly occur upon UV irradiation in argon matrices.

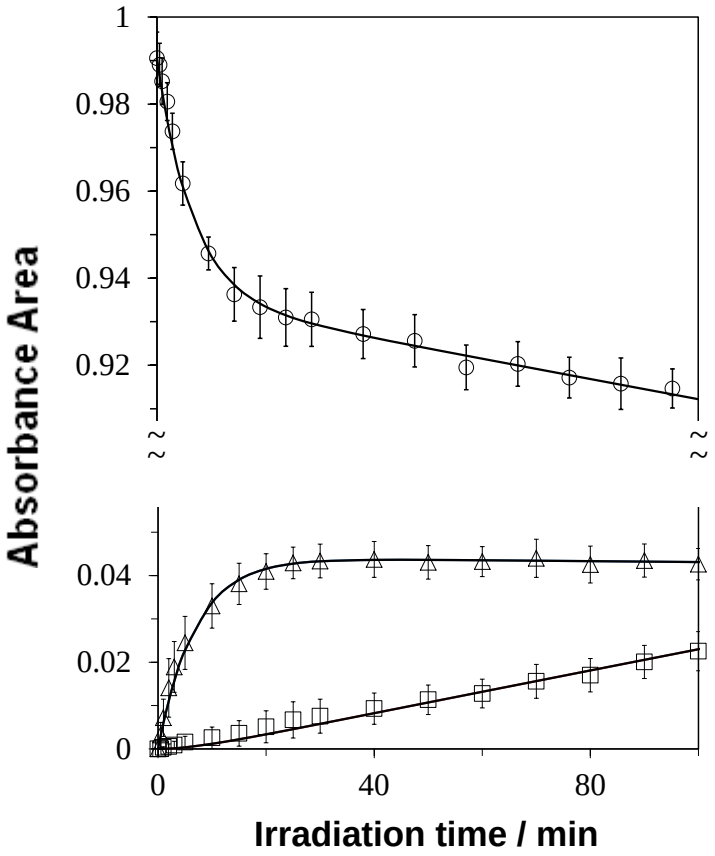

Fig. 5.7. IR-absorbance band-area changes against irradiation time. Symbols of (○), (Δ) and (□) represent the IR bands of TT (3339 cm^{-1}), TC (3562 cm^{-1}) and CC (3571 cm^{-1}), respectively.

5.2.5. Mechanisms of conformational changes upon UV irradiation

To investigate the mechanism of the conformational changes, the author optimized TT and TC in the excited state by CIS/6-31++G** level. The optimized geometrical parameters are listed in Table 5.4. It was found that the dihedral angle of $C_2NC_1C_5$ is 32.8° in TT, indicating the pyridine ring is distorted in the excited state. The length of IMHB is 2.368 Å, which is longer than that in the ground state by 0.359 Å. Thus it was implied that the IMHB is weakened in the excited state and the conformational change from TT to TC occurs to resolve the repulsion between the lone pairs of the two O atoms in the carboxy group. As well as TT, the pyridine ring of TC is also distorted in the excited state, where the dihedral angle of $C_2NC_1C_5$ was 26.5°. The author assumed that the internal rotation around the C−C or C−O bond occurs to avoid the repulsion between the lone pairs of the O atom and the N atom. Note that there are other possibilities that the conformational changes occurred during the vibrational relaxation process.

Table 5.4. Optimized geometry of TT and TC in the excited state. [a,b]

Parameters[c]	TT	TC
$r(C_1-N)$	1.344	1.343
$r(N-C_2)$	1.356	1.351
$r(C_2-C_3)$	1.354	1.354
$r(C_3-C_4)$	1.439	1.439
$r(C_4-C_5)$	1.360	1.358
$r(C_5-C_1)$	1.428	1.429
$r(C_1-C_6)$	1.461	1.444
$r(C_6-O_a)$	1.191	1.199
$r(C_6-O_b)$	1.335	1.334
$r(O_b-H)$	0.944	0.948
$r(N\ldots H)$	2.368	-
$\Theta(C_6C_1N)$	125.5	124.6
$\Theta(C_1C_6O_a)$	122.8	124.6
$\Theta(C_1C_6O_b)$	116.5	113.2
$\Theta(C_6O_bH)$	112.7	107.9
$\Theta(HO_bC_6O_a)$	178.5	-0.3
$\Theta(HO_bC_6C_1)$	-1.2	-179.9
$\Theta(O_aC_6C_1N)$	-176.4	-177.1
$\Theta(O_bC_6C_1N)$	3.3	2.4
$\Theta(C_1C_6NC_2)$	-28.4	-23.0
$\Theta(C_2NC_1C_5)$	32.8	26.5

[a] Calculated at the CIS/6-31++G** level.

[b] Units of r and Θ are Å and degrees, respectively.

[c] Numbering of atoms is given in Fig. 5.2.

5.3. Summary

The UV-induced conformational changes of 2-PA have been investigated by comparison of the IR spectra measured by the low-temperature matrix-isolation technique with the spectral patterns obtained by the DFT calculation. Unlike the previous results in CCl_4 solution, only the most stable conformer, TT having the IMHB of COOH···N, exists in the argon matrix. The presence of TT in 2-PA, the *trans* conformation around the OC−OH bond, is in contrast to general carboxylic acids such as acetic acid and benzoic acid. The second stable conformer, TC having the IMHB of C=O···HC, is produced during the early UV irradiation without optical filters, and the third stable conformer, CC, is produced from TC during the prolonged irradiation time. The back reaction from TC to TT occurs upon the following shorter-wavelength cut-off UV irradiation (λ > 270 nm). The proposed photoreaction pathways are supported by the kinetic analysis of the IR-absorbance band-area changes against the irradiation time.

5.4. References

[1 E.M.S. Maçôas, L. Khriachtchev, M. Pettersson, R. Fausto, M. Räsänen, Phys. Chem. Chem. Phys. 7 (2005) 743.

[2] E.M.S. Maçôas, L. Khriachtchev, M. Pettersson, J. Juselius, R. Fausto, M. Räsänen, J. Chem. Phys. 119 (2003) 11765.

[3] E.M.S. Maçôas, L. Khriachtchev, M. Pettersson, J. Lundell, R. Fausto, M. Räsänen, Vib. Spectrosc. 34 (2004) 73.

[4] E.M.S. Maçôas, L. Khriachtchev, M. Pettersson, R. Fausto, M. Räsänen, J. Am. Chem. Soc. 125 (2003) 16188.

[5] E.M.S. Maçôas, L. Khriachtchev, M. Pettersson, R. Fausto, M. Räsänen, J. Chem. Phys. 121 (2004) 1331.

[6] E.M.S. Maçôas, L. Khriachtchev, M. Pettersson, R. Fausto, M. Räsänen, J. Phys. Chem. A 109 (2005) 3617.

[7] S. Amiri, H.P. Reisenauer, P.R. Schreiner, J. Am. Chem. Soc. 132 (2010) 15902.

[8] A. Halasa, L. Lapinski, I. Reva, H. Rostkowska, R. Fausto, M.J. Nowak, J. Phys. Chem. A, 118 (2014) 5626.

[9] A. Borba, A. G.-Zavaglia, R. Fausto, J. Chem. Phys. 141 (2014) 154306.

[10] I. Reva, C.M. Nunes, M. Biczysko, R. Fausto, J. Phys. Chem. A *in press* (dx.doi.org/10.1021/jp509578c).

[11] R. Song, K.M. Kim, Y.S. Sohn, Inorg. Chim. Acta 292 (1999) 238.

[12] D.M. Stearns, W.I.I. Armstrong, Inorg. Chem. 31 (1992) 5178.

[13] W. Somphon, K.J. Haller, J. Cryst. Growth 362 (2013) 252.

[14] G. Świderski, M. Kalinowska, S. Wojtulewski, W. Lewandowski, Spectrochim. Acta Part A 64 (2006) 24.

[15] E.B. Hughes, H.H.G. Jellinek, B.A. Ambrose, J. Phys. Colloid Chem. 53 (1949) 414.

[16] R.F. Evans, E.F.G. Herington, W. Kynaston, Trans Faraday Soc. 49 (1953) 1284.

[17] H.H. Jaffé, J. Am. Chem. Soc. 77 (1955) 4445.

[18] R.W. Green, H.K. Tong. J. Am. Chem. Soc. 78 (1956) 4896.

[19] Y. Liang, L.K. Noda, O. Sala, J. Mol. Struct. 554 (2000) 271.

[20] J.F. Wojcik, T.H. Stock, J. Phys. Chem. 73 (1969) 2153.

[21] M. Ōki, M. Hirota, Y. Morimoto, Bull. Chem. Soc. Jpn. 39 (1966) 1620.

[22] P. Koczoń, J.Cz. Dobrowolski, W. Lewandowski, A.P. Mazurek, J. Mol. Struct. 655 (2003) 89.

[23] E.M.S. Maçôas, L. Khriachtchev, M. Pettersson, R. Fausto, M. Räsänen, Phys. Chem. Chem. Phys. 7 (2005) 743.

[24] E.M.S. Maçôas, L. Khriachtchev, M. Pettersson, J. Juselius, R. Fausto, M. Räsänen, J. Chem. Phys. 119 (2003) 11765.

[25] E.M.S. Maçôas, L. Khriachtchev, M. Pettersson, J. Lundell, R. Fausto, M. Räsänen, Vib. Spectrosc. 34 (2004) 73.

[26] E.M.S. Maçôas, L. Khriachtchev, M. Pettersson, R. Fausto, M. Räsänen, J. Am. Chem. Soc. 125 (2003) 16188.

[27] E.M.S. Maçôas, L. Khriachtchev, M. Pettersson, R. Fausto, M. Räsänen, J. Chem. Phys. 121 (2004) 1331.

[28] E.M.S. Maçôas, L. Khriachtchev, M. Pettersson, R. Fausto, M. Räsänen, J. Phys. Chem. A 109 (2005) 3617.

[29] S. Amiri, H.P. Reisenauer, P.R. Schreiner, J. Am. Chem. Soc. 132 (2010) 15902.

[30] S. Nishino, M. Nakata, J. Phys. Chem. A 111 (2007) 7041.

[31] S. Nanbu, M. Sekine, M. Nakata, J. Mol. Struct. 1025 (2012) 43.

[32] S. Nanbu, M. Sekine, M. Nakata, J. Phys. Chem. A 115 (2011) 9911.

[33] M. Nagaya, S. Iizumi, M. Sekine, M. Nakata, J. Mol. Struct. 1025 (2012) 53.

[34] S. Iizumi, N. Akai, M. Nakata, J. Mol. Struct. 1037 (2013) 294.

[35] M. Miyagawa, N. Akai, M. Nakata, J. Mol. Struct. 1058 (2014) 142.

[36] M. Miyagawa, N. Akai, M. Nakata, Chem. Phys. Lett. 602 (2014) 52.

[37] J.W. Moore, R.G. Pearson, Kinetics and Mechanism, John Wiley & Sons, New York, 1981.

Chapter 6: General Conclusion

In this thesis, the author investigated photoreaction mechanisms of aromatic carboxylic acids.

In chapter 3, photoreaction mechanisms of salicylic acid were elucidated. In contrast to the previous studies on the dual emission, the author focused on the conformations and the intramolecular hydrogen bonds (IMHBs, hereafter) and found conformational changes from the most stable conformer to the second and the fourth stable ones upon UV irradiation. The latter conformer is the *trans* around the OC−OH bond, which exists stably due to IMHB of COOH···OH−Ph, in contrast to general carboxylic acids. In addition, the dissociation of a water molecule from the carboxy and the hydroxy groups was also observed, and this reaction was related to IMHB.

In chapter 4, a substitution effect of a chlorine atom into the third position of salicylic acid was investigated. The strength of IMHB of Ph−OH···Cl was ca. 11 kJ mol^{-1}. As well as salicylic acid, the UV-induced conformational changes occurred from the most stable conformer (λ > 330 nm), and dissociation of the water molecule from the second stable conformer was observed (λ > 290 nm). In addition, from the fourth stable conformer, which did not react in salicylic acid, dissociation of hydrogen chloride has been implied, producing a five-membered ring ketene compound (λ > 270 nm). Thus it was assumed that the substitution of the chlorine atom induces an additional photoreaction starting from the fourth stable conformer.

In chapter 5, conformations and photoreaction mechanisms of picolinic acid were investigated. Unlike general carboxylic acids preferring the *cis* conformer, only the *trans* conformer was observed in an argon matrix due to IMHB of COOH···N in the pyridine ring. The second stable, the *cis* conformer was produced from the most stable one, and the third was also produced from the second one upon shorter-wavelength UV irradiation. In addition, the back reaction from the second to the most stable one was also observed upon longer-wavelength UV irradiation, and the kinetic analysis revealed the back reaction is ca. 16 times faster than the forward reaction.

In conclusion, the author found conformational changes of aromatic carboxylic acids around C−OH and R−COOH in RCOOH, focusing on IMHB with the *ortho* position. The stable existence of the *trans* conformer was found in the all three

molecules, and also dissociation of hydrogen-bonding atoms was observed. The former finding was quite different from previous studies, and the latter was not reported in the previous studies on the dual emission. Therefore, the importance of IMHB on the conformations and photoreactions of aromatic carboxylic acids was revealed.

Acknowledgement

The author would like to express great appreciation to Professor Munetaka Nakata for his kind discussion, advice and help. The author is very thankful to Professor Kozo Kuchitsu for his helpful discussion. The author also thanks Associate Professor Nobuyuki Akai for his detailed advice about experimental set up and helpful discussion.

The author appreciates Professor Kenji Ogino, Professor Weihua Qian, Professor Masao Takayanagi for evaluation of the author's work with great care and valuable comments and suggestions.

The author thanks the TUAT Research Fellow Program for its financial support.

Research Achievement

1. M. Miyagawa, N. Akai, M. Nakata, UV-light induced conformational changes of 3-chlorosalicylic acid in low-temperature argon matrices, J. Mol. Struct. 1058 (2014) 142-148.

2. M. Miyagawa, N. Akai, M. Nakata, UV-induced photoreaction pathways of salicylic acid: Identification of the fourth stable conformer and ketoketene-water complex, Chem. Phys. Lett. 602 (2014) 52-57.

3. M. Miyagawa, N. Akai, M. Nakata, UV-light induced conformational changes of 2-pyridinecarboxylic acid in low-temperature argon matrices, J. Mol. Struct. 1086 (2015) 1-7.

4. K. Ohyama, K. Goto, T. Shinmyozu, N. Yamamoto, S. Iizumi, M. Miyagawa, M. Nakata, H. Sekiya, Infrared spectroscopic studies on 4-amino-6-oxopyrimidine in a low-temperature Xe matrix and crystalline polymorphs composed of double hydrogen-bonded ribbons, Chem. Phys. Lett. 595-596 (2014) 138-143.